Sustainable Alternative Designs For The Tongzhou Bay Port

J.R.M. Muller

TU Delft

河海大學 HOHAI UNIVERSITY

Cover illustration

Zhang Daqian, 1899–1983
山水 (*Landscape*), 1947
Ink and color on paper

Sustainable alternative designs for the Tongzhou Bay Port

A design study at the potential of alternative reclamation configurations through a 'Building-with-Nature' approach, in preserving and creating valuable habitat based on two specialised coastal shorebird species at the Jiangsu coast

by

J.R.M. Muller

to obtain the degree of Master of Science
at the Delft University of Technology,

Student number:	2042671	
Thesis committee:	Prof. Dr. Ir. S.G.J. Aarninkhof,	TU Delft, supervisor
	Prof. Dr. Ir. Z.B. Wang,	TU Delft, Deltares
	Dr. D.S. Van Maren,	TU Delft, Deltares
Other supervisors:	Prof. Dr. Y.P. Chen	Hohai University
	Prof. Dr. Z. Gong	Hohai University
	Dr. J.F. Tao	Hohai University
	A. Chu	Hohai University

TU Delft

河海大學 HOHAI UNIVERSITY

Preface

Life in China is fast. From the undeniable importance of the internet and smartphone in everyday life, to the rapid urban development and construction of an even faster high-speed rail system, further connecting the vast 'middle kingdom'. This attitude also became apparent when I was offered the opportunity to perform my thesis on the Jiangsu coast at Hohai University. Travel and accommodation arrangements were made fast and soon I was completely settled among my Chinese colleagues. This not only gave me flashing start of my thesis work, but also the opportunity to experience the Chinese culture and university life as well.

During my thesis, I was able to meet and learn from several specialist within multiple fields of the Jiangsu coastal system. As such, the goals were many and the bar was high, which resulted in several highs and lows. Eventually, the combination of these different perspectives led to new insights and served as a continuous motivation throughout the process. The unique circumstances and opportunities that I have encountered made this final part of my studies a truly fantastic experience and a memory I won't soon forget.

First, I would like to thank my supervisors at Delft University of Technology, for their continuous support and feedback. Prof. Dr. Stefan Aarninkhof for always seeing the potential within the topic and keeping me in close contact with several specialists during my thesis. Prof. Dr. Zheng Bing Wang for his valuable feedback and help in arranging my stay at Hohai University. Finally, I want to thank Dr. Bas van Maren for the many technical discussions during the modeling, but also for the not-so technical ones.

Further, I would like to express my sincere gratitude to my Chinese supervisors for the fantastic stay at Hohai University in Nanjing. First, Prof. Dr. Yong Ping Chen for his generous hospitality in making all the arrangements and for the further introduction to all coworkers and students. I want to thank Prof. Dr. Zheng Gong for the insightful discussions on the future development of the Jiangsu coast and the wonderful field-trip along the many study areas. Also, I want to thank Dr. Jianfeng Tao and Ao Chu for helping me setting up the model and the vital cups of coffee. Special thanks for Dr. Peng Yao and Dr. Min Su for their help during the modeling and troubleshooting. Without your continuous support over the last couple of months, these results would not have been possible. During my stay, the office at Hohai became a small second home for me and I'm very grateful for getting to know all of my coworkers. Special thanks goes out to Dan Xu Cao, Zhou Tian Yi and Gan Min for showing me the ropes in the use of smart phones for every little thing, solving my translation problems and looking after my wellbeing.

I also would like to thank the people at NIOZ for their expertize in the migratory bird and providing sighting data. I want to thank Prof. Dr. Theunis Piersma for his enthusiastic response and feedback on the direction of the research. I also want to thank Ying Chi Chan and Hebo Peng for their help and feedback on the sighting data and shorebird characteristics.

Finally, I want to thank my close friends and family for their support and needed distraction.

Jos Muller

Rotterdam, October 2018

Executive summary

Over the last decades, the People's Republic of China experienced large economic development, which has led to severe shortages of usable land. To counteract this, the Chinese central government promoted the development of coastal provinces by reclaiming large sections of coastal zones. One of these regions is Nantong Binhai Park or Tongzhou Bay on the Jiangsu coast. This region is characterized by large intertidal mudflats with deep tidal channels and has a high potential for the development of agri-aquaculture and the construction of a deep-sea port. However, these intertidal mudflats also provide vital ecosystem services and support numerous species, such as several endangered migratory shorebirds within the East Asian–Australasian Flyway. Acknowledging the importance of both port development and existing endangered ecosystems, a more integrated coastal development strategy is needed. A possible solutions could be found following the 'Building with Nature' approach, in which natural processes and ecological needs are included during the design process. This requires a good understanding of the governing processes as well as the requirements from society, ecology and engineering perspectives.

In this thesis, a study is performed to find a more sustainable alternative for the planned Tongzhou Bay port. It aims at making the connection between engineering and ecological point of view. A previous developed hydro-morphodynamic numerical model was made available and is further developed to gain a better understanding of the local governing processes, such as tidal features, sediment transport and siltation patterns. Several simplifications and an additional cohesive fraction were added to the model setup, which showed satisfying results during validation. Model results show a net inward flux of tidal volumes and sediments though the main tidal channels; Xiaomiaohong, Sanshahaong and the upper tidal channel. At the Yaosha shoal, most of tidal volume flux flow through the Xiaomiaohong channel and cross over the shoal in a northward direction. Transport fluxes tend to follow these current patterns closely and show a similar south-north sediment flux over the Yaosha and Lengjiasha shoal. In order to model the Tongzhou Bay morphology in an efficient manner, a morphological acceleration factor was used. This approach was verified through a test case, hindcasting the morphodynamic developments due to the most recent reclamation activities at Tongzhou Bay. Qualitative verification of the testcase results show the models capability in predicting similar morphodynamic features with respect to measured elevations. The model is setup to predict 8 years of morphological development with no further reclamations, serving as a reference case. Heavy siltation was found at the higher elevated regions and outer edges of the intertidal mudflats. Most of the erosion takes place in the channels, indicating the gradual steepening of the mudflat profile.

The Tongzhou Bay ecosystem and potential occurrence of a certain habitat is quantified by classifying the region in to specific ecotopes, based on previous model results. These ecotopes are individual regions, which describe relative homogeneous characteristics. Referencing of the ecotope map with satellite-tracked home range data of two shorebird species at Tongzhou Bay, indicate the relative preference of these species on mid- and low-range littoral zones. These ecotopes are subsequently used as an indication for the potential occurrence of valuable habitat for these shorebird species survival.

The better understanding of the governing processes in development of the intertidal mudflats and corresponding ecotopes is used to design alternative port configurations through several design cycle iterations. A set of three design criteria were determined, requiring each configuration to preserve existing high-value ecotopes, enhance the development of these ecotopes and create potential area for future port development. The full reclamation of the Yaosha shoal will result in the loss of high-value ecotopes at the shoal. Partial reclamation of the southside of the Yaosha shoal, leads to the blocking of current and transport fluxes supplied through the Xiaomiaohong channel. Oppositely, the partial reclamation of the northside of the Yaosha shoal, still allows sediment supply to the Yaosha shoal by the Xiaomiaohong channel, only to be blocked on the backside of the shoal. As a result, siltation rates and therefore ecotope accretion is enhanced. However, ebb velocities on the shoal are stronger and the formation of creeks and new tidal channels over the shoal are predicted. Similar developments are found by comparable reclamation scenarios at the Lengjiasha shoal. Evaluation of all alternative designs revealed that the optimum configuration is the offshore reclamation of the Lengjiasha shoal. This is mainly due to restricting reclamation activities and the reduction of local flow velocities at the Yaosha shoal.

This thesis explores the potential of more sustainable alternative port designs through understanding governing processes in natural development at Tongzhou Bay. The Yaosha shoal can be classified as the most vital habitat for several migratory birdspecies. Reclamation activities at the Yaosha shoal will lead to a clear loss of habitat and blocking of the driving processes for the development of new habitat zones. It is found that alternative reclamations of less important zones, such as the Lengjiasha shoal could preserve valuable habitat and increase the natural development of these habitats. However, this far offshore reclamation implies large challenges regarding port operations and logistics with the hinterland.

Contents

List of Tables

List of Figures

List of abbreviations

AYD	Abandoned Yellow river Delta
BTG	Bar-Tailed Godwit
BP	Before Present
ECS	East China Sea
GDP	Gross Domestic Product
GK	Great Knot
JCC	Jiangsu Coastal Current
JRM	Jiangsu Regional Model
ME	Model Efficiency
morfac	Morphological acceleration factor
MZCC	Min-Zhe Coastal Current
NRSR	Northern Radial Sand Ridges
OBOR	One Road, One Belt
PB	Percentage Bias
RSR	Radial Sand Ridges
SRSR	Southern Radial Sand Ridges
SSH	Sanshahong
SYS	Southern Yellow Sea
TBM	Tongzhou Bay Model
USD	United States Dollar
WCH	Wangcanghong
XMH	Xiaomiaohong
ZES	Zoute wateren Ecotopen Stelsel (Salt waters Ecotope System)

Nomenclature

ϕ	Krumbein phi scale	–
τ_{ce}	Critical bedshear stress for erosion	N/m^2
τ_c	Current-induced bedshear stress	N/m^2
τ_{cw}	Wave- and current-induced bedshear stress	N/m^2
A	Cross-sectional flow area	m
A_e	Empirical cross-sectional flow area	m^2
A_{port}	Area for port development	hec
$A_{port,max}$	Maximum area for port development	hec
$\bar{m}$	Mean measured value	–
c_{SB}	Suspended sediment concentration at the boundary	mg/L
D	Particle diameters	μm
d	Local water depth	m
d_{mud}	Initial bed layer thickness	m
D_0	Reference diameter	μm
Δm	Measurement error	
f_{eco}	Ecotope weight factor	–
g	Relative ecotope area growth w.r.t. the reference case	hec
g_{max}	Maximum ecotope area growth w.r.t. the reference case	hec
H	Initial waterdepth	m
H_s	Significant wave height	m
m	Measured value	
M	Erosion parameter	$kg/m^2/s$
ME	Nash-Sutcliffe Model efficiency	–
n	Ecotope type	–
n_{rough}	Manning roughness coefficient	$s/(m^{1/3})$
p	Predicted value	–
P	Tidal prism	m
PB	Percentage bias	%
q	Initial preserved ecotope area	hec
q_{max}	Maximum initial preserved ecotope area	hec
$t_{dryfall}$	Dryfall duration	s
T_p	Peak wave period	s
v_{wind}	Wind velocity	m/s
w_s	Settling velocity	mm/s
Y	Variant performance score	–
$\tilde{Y}$	Unweighted variant performance score	–
z_a	sediment transport type reference height	m

1 Introduction

In this chapter, an overall introduction is given to the area and problem of interest, which is the subject of this thesis. From the problem definition, the objective and corresponding research questions are formulated. Finally, the general structure of this thesis is outlined as a reading guide.

1.1. Background

The People's Republic of China is one of the most populated and developing countries in the world. With the world's second largest GDP of 11,200,000 million USD and a net growth of 6.7% in 2016, China has become a major global economy (National Bureau of Statistics, 2017; World Development Indicators database, 2017). Most the economic development takes place in the metropolitan areas and ports within the coastal provinces, which contain 43.3% of the total population or 1.4 billion people (National Bureau of Statistics, 2016).

One of these regions is the Jiangsu coastal province, which is situated at the Southern Yellow Sea (SYS) between the Shandong province to the north and the Yangtze river estuary to the south, as shown in Figure1.1. The Jiangsu coastline stretches over 994 km long and hosts several main national ports, such as the the Lianyungang port, Nanjing port, Zhenjiang port, Nantong port and Suzhou port and several important regional ports (Li et al., 2014; Huo et al., 2018; Jiangsu Yangkou Port Co., Ltd., 2018). The coast is characterized by muddy shores and large inter-tidal mudflats that can reach up to 40 km offshore (Chen and Zhang, 2011; Wang and Zhu, 2006). Due to the abundance of large inter-tidal flats, coastal reclamation activities serves as a solution for the increasing demand of usable land (Zhao et al., 2015; Wang et al., 2014a; Tian et al., 2016). Main utilization of these reclaimed areas is used for modern agriculture, aquaculture, planted forests, ports and related industries, coastal tourism and other uses (Wang and Wall, 2010; Economic Daily, 2017). Since 1950, these reclamations were carried out at roughly the same rate as the tidal flat accretion rate, allowing nature to keep up (Fan et al., 2017).

With initiatives for further economic development such as the "One Road, One Belt" (OBOR), there is an increased demand for a higher capacity of coastal and riverine ports (Wang and Wall, 2010). To sustain further economic development, the Chinese central government upgraded the development of Jiangsu coastal zone to be part of national development strategy and approved a plan to reclaim large sections of the Jiangsu coastal zone for 2030 (Zhang and Chen, 2011). Essential part of these reclamations are the development of two new deepsea ports at Jianggang and Lüsi, reclaiming the Dongsha-Tiaozini and Yaosha-Lengjiasha mudflats respectively. After the final stage, these two proposed projects would have a combined reclaimed area of over 960 km^2 (Zhang and Chen, 2011). With unique topographic setting of deep natural tidal channels and large shallow shoals, these zones have a high potential for port development (Zhang et al., 2011; Zhang and Chen, 2011). The proposed port reclamation at the Lüsi port is known as "Nantong Binhai Park" or Tongzhou Bay (Encyclopedia, 2018) and is part of the Nantong Port Group Cooperation (Nantong Port Group Co., Ltd., 2017; China Daily, 2017). Together with the adjacent offshore Yangkou port and the Lüsi port itself, the complete proposed Tongzhou bay port would consists of 280 km^2 under the slogan "two wings, one body" (Encyclopedia, 2018; Wang and Wall, 2010).

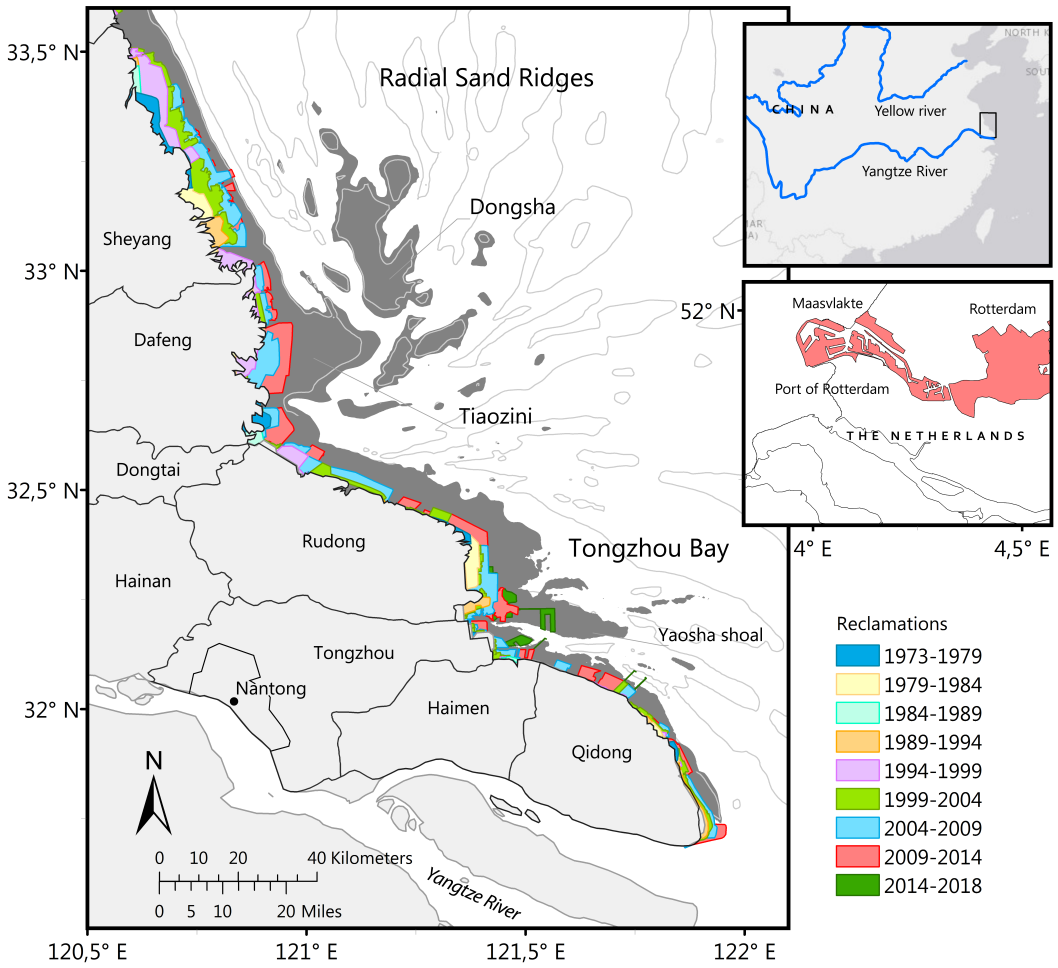

Figure 1.1: Overview of the Jiangsu coast and intertidal mudflats. Indicated are the previous reclamations. Also the Port of Rotterdam in the Netherlands is shown with similar scale as a reference.

1.2. Problem statement

The extend of these large-scale reclamations will have a significant effect on local tidal conditions and moderate on local wave action (Cong and Zhu, 2017; Lu and Dou, 2011; Tao et al., 2011; Zhu et al., 2016; Fan et al., 2015). Muddy coastlines, such as the Jiangsu coastline, are highly complex in processes and sediment characteristics and react strongly to changes in the driving hydrodynamic forces (Le Hir et al., 2000; Liu et al., 2011; Roberts et al., 2000). As a consequence, these anthropogenic interventions will affect the driving morphodynamic processes and overall shape and morphology of the coastal profile (Song et al., 2013; van Maren et al., 2016; Wang et al., 2012b, 2014b).

Furthermore, large concerns have been raised about the impact of large-scale reclamations on the natural habitat and ecological diversity of the saltmarsh ecosystem at the Jiangsu coast(Sun et al., 2017; Wang et al., 2014a; He and Zhou, 2016; Yao, 2013). The ongoing reclamation activities lead to a gradual degradation of the environmental quality (Wang and Zhu, 2006). The Yellow Sea coastal zones form an essential part of the Asia-Australian Flyway. Within this flyway, over 36 migratory shorebirds species or 40% of all resident birds are reliant on this habitat, including the Jiangsu coastal area (Barter, 2002; Piersma et al., 2017). The past 50 years, these ecosystems have been reduced by 50% and are considered as endangered (Murray et al., 2015). Recent studies show that the reclamation activities at the Jiangsu flats can be linked directly to the decline of these endangered shorebird species(Piersma et al., 2017; Peng et al., 2017). Construction within

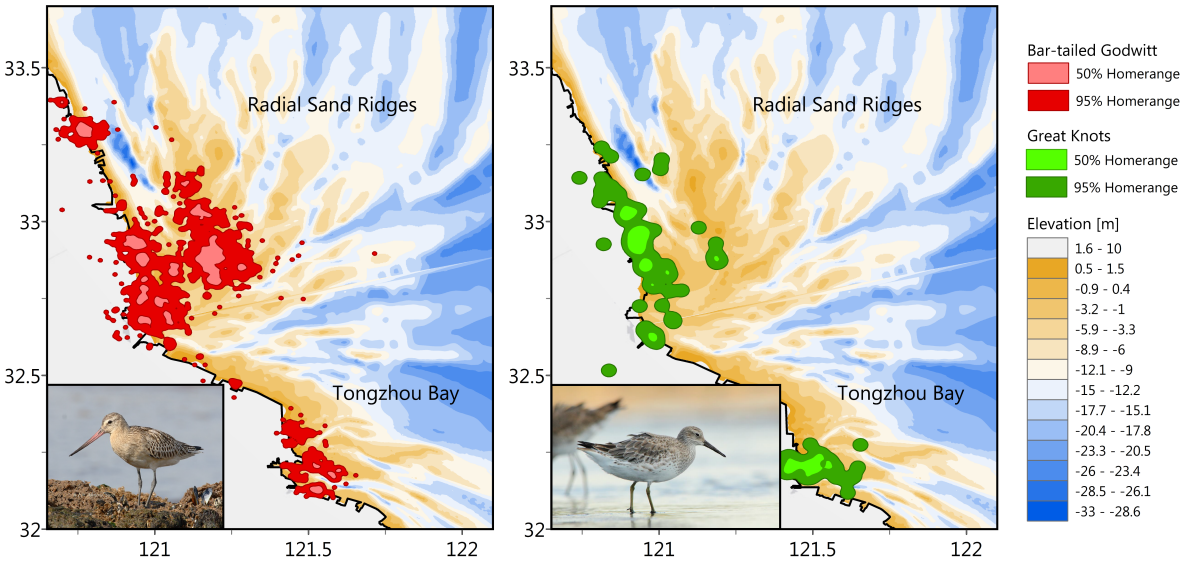

Figure 1.2: Satellite tracked home-range of two migratory bird species at the Tongzhou Bay, namely the Bar-Tailed Godwitt and the Great Knot as provided by Chan et al. (2018)

.

the Yellow and Yangzte River also lead to a reduced amount of sediment import and a reduced accretion of these intertidal areas (Barter, 2002). The proposed Tonghzou Bay port would strongly interfere with this habitat. Figure 1.2 show the extend of the proposed port with the satellite tracked, home-range data of two endangered shore-bird populations, namely the Bar-tailed Godwit (BTG) and the Great Knot (GK).

In 2013, the first phase of the Tongzhou Bay port at the Yaosha-Lengjiasha shoals was constructed, which further reduces the tidal flat area and increases pressure on the ecosystem (Huang and Zhang, 2017). Due to the raised ecological concerns, the Chinese national authorities put a halt on all the large-scale reclamations on the Chinese coast until a better understanding is obtained on the state of the coastline and the impact of new reclamation projects (BirdLife International, 2018; China Daily, 2018; Xinhua News Agency, 2018). Acknowledging the importance of both the development of a new port and related industries and the ecological value of the inter-tidal flat habitat, there is need for a more integrated coastal development in which both socio-economic and ecological requirements are included (Forst, 2009; Wang and Zhu, 2006; Cui, 2017; Liang et al., 2015; Zhang et al., 2016).

The last decade, several coastal engineering projects have adopted these integral design strategies in order to provide a robust and sustainable solutions. These concepts, also known as Building with Nature (or Working with Nature (PIANC, 2011)), is an engineering practice that aims at pro-actively using and providing for engineering purposes as well for socio-ecological services as part of the design solution (de Vriend et al., 2014a; van Slobbe et al., 2013). The implementation of these strategies is very dependent on the local conditions and require a profound understanding of the different perspectives, needs and the governing natural processes (Baptist et al., 2017; de Vriend et al., 2014b). Despite some preliminary studies on tidal velocities and siltation rates for the proposed Tonghzou Bay port or other smaller reclamation projects (Huang and Liu, 2017; Nantong Port Authority, 2013), ecological requirements are not yet included in the design of Tonghzou Bay port. This is often due to a knowledge gap between engineering practices and the governing processes in the current state and development of wetland ecosystems (Ma et al., 2010; Borsje et al., 2011). It is therefore not clear, if alternative port configurations for the proposed Tonghzou Bay port could provide for both port development and aid in the state of valuable wetland ecosystem .

1.3. Objective

The problem statement shows the need for a more integrated design strategy for finding a solution for the conflicting interests between port development and the state of the Tongzhou bay ecosystem. Consequently, the objective of this thesis is to study the effectiveness of alternative designs for the Tongzhou bay port, in

which benefits both the state of the wetland ecosystem and the development of a deep-sea port. This is attempted by bridging the knowledge gap between ecologic and engineering practices.

This main objective is further divided into two sub objectives. The first objective of this thesis is aimed at obtaining a better understanding of the hydro- morphodynamic governing processes for the development of the Tongzhou Bay system with the use of numerical modeling. The second objective is to use the gained insight in the design of alternative port configurations for the Tongzhou Bay port and evaluate the performance of these alternatives in providing for both port and ecology developments.

1.4. Research questions

In order to quantify the defined objectives, the following research question is expected to be answered with the results of this thesis.

Could the reclamation of alternative port configurations for the Tongzhou Bay port benefit the development of valuable ecosystems at Tongzhou Bay?

This question is divided into the following sub-questions;

- Which processes are governing for flow and transport characteristics at Tongzhou Bay ?
- What types of ecosystem exist at Tongzhou Bay ?
- What is the state of development of these ecosystems without anthropogenic influence ?
- What is the impact of alternative port reclamations on this ecosystem development ?

1.5. Methodology and thesis outline

According to the questions that need to be answered, this thesis is divided into 3 phases. These phases are further divided into several processes as shown in Figure 1.3.

The 1^{st} phase is aimed at understanding the governing processes such as tidal features, sediment transport and siltation patterns at Tongzhou Bay. This is done by means of a review of the literature on the Jiangsu coast and the Tongzhou Bay region and can be found in Chapter2. In order to study the region and test different scenarios, a 2DH hydro-morphodynamic numerical model, previously setup for the Jiangsu coast was further developed and applied on the Tongzhou Bay region. The model description and setup will be covered in Chapter 3. Subsequently, the model results will be validated with help of earlier work, such as field observations, measurements and referencing the modeling results. These modeling results are the first part of the overall results and can be found in Chapter 4.

In the 2^{nd} phase, the validated model results are used to quantify the types of ecosystems at Tongzhou bay based on abiotic characteristics. The classification of these characteristics lead to the creation of a so-called ecotopemap, which can be referenced with satellite-tracked shorebird data at the Tonghzou Bay region. This leads to the determination of high-value ecotopes, which will serve as an indication of the value of the overall ecosystem in alternative designs. Next, the natural development of these ecotopes is determined as a reference case. The quantitative description of the ecosystem at Tongzhou bay is covered in Chapter4.

In the 3^{rd} phase, alternative port configurations are designed, following an iterative design cycle. The gained insight in the governing processes and ecosystem development are combined with port and ecology requirements. These lead to design criteria at which the alternative designs have to suffice. Their effectiveness will be tested using the validated model setup during simulation. Finally, the performance of each alternative is evaluated based on the hydro- morphodynamic behavior and ecotope development. Based on this value of each alternative, a new generation of designs can be simulated. The design and results of the conceived scenarios are treated in Chapter 5

Finally, the overall behavior of each alternative will be discussed in Chapter 6. Subsequently, the results are further assessed by referencing with other relevant findings in previous work. The set research questions are revisited in the final conclusions and recommendations for further approaches for this work and topic are stated. This will be covered in Chapter 7.

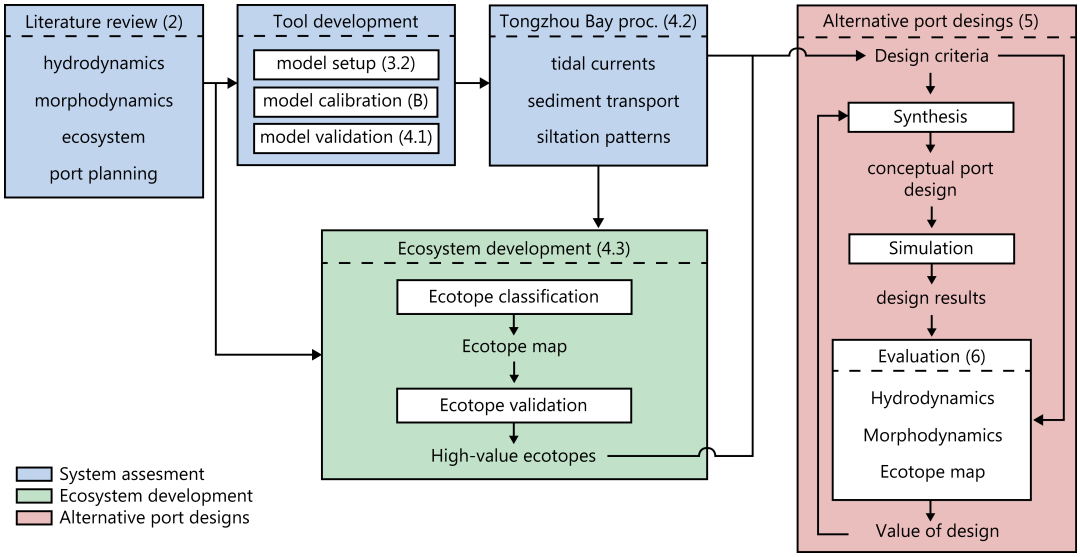

Figure 1.3: Schematic overview of the structure of the thesis. Indicated within the parentheses are the corresponding chapters and sections of each process. The colored blocks correspond with the three phases as described

2

System description of Jiangsu Coast and Tongzhou Bay

2.1. Topography

The Jiangsu coast is characterized by muddy shores and large intertidal mudflats that can reach up to 40 km offshore (Chen and Zhang, 2011; Wang and Zhu, 2006). The Jiangsu coast can be divided into two characteristic domains *e.g.* the northern situated Abandoned Yellow River Delta (AYD) and the Radial Sand Ridges (RSR), situated in the south (Liu et al., 1989; Xue, 1993). Both systems are the result of the combination of two large-scale tidal current patterns that are active at the Jiangsu coast since 7000 years BP (Zhu and Chen, 2005).

The Abandoned Yellow River Delta has mainly been developed due to the abundant sediment supply by the old course of the Yellow River before 1855. Large volumes of sediment have been deposited before the Yellow River changed his course to the current position (Woodroffe and Saito, 2011). Subsequently, tidal current patterns that consist due to the interaction of the radial tidal current in the Northern Yellow Sea and the progressive tidal wave in the south reformed this delta to the current shape (Su et al., 2017b).

The second system is the radial sand ridges, which consist of a large fan-pattern radiate system of mudflats and channels that vary from $2m$ to $20m$ deep (Wang et al., 1999). The origin of this system dates back to the late Pleistocene, when the Paleo-Yangtze River Estuary was still situated at the Southern Yellow Sea (SYS) and large volumes of sediment were deposited and reworked by the unique tidal current system (Zhu and Chen, 2005; Zhu and Chang, 2001). Other sediments types, such as silt and mud were deposited on top of these areas especially in the northern RSR and originated from the AYD, or more recent Yangtze sediment discharge (Li et al., 2001; Su et al., 2017a; Wang et al., 1999, 2012a). Due to the erosion of the AYD, the tidal current along the Jiangsu coast shifted southward, enhancing the rotary tidal wave in the north and shifting the meeting point of the two tidal systems also southward (Chen et al., 2017). The characteristics tidal current pattern in the RSR area, reworked the sediments in to the typical sand ridges (Yao et al., 2013; Zhang et al., 1999; Zhu and Chang, 2001; Zhu and Chen, 2005). Sediments from the AYD not only supplied the RSR, but also other sediment fluxes (*e.g.* from the Yangtze river) where active during this later development (Zhou et al., 2014).

The RSR system can be divided further into a northern and a southern Radial Sand Ridge system (NRSR and SRSR respectively), based on their own characteristic tidal forcing, sediment fluxes and tidal flat topography (Xing et al., 2012; Xu et al., 2016; Zhang et al., 2013). Tongzhou Bay is located in this southern part of the RSR at the central Jiangsu coast. It consist of several long and narrow intertidal ridges with deep tidal channels (Xing et al., 2012). The largest topographic features are the Lengjiasha and Yaosha shoals and the Xiaomiaohong (XMH), Sanshahong (SSH) and Wangcanghong (WCH) channels, as shown in Figure 2.1. The sand ridges are typically discontinuous (*e.g.* Hetunsha Ridge and Jiangjiasha Ridge) (Xu et al., 2016).

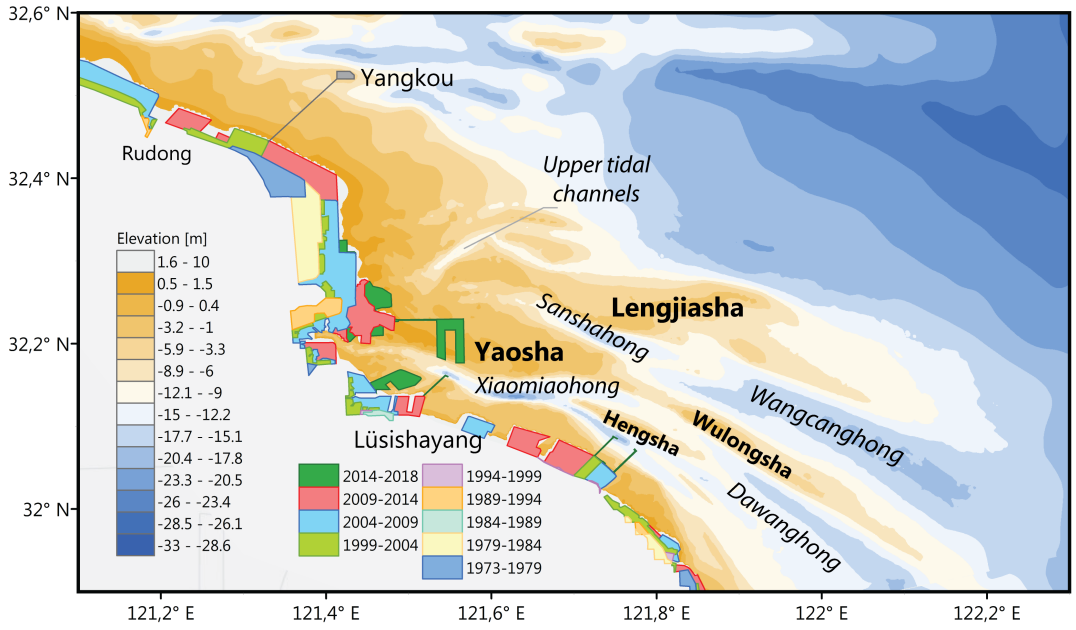

Figure 2.1: Overview of the Tongzhou Bay topography, with the Yangtze river mouth located at the south and the Tiaozini shoal to the north. Recent reclamations at this region are indicated for the period from 1973 to the present. Indicated are the measuring stations, including 6 tidal gauges for water levels (blue) and 14 temporary mooring stations (red)

2.2. Hydrodynamics

2.2.1. Tide and currents

The Jiangsu coast is influenced by two distinct large-scale tidal circulations. These are the anti-clockwise rotary tidal wave in the northern part of the Southern Yellow Sea (SYS) and the progressive tidal wave in the South Yellow Sea coming from the Pacific (Liu et al., 1989; Wang et al., 1999; Xing et al., 2012; Yan et al., 1999a; Zhang et al., 1999) (Figure 2.2). These two tidal systems converge at the coast at Jiangang and is the main driver of the current pattern at the central Jiangsu coast. (Su et al., 2015; Yan et al., 1999b). Due to this feature, a semi-diurnal vertical tide can be observed along the Jiangsu coast with its largest tidal range of 9.5 m between HWS and LWS at Jianggang at the Tiaozini tidal flat. North and southward of this point, the tidal range is declining, creating a rope-skipping pattern (Kang, 2015). Similar pattern was found at Tongzhou Bay, with a mean tidal range of 4.5 m, 3.9 m and a peak of 6.2 m, 5.2 m at Yankou and Lüsishayang stations respectively (Kang, 2015). In Xiaomiaohong channel, the spring tide can be twice as high than during neap tides (Chen, 2013).

The overall current patterns differ over the RSR, showing a more diffused pattern in the Southern Radial Sand Ridge (SRSR) system than the concentrated bidirectional flow in the Northern Radial Sand Ridge (NRSR) system. This results in multiple shallower channels at Tongzhou Bay, compared to Xiyang channel in the NRSR system (Xu et al., 2016; Kang, 2015). The tide is propagated through the channels, leading to higher velocities in the main tidal channels and lower over the shoals and nearshore areas. The mean velocities during flood and ebb current do not differ significantly, with magnitudes of $0.2 \sim 0.4$ m/s above the 0 m isobaths, $0.4 \sim 0.6$ m/s between -5 m and 0 m, $0.6 \sim 0.8$ m/s below the -5 m and $1.0 \sim 1.2$ m/s inside through of the channels (Chen, 2013).

As a results of tidal asymmetries and other processes, mean tidal fluxes occur during a tidal cycle (Xing et al., 2012; Xu et al., 2016). Figure 2.2 show the main tidal currents as found by (Zhang et al., 2013). In the northern RSR, the main tidal currents propagate through major tidal channels, such as the Xiyang channel towards the RSR field. Another flux bypasses the RSR and merges with the rotary system in the upper part of the SYS. As a result of the collision of the rotary tidal wave and the progressive tidal wave, smaller circulation develops at the RSR field. In the SRSR, the main current pattern consists of the merging of two fluxes. The first flux follows the Qidong coastline in south-north direction, which merges with the second flux that originates from offshore waters in a east-west direction. This mean flux continues in a south-north direction into Tongzhou Bay. A small scale circulation flux is formed due to the collision with the earlier mentioned

circulation pattern within the central RSR. These residual patterns are largely similar during either spring or neap. However, the overall strength of the two tidal systems is relatively weaker during neap tide and the point of convergence shifts towards the north-east (Zhang et al., 2013). Zhu and Chang (2001); Su et al. (2015) found that initial bathymetry, river discharges or tide-generated forcing do not have a governing effect on these large-scale tidal current patterns .

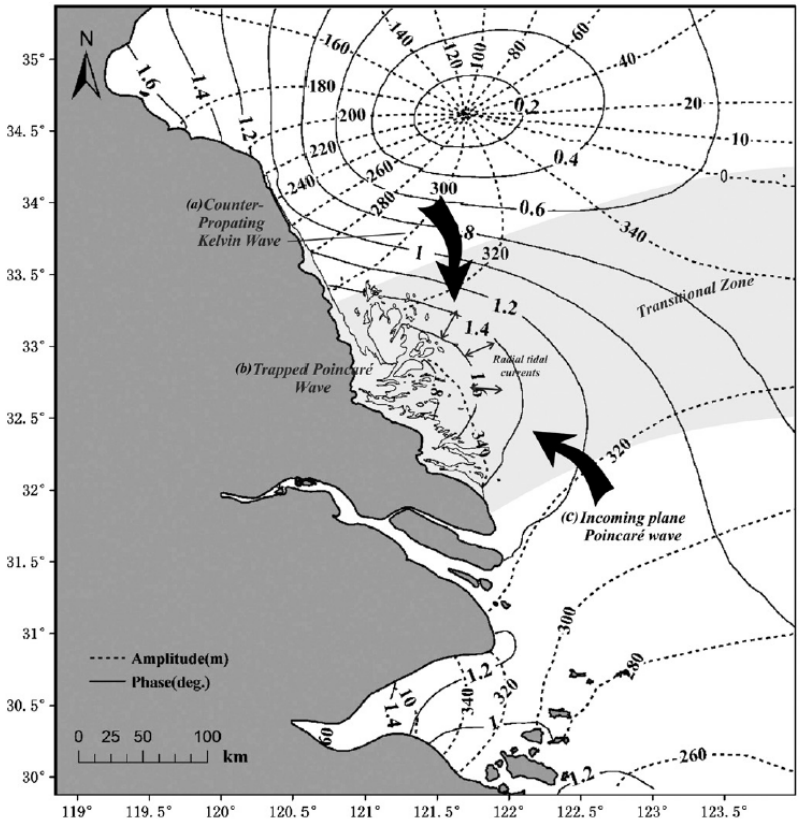

Figure 2.2: Large-scale tidal currents at the Jiangsu coast, with the rotary wave in the Yellow Sea and the progressive wave, coming from the East China Sea (from Xing et al. (2012))

2.2.2. Yangzte and minor river discharges

Several river discharges are present at the Jiangsu coast. These range from smaller agricultural drainage channels to larger natural river discharges. Southward of Tongzhou Bay is the Yangtze River Estuary. The discharge plume of the river is mainly directed southward and deposits mud and silt sediments alongshore, starting from the Yangtze River mouth down to the Taiwan strait Lee and Chough (1989). This is mainly caused by longshore coastal currents (*e.g.* the Min-Zhe Coastal Current (MZCC) and Jiangsu Coastal Current (JCC)) which are river-induced buoyant coastal currents (Deng et al., 2017; Liu et al., 2007).

Samples were taken in the Yangtze river plume and showed that suspended sediment concentrations in the lower estuary and adjacent coastal waters are decreasing. The small concentration that is measured mostly originates for local resuspension as it shows significant seasonality and coincides with semi-diurnal tides during neap and spring (Li et al., 2012; Liu et al., 2007). This means a coastal erosion of the Yangtze mouth which is closely related to trapping of upstream sediment due to the construction of the Three Gorges Dam (Deng et al., 2017). It is found that smaller river discharges are negligible on the tidal features nor does it create significant density differences (Yao, 2016)

2.2.3. Waves

Aside large episodic events such as typhoons, overall wave height is relatively calm at the Jiangsu coast. The wave field at the Yellow and East China Sea is generally consistent. However, nearshore wave action is stronger throughout the RSR system than in the upper Jiangsu coast (Chen et al., 2013). (Storm) waves and incidental events, such as typhoons have a significant role in the evolution of the RSR (Liu et al., 1989; Zhang et al.,

1999). Large typhoon waves that penetrate through the channels, however, experience heavy damping effects by the fine suspended particles or mud layer that is formed and reduce the wave height (Xu et al., 2015). The wind and wave field varies seasonally. In winter, surface waves with relative large wave height would be generated in southeast, due to the strong local wind forcing from the north and the corresponding large fetch. In summer, the wind speeds and wave height are the smallest (He and Xu, 2016; Liu et al., 1989; Zheng et al., 2014).

The yearly significant wave height at the southern Jiangsu coast and Tongzhou Bay is 1.1 m and mean wave period of 5.5 s in the East China Sea . The seasonal variation of the mean wave height is found 0.9~1 m in spring and summer, 1.0~1.3 m in autumn and 1.1~1.5 m in winter (Chen, 2013; Zheng et al., 2014). Further identification shows that 36.3% of single-peaked wind waves have a high occurrence in the SE, SSE and WNW directions. The rest are identified as young swells with high occurrence in the WNW, ESE to SSW directions (Yang et al., 2014).

At Tongzhou Bay, the wave pattern are more complicated due to the complex bathymetry and seasonal variation. Overall wave action is wind generated and has a significant wave height of $H_{1/3}$=0.15~2.2 m with a mean wave period varying between 2.06~6.82 s. These values are lower with respect to the average magnitude at the overall Jiangsu coast, due to shoaling effects and sheltering by the local ridges and channels (Yang et al., 2014).

2.3. Sediment characteristics

2.3.1. Bed composition

The sediments in the bed along the Jiangsu coast mainly consists of silt patches along the coastline (3.9~62.5 μm), sandy silt (also between 3.9~62.5 μm but with higher sand content), fine sand more offshore (125~250 μm) and patches of clayey silt originating from the Yangtze sub-aqueous delta (0.98~3.9 μm) (Liu et al., 1989; Wang and Ke, 1997; Zhu and Chang, 2000; Sun et al., 2014) (Table 2.1). The grain size diameter decreases from offshore towards nearshore zones. Furthermore, these offshore sediments are more sorted than sediments in the nearshore. This is due to fine sand particles, located at MLW have a higher chance to be reworked by waves and subsequently mixed over the watercolumn due to currents and is common for mudflats (Fan, 2012). Clayey silt or clay predominantly deposited near the MHW, where flow dominates, with the exception during storms. Overall, the tidal flats are narrower and composed of coarser sediments in the SRSR and wider and with finer sediments in the NRSR (Wang and Ke, 1997). These fines mainly originate from either the AYD for the NRSR or Yangtze sub-aqueous delta for the SRSR Lee and Chough (1989). The overall compositions over the whole RSR show an increase in average grainsize, signifying the depletion of fines and the supply from these deltaic zones towards the RSR (Wang et al., 2013). Figure 2.3 shows a tertiary diagram from bed samples taken during 2006~2007 at the AYD and the RSR (Wang et al., 2013). It can be seen that finer material is present at the AYD and the southern RSR and more coarse material in the central and northern RSR.

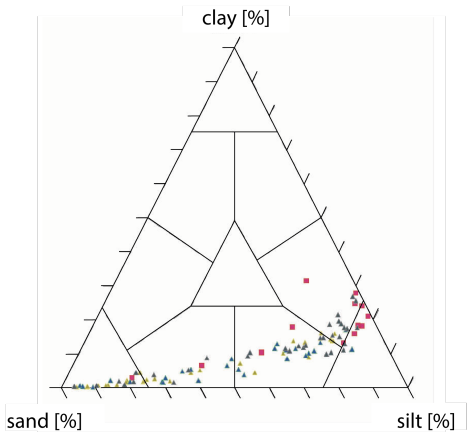

Figure 2.3: Tertairy diagram depicting the bed composition for seveal location at the Jiangsu coast, sampled during 2006~2007 (Wang et al., 2013). The red squares indicate samples, taken at the abandoned Yellow river Delta (AYD), yellow triangles the Northern Radial Sand Ridges, green triangles the Central Radial Sand Ridges and dark green triangles the Southern Radial Sand Ridges

Sediment type	Content			Mode(s)	Median grain diameter
	Sand	Silt	Clay		
Fine sand	70-90	10-20	<5	2-3ϕ ;single mode	62.5 - 250 μm
Sandy silt	30-40	>50	<10	4-5, 6-7 ϕ; single/double modes	62.5 - 125 μm
Silt	5-20	65-75	<10	4-5, 7-8 ϕ; single/double modes	16 - 39 μm
Clayey silt	5-10	>60	20-25	5-6, 8-9 ϕ; double modes	8 - 39 μm
Clay	<15	20-25	45-70	8-9, 4-5 ϕ; single/double	4 - 8 μm

Table 2.1: Dominant types of sediment found along the Jiangsu coast, from Wang and Ke (1997). Indicated is the sediment classification along with the characteristic modes and median grain diameter, with ϕ the Krumbein phi scale ($\phi = log_2 \cdot D/D_0$)

2.3.2. Suspended sediment and transport

The suspended sediment fluxes closely follow the residual tidal current fluxes. During spring, the tidal currents are stronger and a smaller circulation is formed at the convergence of the northern and southern flux. During neap tide, the current and transport energy is much lower, therefore the convergence shifts towards the north (Zhang et al., 2013). Tidal currents and transport capacity also vary seasonly, resulting in a larger suspended sediment concentrations during winter. (Xing et al., 2012). This is partly caused by stronger local wind waves, that have an important role in the resuspension of the fine sediment and the generation of wave-induced currents (Xu et al., 2014). This effect even more apparent in the northern RSR, which is a more open coast compared to southern region, which is more sheltered by shoals (Wang et al., 2011). Overall, it is found that the wind and wave-induced bed shear stress enhancement causes for more entrainment of sediments, which are subsequently mixed over the water column and transported by tidal currents and residual fluxes (Zhang et al., 2013; Zhu and Chang, 2000). Transport patterns may differ for the various sediment types found at the Jiangsu coast, based on their critical shear stress for entrainment (Zhu and Chang, 2000)

The nearshore topography and vegetation also have a significant effect on the transport of fines at the Jiangsu coast. The fine sediments particles (<±62.5 μm) behave differently during a tidal cycle and remain in suspension much longer then fine sand or silt. Together with the asymmetric tidal velocities during the ebb and flood flow, the suspended fine sediment is being transported depending on the dominant flow. This net transport per tidal cycle or lag effect causes fines to be transported in shallower regions, where the water depth and vegetation reduces the flow even more. These combined effects contribute to the sorting of sediment types and creation particular regions of fine sediment siltation (Gong et al., 2017; Hu et al., 2011; Su et al., 2017a; Wang et al., 2012b; Xing et al., 2012).

At Tongzhou Bay, the tide-averaged suspended sediment concentration is about 3 times higher than at the entrance of the Xiaomiaohong and Sanshahong channels, showing a gradual decrease Chen (2013). It was found that the main source of suspended sediment in the channel are stirred-up sediments by waves on the shoals and subsequently diffused into the channel by the currents. Little sediment is supplied from outside the channel (Chen, 2013). Net transport fluxes are mostly driven by local residual currents due to the discontinuous channels and ridges. Also net transport patterns into the channels occur due to non-instantaneous response in the transport of fine sediments (Xu et al., 2016)

2.4. Morphology

The morphologic development of the Jiangsu coastline is governed by the particular large-scale tidal currents and transport fluxes. After the shift of the Yellow river towards the Bohai Sea, the northern Jiangsu coast shows a trend of erosion, due to a lack of sediment supply (Cai et al., 2009; Su, 2016) (Figure 2.4). Over the last decades, these sediments are transported by the rotational tidal current towards the southern Jiangsu coast, such as the RSR system, Yangtze River delta or further offshoreHwang et al. (2014); Zhou et al. (2014). Typically, tidal flats with the abundance in sediment supply can steadily prolongate seaward maintaining a convex-up cross-shore profile (Fan, 2012; Liu et al., 2011). As a results, the RSR system is in an overall trend of accretion (Figure 2.4) (Li et al., 2001; Xing et al., 2012; Yao, 2016; Zhang et al., 2013; Gao et al., 2009). It was found that these large-scale currents and sufficient sediment supply are the driving forces in the creation of the typical sand ridge field at the Jiangsu coast and not so much on initial bottom topography (Zhu and Chang, 2000, 2001; Zhu and Chen, 2005). Other driving forces in the morphology of inter-tidal mudflats are longshore transport and net transport processes due to settling and scour lag effects and less on sediment supply (Shi and Chen, 1996; Gong et al., 2012).

The continuous erosion of AYD leads to the smoothing of the rotary tidal wave in the north and a south-

ward shift of the earlier mentioned convergence point of the two current patterns at the Jiangsu coast Chen and Wang (2009). This shift in the driving tidal currents results in an overall shift in transport and sediment supply of the whole RSR system. This causes the tidal channels and shoals in the RSR to steadily migrate southward (Chen et al., 2017; Gu et al., 2014; Ding et al., 2011). As such, a comparison of 40 years of bathymetric data showed deposition at the northside of the Xiaomiaohong channel and erosion at the southside, indicating the southward migration of channel Chen and Yu (2011). Similar southward migration is found at the Tiaozini shoal and the Xiyang and Lanshayang channel (Ding et al., 2011; Zou et al., 2006; You et al., 1998)

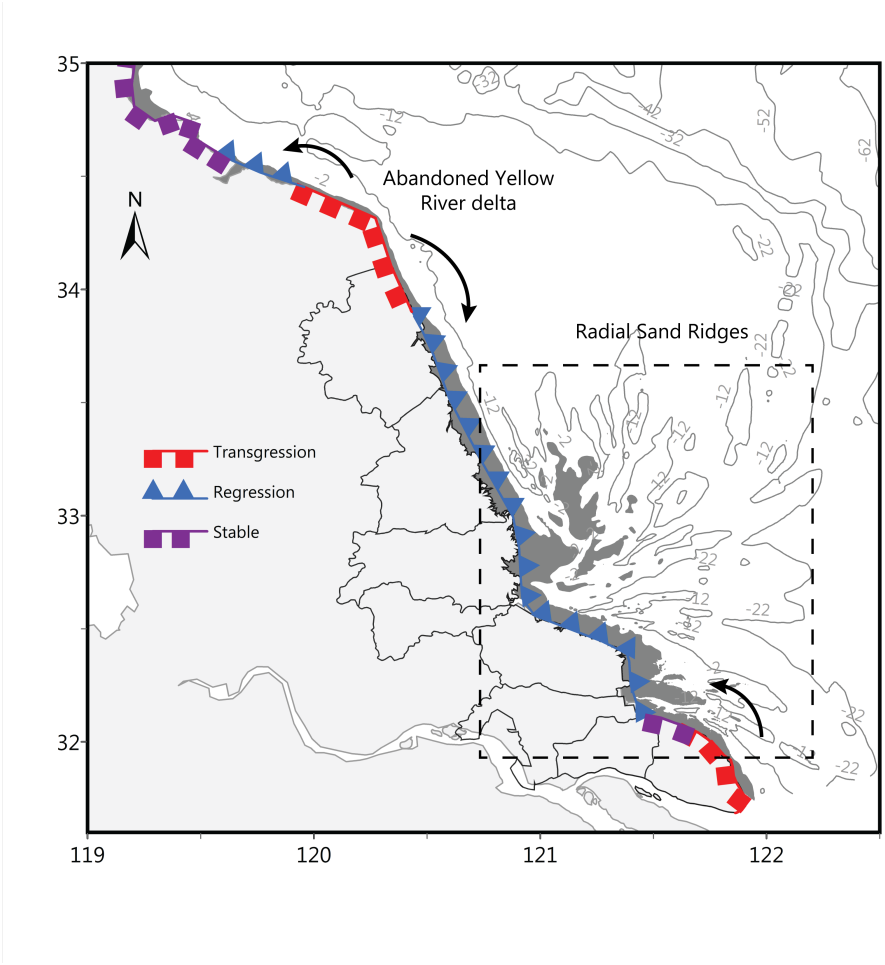

Figure 2.4: Long-term coastline changes along the Jiangsu Coast over the last decades, according to Li et al. (2014); Zhou et al. (2014); Liu et al. (2011)

2.5. Ecology and shorebird species

The Bohai and Yellow Sea coastal zones provides ecosystem services for a large variety of species and are therefore included in the UNESCO world heritage list (UNESCO World Heritage Centre, 2017). These coastlines form an essential part of the East Asia-Australian Flyway (Figure2.5)(Peng et al., 2017). The Jiangsu coast and Tongzhou Bay region is estimated to support at least 2.000.000 shorebirds or 40% of all migratory shorebirds in the flyway, during northward or southward migration and more than 30% of the estimated flyway breeding populations (Barter, 2002; Piersma et al., 2017). The majority of shorebirds use these regions as migration stop-over areas, depending on the season and species. However, smaller groups of species have also been sited during non-breeding seasons(Peng et al., 2017).

Different types of shorebird species can be classified based on habitat preferences. Important indications for preferred habitat is based on necessities such as nest building, breeding grounds and suitable forage areas. One of the most important habitat variables is the waterdepth and waterdepth fluctuations, as it limits the access to preferred food sources. The largest density and diversity of food sources in water is found at relative

Figure 2.5: Schematic view of the East Asian-Australasian Flyway with the Yellow Sea (yellow), from Piersma et al. (2017). Several migrations form northern regions of Russia and Alaska meet with stream from southern regions such as India, Australia and New Zealand

shallow waters and the most dominant bird type uses wadding or dabbling to find food. Suitable water depths ranges from 5 to >25 cm for small shorebirds to diving large species (Ma et al., 2010) (Figure 2.7). Other biotic and abiotic habitat variables to support various shorebird species was elaborated by Ma et al. (2010) and are stated in Table 2.2.

Over the inter tidal mudflats, different species can be divided based on their feeding modes. Some species are either bounded to the waterline (i.e. tide-followers), feed intensively at upper zones of the mudflat (i.e. zone specialists) or feed over the whole length of the intertidal flats (i.e. generalists). As such, these species vary in their dependency for certain region and have different vulnerabilities to environmental change Piersma et al. (2017). Figure2.8 gives a schematic view of the regional dependency of several shorebird species as found at the Yangkou foreshore at Rudong county Piersma et al. (2017)

Most species use higher elevated regions for nesting and roosting, often behind constructed seawalls. Other preferred nesting regions are on well-vegetated mudflatregions (Peng et al., 2017). Common species of vegetation at the Jiangsu coast are *Spartina antiflora* or Cord Grass and the more native *Phragmites Australis* and *Suaeda Salsa* (Sun et al., 2017). The ongoing reclamation activities and the invasive nature of *S. Antiflora* lead to a gradual degradation of the saltmarch diversity and the environmental quality (Sun et al., 2017; Wang and Zhu, 2006).

The exploitation of intertidal mudflats also leads to a large threat to the bird populations (Piersma et al., 2017; Peng et al., 2017). The past 50 years, these ecosystems have been reduced by 50% and are considered as endangered (Murray et al., 2015). Several shorebird species heavily depend on these mudlfat regions during migration, such as the Red Knots (*Calidris canutus*), Great Knots (*Calidris tenuirostris*) and Bar-tailed Godwits (*Limosa lapponica*). Due to this linked dependency on the Yellow Sea intertidal zones, the comparable decline in their population size can be directly linked on the exploitation of these zones (Piersma et al., 2017, 2016).

2.6. Tongzhou Bay Port

Recently, the coastal region of Jiangsu is promoted to be included in China's national development strategy (Zhang and Chen, 2011). Due to economic development in industry and export has led to a high demand in port capacity and land resources for economic development (Figure 2.9) (Cai et al., 2017). Over the last decades Jiangsu major national ports have show an rapid increase in turnover and overall volume, as shown in Figure 2.9 (Wang and Wall, 2010).

As part of the OBOR strategy, an essential part is infrastructure projects, such as port development and reorganization (Huo et al., 2018; Swaine, 2015). Nantong Binhai Park or Tongzhou Bay Port is part of the Nantong port group and is one of potential port development locations, in close cooperation with Shanghai port (China Daily, 2017; Nantong Port Group Co., Ltd., 2017). In December 2016, the "Tongzhou Bay Port Mas-

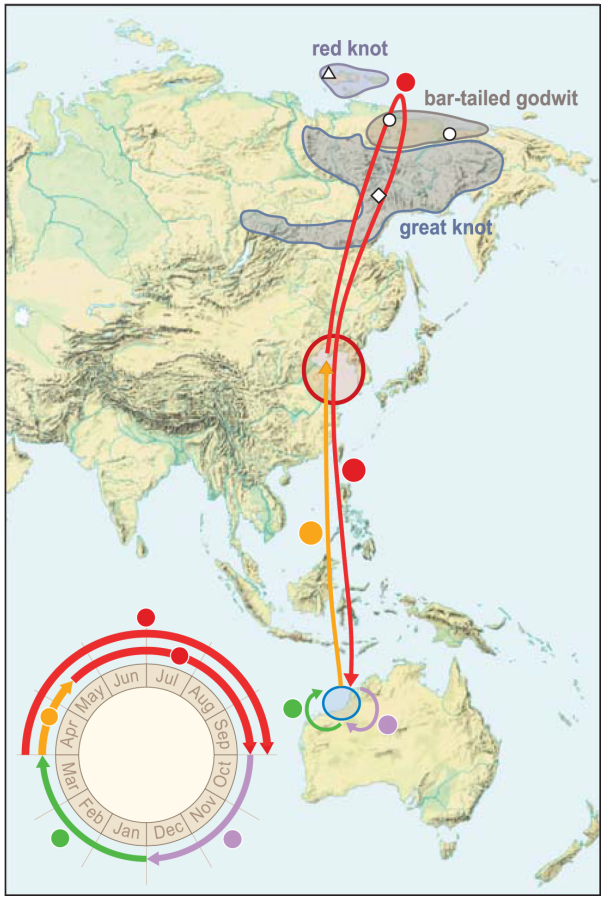

Figure 2.6: North and southward migration route for the Red-knot, Great knot and Bar-tailed Godwits, from Piersma et al. (2016)

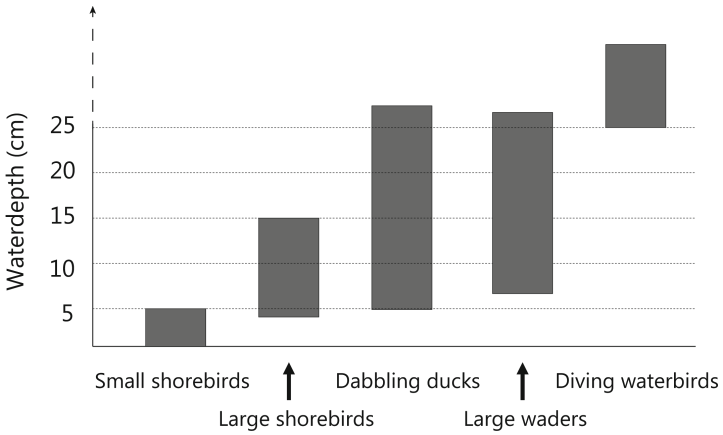

Figure 2.7: Preferred waterdepth fluctuations for different types of shorebirds, from Ma et al. (2010)

Habitat variable	Relevance
Water depth	Determines the accessibility of potential foraging habitats for shorebirds. Also availability of fish and pray may decline as locomotion of birds is higher in shallow water and therefore a higher net energy intake
Water level fluctuation	Fluctuations lead to spatio-temporal varying habitat. This provides more foraging opportunities and consequently supports a high richness of species and abundance of waterbirds. More stable water levels benefits the breeding by providing suitable nest sites.
Vegetation	Provides shelter, benefits nest building and food density and diversity. A higher vegetation cover increases species richness and abundance of waterbirds, especially during breeding periods. However, too much vegetation can limit the accessibility and adversely affect foraging. This depends on type of birds species.
Salinity	A high level of salinity affects the overall body weight due to dehydration, thermoregulation reduction of feathers, composition of aquatic plant communities, distribution of zoobenthos and aquatic animals and thus foraging sites.
Topography	Higher eleveated placesregions are preferable for resting, roosting, preening and even nesting. Combination of variable topography with suitable water depths creates diverse habitats which is accessable for multiple water birds species.
Food types	Understanding food resources in wetlands is important for determining the potential carrying capacity of the wetlands for waterbirds. Food can vary per species and season.
Wetland size	Increases the probability for a wetlands to have a high habitat heterogeneity. Larger wetlands can support area-dependent and independent species. However, the accessibility of a habitat is more important then the actual size of the wetland.
Connection to other wetlands	Connected wetlands to other larger habitat areas can support waterbirds more efficient. Foraging by traveling is more effective than remaining is a single one and this connectivity improves exchange and movement of aquatic animals and plants, thus increasing potential food.

Table 2.2: Governing habitat variables for shorebird species and smaller species Ma et al. (2010)

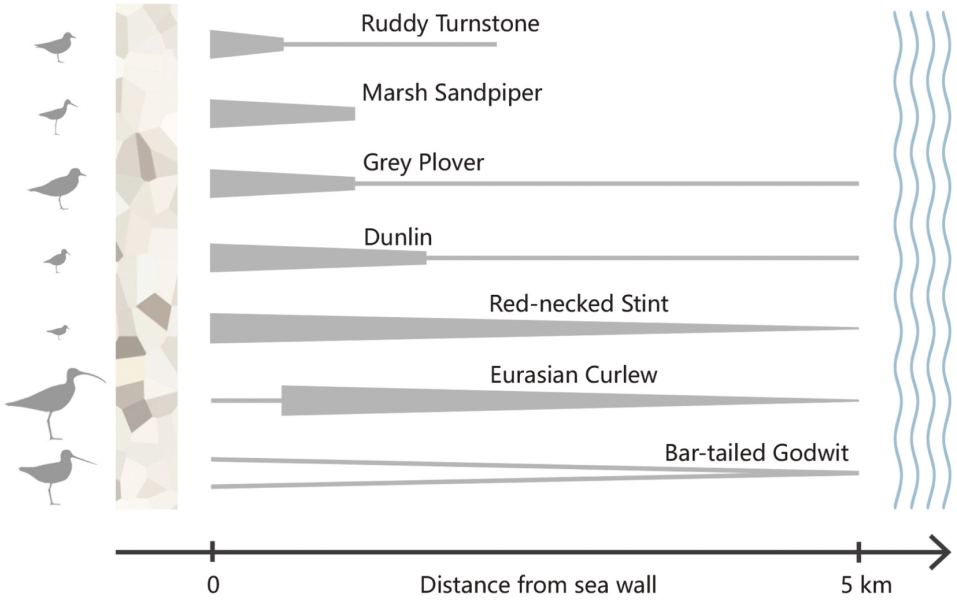

Figure 2.8: Schematic view of the feeding shorebirds species and distribution on the Jiangsu intertidal mudflats, from Piersma et al. (2017)

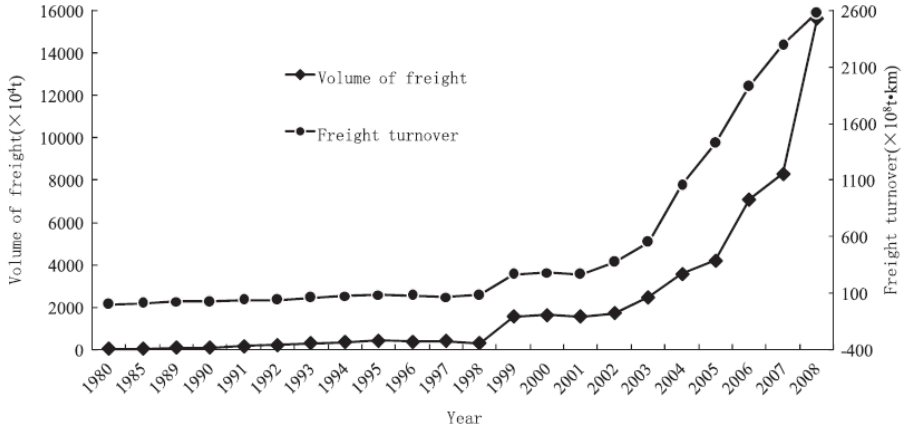

Figure 2.9: Rapid increase in turnover and total freight volume for Jiangsu coastal ports from Wang and Wall (2010)

ter Plan" was formally approved by the Ministry of Transport and the Provincial Government (Encyclopedia, 2018). Within this plan, the overall layout and capabilities of the Tongzhou Bay port was layout. Together with the existing Lusishayang and Yankou deep sea ports, the Tongzhou Bay port is designed under the vision of "One Core, Two Wings" (一体两翼). This consists the complete reclamation of the Yaosha shaol and developed into port and coastal industry, with a total area of 100 square kilometers. These port developments would provide for 10 berths on the north and south sides with a projected capacity of 50,000 to 100,000 tons by 2020, achieving 6-8 million tons of port throughput.

The next phase contained the area around the Lengjiasha, with an area of 185 km^2 from 2021 to 2030, including 300 tons of terminals. In 2030, Lengjiasha will have 75 quay berths of 50,000 to 100,000 tons and achieved a 120 million tons port throughput. This also includes the further deepening of the tidal channels to a 300,000-ton waterway. The natural depth of the SSH channel is comparable to XMH, and it has the prospect of developing a waterway of 100,000 to 150,000 tons. Nantong Port Authority (2013); Huang et al. (2015)

The Tongzhou Bay Port is mainly designed for the creation of an industrial port for petrochemical, fossil fuels, bulk and container terminals. Furthermore, the port should function as a transportation hub with the hinterland and inland shipping and setup close relation with Nantong and Shanghai ports (China Daily, 2017). This should further develop port related industries on the mainland and should also promote (eco)tourism, such as cruise and a marine.

At the time of writing, two basins of the original port have been constructed according to the first phase of the reclamation and makes up for 11.3 km^2 (Huang and Zhang, 2017). Due to constraints of economic development and ecological impact on mudflat ecosystems, further construction was halted until the full impact is clear (China Daily, 2018; Xinhua News Agency, 2018; BirdLife International, 2018).

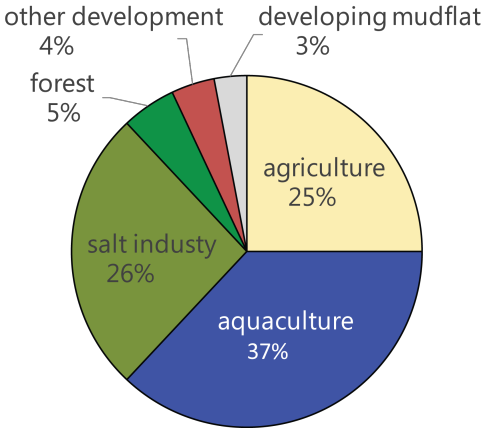

Figure 2.10: Exploitation purposes of reclaimed mudflat areas at the Jiangsu coast, adapted from Wang and Wall (2010)

3

Methods

In order to investigate the tidal currents and transport patterns, a previously developed and well calibrated numerical model of the Jiangsu coast was made available and further developed for the Tongzhou Bay region. The outcome of the model used for the quantitative description of the types of ecosystems. In this chapter, this model, the set-up and validation methods are described, as well as the method for quantitative describing the occurrence of ecosystems using the models output.

3.1. Numerical model

In order to test several hydro,- and morphodynamic processes at the Tongzhou Bay and simulate the effect of different port configurations, use will be made of the open-source numerical model Delft3D, developed by Deltares (Deltares, 2018)

The Delft3D model consists of several modules which can be coupled, which describe flow, transport, morphodynamics, water quality and other phenomena. The flow is calculated with Delft3D-FLOW by solving the Reynolds-averaged Navier-Stokes equations, under the shallow water and the Boussinesq assumption. It does this on a staggered grid by a finite difference scheme for a 2D (depth-averaged) or 3D environment.

The total sediment transport is divided in bed and suspended transport mode, based on the reference height as proposed by van Rijn (1993). The sediment transport is calculated by the transport formula as proposed by (van Rijn, 2007a,b,c). Here, the sediment transport is divided in bed and suspended load based on the introduced reference height z_a (van Rijn, 1993) and is determined at each half time step with input from the flow calculations. The bedload transport (below the reference height) is assumed to react instantaneous with the flow. The suspended sediment transport is defined as the transport above the reference height. In this setup it is calculated by solving the two dimensional, averaged over the vertical (2DH) diffusion-advection equation. By taking samples and performing flume experiments, Yao et al. (2015) suggests using multiple fractions in calculating sediment transport for silt-sand mixtures such as the Jiangsu coast. Therefore, the total suspended transport consist of solving the diffusion-advection equation for each fraction separately and finally summation of all these transports. Additionally, Yao et al. (2015) found that the conventional sediment transport formulations, as described by van Rijn (2007a,b), underestimated the sediment concentrations and overall transport for sand-silt enriched mixtures, typical for the Jiangsu coast. As such, they recalibrated these sediment transport formulations to extend it for the silt range of 8 μm to < 250 μm and implementing them within Delft3D-FLOW module. For further elaboration on these modified transport formulations, the reader is directed to Yao et al. (2015); Yao (2016).

In this study, the model is extended with an extra cohesive fraction. As such, an additional set of transport formulations were used for the calculation of the exchange between the bed and the watercolumn, as proposed by (Partheniades, 1965). More on this additional fraction and application the transport formula in Section C.2. The bedlevel change is calculated at each corresponding time step, according to the sediment mass balance. This morphological update of the bed can be accelerated by several methods. More on this in section 3.2.1.

The current processes that are resolved by the model are identical to the setup as suggested by Yao (2016). These include flocculation effects of finer fractions (*e.g.* grain size < 40 μm); hindered settling effects for all fractions; effects of the cohesion and packing density of fresh deposits on the critical bed shear stress for a

median grain size of the mixed sediment bed smaller than 62 μm; cohesion effects on the critical bed shear stress for a median grain size of the mixed sediment bed larger than 62 μm; hiding and exposure effects on the adjustment of the critical bed shear stress of each fraction when the median grain size of the mixed sediment bed is larger than 40 μm; stratification effects (turbulence damping through eddy viscosity of flow) in case of a high sediment concentration; bed slope effects on the critical bed shear stress and the bed-load transport. For cohesive fractions, the sediment mixing is not enhanced by waves. Only the critical bed shear stress is enhanced due to the interaction between waves and flow, according to (Fredsøe, 1984) as described by Yao (2016).

3.2. Model Set-up

3.2.1. General Tongzhou Bay Model configuration

Domain and coupling To simulate the governing tidal processes and transport with an acceptable level of accuracy, a multi-nested model approach is adopted and further developed in this thesis. The overall tidal currents, were successfully modeled by a large-scale hydrodynamic model that encompasses the entire Bohai, Yellow and East China Sea (Su et al., 2015). Subsequently, the model results on tidal propagation were used as hydrodynamic boundary conditions for a stand-alone model of the Jiangsu coast (Su et al., 2017b,a; Yao, 2016). This Jiangsu Regional Model (JRM), encompasses the entire Jiangsu coast, having its boundaries just north of the Yangtze river mouth up to the Shandong peninsula. The model uses a computational grid of 573 by 346 gridcells with a resolution varying form 608 ~ 1216 m. The model was made available for this thesis and is able to simulate the hydrodynamic processes with higher resolution as well as sediment transport and morphodynamic processes.

In order to simulate the flow and transport with a higher resolution at the Tongzhou Bay region, a smaller finer domain was 'online' nested within the JRM with use of the Domain Decomposition (DD) approach (Deltares, 2018), which means a constant feedback of the base and sub-domain. Due to the expected boundary inconsistencies from the complex shoal-channel topography and the concentrated tidal currents, preference to this DD approach was given instead of more conventional nesting. Due to this 'online' set-up, the boundaries of this smaller model were required to be defined along the existing grid lines of the JRM, to form a square outcrop at Tongzhou as shown in Figure 3.1. The Tongzhou Bay Model (TBM) covers the Yaosha-Lengjiasha ridges as well as the more nearshore areas of Lusishayang and Rudong. The computational grid consists of 269 by 468 gridcells with a resolution varying from 287 ~ 397 m. This grid size refinement corresponds to 3 : 1 compared to the JRM computational gird. The northern boundary is set around the Lanshayang channel, south of the Tiaozini shoal. Reason for this is retaining a relative compact model domain and reduce the amount of inconsistencies along the in- and outgoing constituents along the boundary. The southern boundary is set close to the original calibrated boundary of at the Yangtze river mouth. Generally, sufficient computational domain is provided in order to correctly simulate incoming constituents. Unfortunately, the southern boundary of the JRM computational domain is relatively close to the Tongzhou Bay region.

Bathymetry The Tongzhou model bathymetry is based on the bathymetry from the JRM. This bathymetry is compiled from measurements taken at the Radial Sand Ridge system during 2006 (Zhang and Ed., 2012) and Electronic Navigational Charts published by the Navigation Guarantee Department of the Chinese Navy Headquarters (Yao, 2016). During the calibration phase, the JRM bathymetry was updated with higher resolution bathymetric data of the Tongzhou Bay domain, which was surveyed during October 2010. The local refinement led to a more up-to-date bathymetry with the situation of 2012. Preliminary results showed an increased in accuracy of the TBM in reproducing water levels and current velocities and was adopted for further simulations (see section C.2). The difference between the old and new bathymetry is shown in Figure 3.2. Significant change can be observed from a deepening of several meters of the main tidal channels and heightening somewhat smaller rates at the intertidal shoals. These changes could be due to bedlevel changes during the period 2006-2010 and higher sample resolution of the 2010 bathymetric data.

Boundary conditions The TBM computational grid is defined as an outcrop of the JRM grid and is 'online' coupled at its three open borders, as shown in Figure 3.1. At these boundaries, the models exchange information including the waterlevel, current velocities and sediment concentrations with morphological timestep of 2 minutes by means of the domain decomposition approach (Deltares, 2018). This means that the TBM

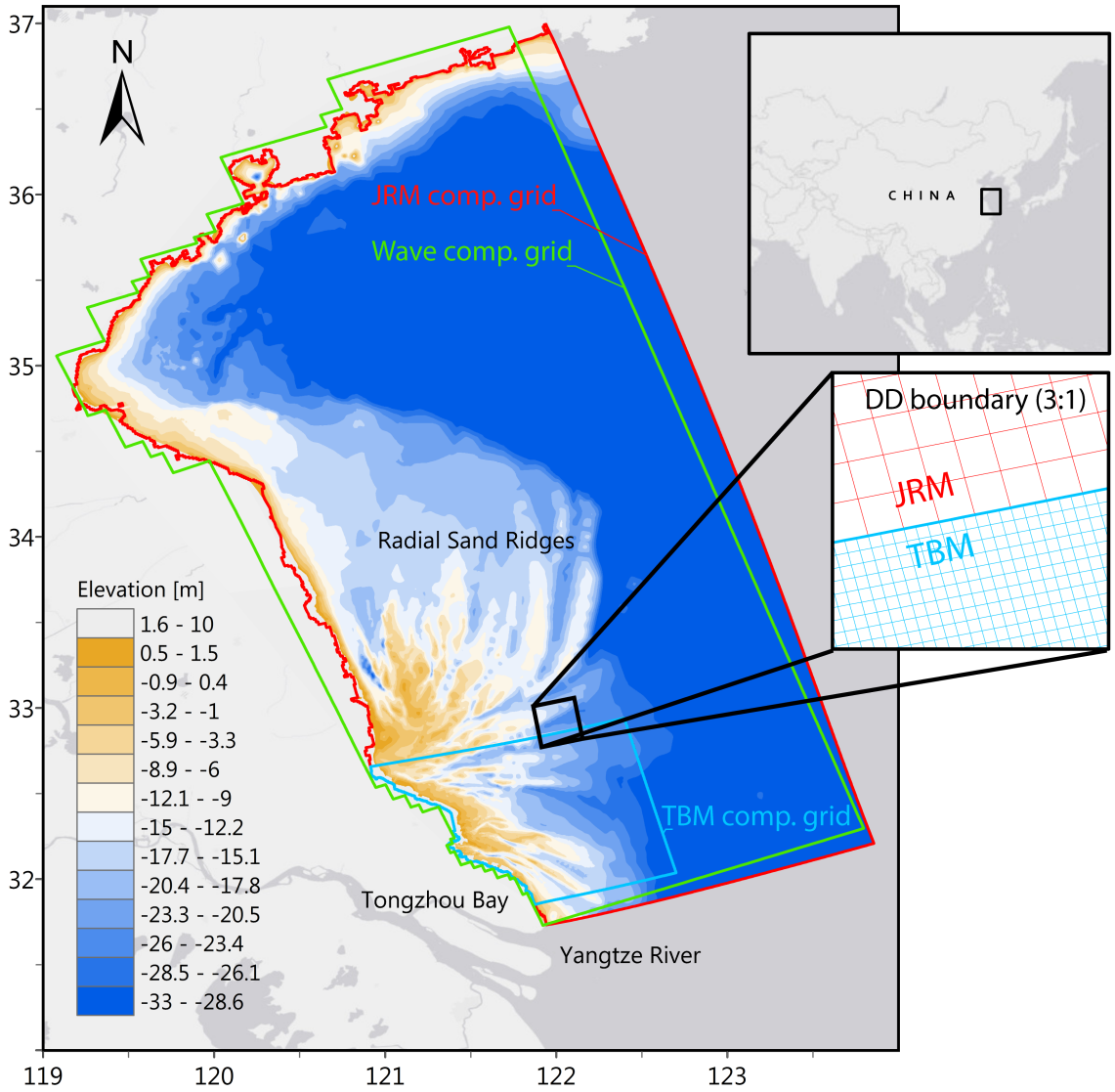

Figure 3.1: Computational domains of the Jiangsu Regional Model (red), Tongzhou Bay Model (blue) and wave computational grid (green). A close-up of the grid domain shows the coupling and different resolutions between the two 'online' coupled grids of the JRM and TBM.

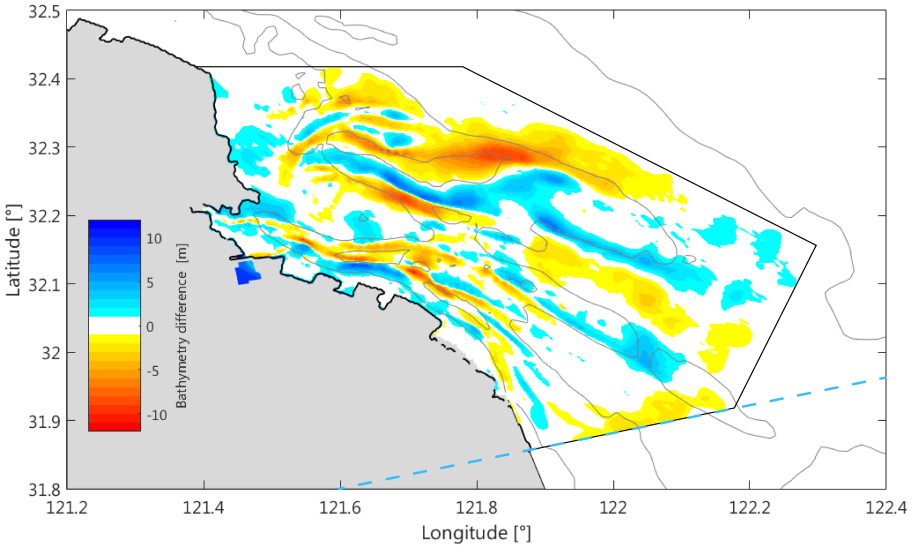

Figure 3.2: Difference between JRM bathymetry based on 2006 and more recent retreived bathymetry in the TBM for 2010 situation. Black circumference indicates the domain of the new bathymetric data. The area overlaps and is cut by the Tongzhou Bay Model domain, indicated with the blue dashed line.

does not require specific defined boundary conditions as it provided by the JRM at each new timestep. As such, the set boundary conditions at the JRM will be discussed.

The waterlevel, as calculated by the JRM is driven by a series of astronomical tides at its two open boundaries (Yao, 2016). These were derived from a set of 13 tidal harmonic components (i.e. M2, S2, K2, N2, K1, O1, P1, Q1, M4, MS4, MN4, MF, MM) from a large-scale tidal wave model for the Bohai, Yellow and East China Sea (Su et al., 2015). These components consisted of a full morphological year time-series with a 10 minute output interval. This model also included the influence by the discharge of Yangtze river, which is situated just south of the JRM domain in the waterlevel boundary conditions (Su et al., 2015; Yao, 2016).

Sediments found at the Jiangsu coast ranges from fine sand to silt, as shown by measurements taken at the Tiaozini shoal by Yao et al. (2015). In order to model the sediment dynamics over such mixed beds, they proposed a multi-fractional approach in which the bed consists of multiple sediment fractions and the transport is calculated separately for each fraction. As such, the JRM was set-up with 4 representative sediment fractions including 16, 45, 90 and 180 μm resembling fine silt, silt, very fine sand and fine sand respectively. The initial Tongzhou Bay Model was set-up with these same sediment fractions as defined in the JRM with inclusion of an additional cohesive sediment fraction, which will be further explained in section 3.2.2

At the two open boundaries, the JRM is supplied by a constant sediment concentration. Yao (2016) argues the incoming sediment concentrations from offshore are relatively small and defines a constant concentration for the 16 μm fraction of 5 mg/L at its eastern boundary. As mentioned earlier, the southern boundary is under the influence of the Yangtze river discharge and sediment flux. Previous studies found that most of the sediment is transported southward with the Min-Zhe Coastal Current and deposited along the East China Sea coast (Deng et al., 2017; Liu et al., 2007; Wang et al., 2007). With the lack of a clear value for the sediment flux at the southern boundary of the JRM, Yao (2016) performed a sensitivity analysis for different values corresponding to different seasonal discharges. They found that due to the lack of northward transport pattens, the Yangtze-derived sediment from the southern boundary is negligible. Furthermore, they found that the morphologies calculated by the JRM are independent on the set SSC at the open boundaries and can be regarded as a quasi-closed coastal system. As such, the southern boundary of the JRM is set with a linear decreasing concentration of 300 mg/L for the 16 μm fraction at the nearshore zone (from shore to a water depth of 30 m) to 15 mg/L at the offshore end. No further boundary concentrations were set for the other fractions.

Waves The role of waves in the entrainment of fine sediment at the Jiangsu coast is a topic that has been treated in numerous studies at the Jiangsu coast. Several studies suggest the influence of wind, waves and river discharges are minor on overall suspended concentrations and transport the Jiangsu coast (Xing et al.,

2012). On the other hand, a strong enhancement in the local bedshear stresses was measured due to the wave-current interactions along the Jiangsu coast with respect to bedshearstresses induced by tides only (Wang et al., 2006). As a result, more sediments are resuspended and transported by the tidal currents (Zhang et al., 1999). For instance, large turbitiy maxima were measured along the Jiangsu coast, which were closely linked to surface wave action (Wang et al., 2011). However, the effect of waves vary, both spatially and temporally.

Therefore, the effect of waves is further elaborated during calibration of the additional cohesive sediment fraction. Preliminary results show that the combination of wind-induced waves with an additional fraction gives the best estimation of suspended sediment concentrations during both neap and spring tide (see Section C.4). However, it is argued that long-term morphology of the Jiangsu coast and Tongzhou bay is mainly driven by tidal patterns (Zhang et al., 1999). Furthermore, due to computational limitations, the effect wind-induced waves will not be further included in the simulation of alternative reclamation scenarios.

Salinity Aside some small drainage channels and the Yangtze River discharge being deflected towards the south, no large fresh water discharges are present at Tongzhou Bay (Li et al., 2012). With the lack of fresh water sources, the overall region can be regarded as a brackisch/salt regime. Measurements obtained at 14 mooring stations at Tongzhou Bay during a 2012 campaign show confirming values, with a mean value of 30.74 ppt and relative small fluctuations (see appendix A) (CCCC Third Harbor Consultants Co. Ltd, 2012). As such, both the JRM and the TBM are setup with a constant salinity of 30 ppt.

Tidal forcing, secondary flow The JRM includes tidal forcing from the tidal constituents. This forcing is deemed to only have significant effect on larger scales. Since the TBM focuses on the nearshore region of Tonghzou Bay, tidal forcing is not included. Due to the complex combination of shoals and channels in a relative small region, secondary flow effects play a significant role in sediment transport. When tidal flow in side the channels is higher than at the shallow ridges, a velocity gradient is created along the channel's cross-section. This generates a secondary circulation, which is important for sediment transport (Lu and Dou, 2011). As such, the secondary flow is included in the JRM and TBM.

Morphological scale factor The morphological change at each time step was multiplied by a morphological acceleration factor (Roelvink, 2006), to increase the bedlevel changes and thereby efficiently model long-term morphology. However, this approximation of the long-term bedlevel update introduces spatially and magnitude errors, which could lead to unrealistic siltation and erosion patterns. Furthermore, by multiplying the local morphological change, the net effect of large-scale fine sediment fluxes are not represented correctly, as these react non-instantaneous to flow and occur over longer timescales. To maintain small inconsistencies in modeling the morphodynamics in Xiyang channel (*e.g.* 9 years), Gong et al. (2012) suggested *morfac* = 1. Su et al. (2017a) performed a hindcast on the evolution of the Jiangsu coast as a whole over longer timescales (*e.g.* 300 years) and found satisfying results with *morfac* = 108. In the development of the JRM, Yao (2016) argues the difficulty of using a morphological acceleration factor in combination with multiple sediment fractions. Judging from previous modeling setups and corresponding timescales, it is uncertain if applying a morphological accelerations factor to allow for the efficient modeling of Tongzhou Bay morphologic development (*e.g.* 8 years) will show satisfying results.

In order to obtain an indication of the effect of applying *morfac*, a verification case was defined. The model was setup to hindcast the bedlevel changes as result of the most recent constructed reclamations at Tongzhou Bay. This consisted main reclamation of around 11.3km^2 at the center of the Yaosha shoal and a connecting elevated construction road with the main land (Huang and Zhang, 2017). The reclamation activities started around 2013 and took approximately 4 years to complete (Figure 3.3). The model was set-up to run from 8 January to 8 March 2014 with an acceleration factor of *morfac* = 24, thereby effectively modeling 4 years of morphological development. Topographic data of the Yaosha shoal was surveyed for January 2018 with satellite altimetry. These datasets were made available (Kang, 2017) and together with visual observations (see Appendix B), will be used to verify the modeled morphodynamic development. The verification results will be further elaborated in section 4.1.3

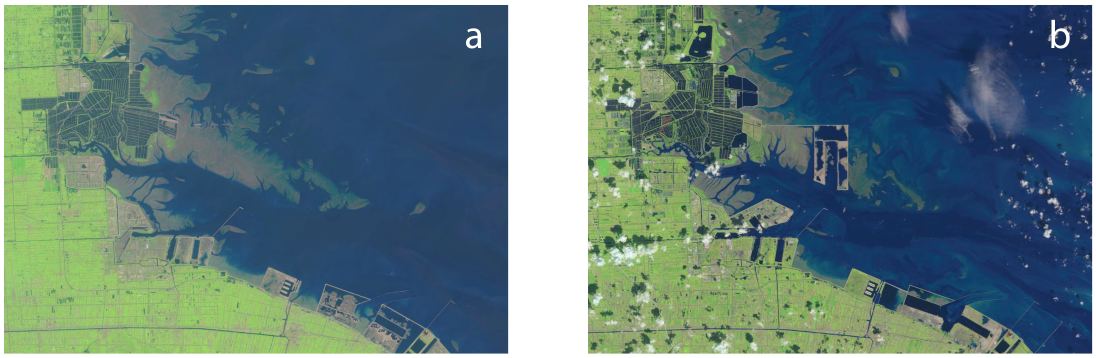

Figure 3.3: Satellite images of reclamation extend at Tongzhou Bay. Images were retrieved on 29-Aug-2013 before construction (a) and 28-Sep-2018 showing the current situation (b) (USGS, 2018)

3.2.2. Suspended sediment concentration calibration

From the data analysis, it became clear that an even finer fraction in the suspended matter was measured at Tongzhou Bay (see Appendix A). Further, during preliminary simulations, the computed depth-averaged SSC, did not show a strong dependency on the local flow velocities. This is especially the case during neap tide when the tidal velocities are low *e.g.* <0.5 m/s, suggesting the observed SSC is made up of more easily suspended fines (see section C.1). Previous studies measured 'soft' surface layers or fluid mud at similar locations along the Jiangsu coast (*e.g.* Dongsha shoal and Nanhui mudflats). It was found that this material is resuspended at relatively lower bedshear stresses with respect to the material in more drained sub-surface layers (Shi et al., 2016; Zhu et al., 2014).

Additionally, windspeeds and directions were measured at the 14 mooring stations as well (CCCC Third Harbor Consultants Co. Ltd, 2012). Measurements showed averaged windspeeds of 2 m/s during spring tide and increased to a maximum of 9 m/s during neap conditions. These strong winds suggest the presence of wind-induced waves, especially during neap tide. The effect of wave action could have a significant role in the resuspension of fines and increase in overall sediment concentrations (Wang et al., 2006; Zhang et al., 1999).

Additional cohesive fraction case Preliminary simulations were carried out to identify the effect of an additional cohesive fraction, wave-action or the combination of the two on overall sediment concentrations and agreement wit measured concentrations.

The modified sediment formulations, as described in section 3.1, includes the flocculation of pseudo-cohesive material in the effective fall velocity per fraction, with a minimum flocsize of 16 μm. This limits the possibility of including fractions smaller than 16 μm with the above mentioned transport formula. Therefore, the smaller fraction was modeled by use of the well known transport formula for cohesive sediments, as described by (Partheniades, 1965), which are included in the Delft3D model. The final sediment parameters of the additional cohesive fraction are shown in Table 3.1. According to Shi et al. (2016), corresponding bed shear stresses for fluid mud layers at the Jiangsu coast, is $\tau_{ce} = 0.18\ N/m^2$ for the uppermost 0.02 m of sediment and 0.29 N/m^2 for the subsurface layers. Yang et al. (2016) even proposes 0.11 N/m^2 for bedsurfaces at lower depths, offshore of Tongzhou Bay. In this study, the critical bed shear stress for erosion or resuspension is set to 0.2 N/m^2. Other parameters, such as the settling velocity, w_s and erosion parameter, M are determined by means of several sensitivity analyses during the calibration phase. The full calibration process is further elaborated in Appendix C.

At open coasts with fine sediments, high concentrations are mostly situated in nearshore and remain bounded to the coastline through spatio-temporal large-scale processes, such as longshore residual currents, baroclinic circulations and other 3D patterns. Wang et al. (2011) compared remote sensing data with a large scale 3D hydrodynamic circulation model updated with 3D sediment transport and found similar nearshore concentrations. The JRM and TBM does not incorporate these depth-varying processes, nor is it explicitly setup with residual currents, beside tidal non-linearities due to bathymetry. To achieve similar nearshore concentrations, the fine sediment is supplied by carefully determined boundary conditions.

The southern boundary of the test model and TBM is situated just north of the Yangtze estuary. Mea-

Specific density	2.65E+03	kg/m^3
Settling velocity	1.00E-04	m/s
Critical bed shear stress for sedimentation	1.00E+03	N/m^2
Critical bed shear stress for erosion	2.00E-01	N/m^2
Erosion parameter	4.00E-03	$kg/m^2/s$
Dry bed density	3.00E+02	kg/m^3

Table 3.1: Final calibrated sediment properties for the additional cohesive sediment fraction

surements at the southern Jiangsu coast and ECS have shown that the nearshore suspended sediment concentrations are influenced by Yangtze discharge and sediment transport (Li et al., 2012; Liu et al., 2007). This suspended material mainly consist of clayey-silt, and silty-clay with a "quasi-bimodal" grain-size distribution of 6-9 ϕ (Liu et al., 2006). Yao (2016) included the Yangtze-derived SSC, by defining a varying concentration along the southern boundary for the 16 μm fraction, defining a nearshore concentration of 300 mg/L which linearly declines to 15 mg/L at the offshore end of the boundary. A similar approach was adopted for the southern boundary concentrations of the newly added cohesive fraction.

The TBM boundaries were coupled with the JRM and therefore boundary conditions need to be set at the JRM boundaries. Since, we are mainly interested in the dynamics inside the TBM, a initial condition of 200 mg/L for the cohesive fraction was set over the whole JRM domain. The eastern boundary of the JRM was set at relatively low concentrations, as no significant fluxes of fines are present at offshore depths. The southern boundary of the JRM is extended with a linear decreasing concentration of 300 mg/L nearshore and the same 15 mg/L at the offshore end of the boundary. Finally, by observing the sediment concentration in the domain after 6 months of morphological time of solely described boundary conditions, an initial concentration of 200 mg/L throughout the TBM domain for the cohesive fraction was chosen to speed up the simulation duration. For a full elaboration on these values, the reader is directed to section C.2.

Waves inclusion case The effect of waves were included by means 'online' coupling of the numerical model Delft3D-WAVE with the Delft3D-FLOW module (Deltares, 2014). Wave calculations were made on a separate computational grid, as shown in Figure 3.1. It consists of 139 x 238 gridcells with a resolution of 836 ~ 4.212 m. The grid was enclosed by one landboundary at the Jiangsu coast and two open boundaries. The wave and hydrodynamic model exchange information, such as water depth and current velocity with a timestep of 20 min. Wave-current interactions on the bedshear stresses are calculated as described by (Fredsøe, 1984).

Due to the lack of clear wave data at the Jiangsu domain, wave conditions consisted of the combination of incoming waves at the offshore boundary and local wind-induced waves. The incoming wave condition at the eastern offshore boundary was defined as a single wave condition with a mean significant waveheight of $H_s = 1.1m$ and a peak wave period of $T_p = 8s$, as found in previous studies Chen et al. (2013); Yang et al. (2014). Further, a spreading of 10 and normal incident wavedirection was assumed. Data analysis showed that the wind velocity, v_{wind} and phase did not differ significantly over the 14 measuring locations (see section A.2.2). As such, a spatially constant wind timeseries was assumed over the whole computational domain. Missing data between measuring periods were linearly extrapolated with a minimum of 2 m/s

Preliminary results Figure 3.4 shows the modeled preliminary results for station N7, which is located inside the Sanshahong channel. This includes the measured windspeeds and calculated wave heights, current velocities and direction and calculated sediment concentration for the initial model setup, inclusion of an additional fine fraction and the inclusion of waves with this fraction. The inclusion of a fine cohesive fraction increases overall sediment concentration and shows better match with measured concentrations. The carefully selected sediment parameters lead to a very easily entrain fraction that remains in suspension during lower current velocities. The role of waves lead to an additional increase of concentration during periods of strong wind velocities. Main contribution to this higher sediment concentration is from the cohesive and 16 μm fraction and is several order smaller for the larger fractions (*e.g.* 45, 90 and 180 μm). In case of the combination of an additional cohesive fraction and waves, the restuls show an even better approximation of the measured values. Wind-induced waves lead to an increased entrainment of the cohesive fraction and 16 μm fraction. However, the model is setup with a simplified bed composition. Significant peaks in sediment concentration could also be caused by a higher local availability of certain fractions. From these results, the influence of waves, especially during low current velocity at neap tide, can be significant. Together with the

inclusion of a cohesive fraction, similar concentrations could be predicted with respect to the measured values. However, in order to apply the model for the testing of further port reclamation in an efficient manner, the influence the added cohesive fraction is given priority and waves are not included within the model setup.

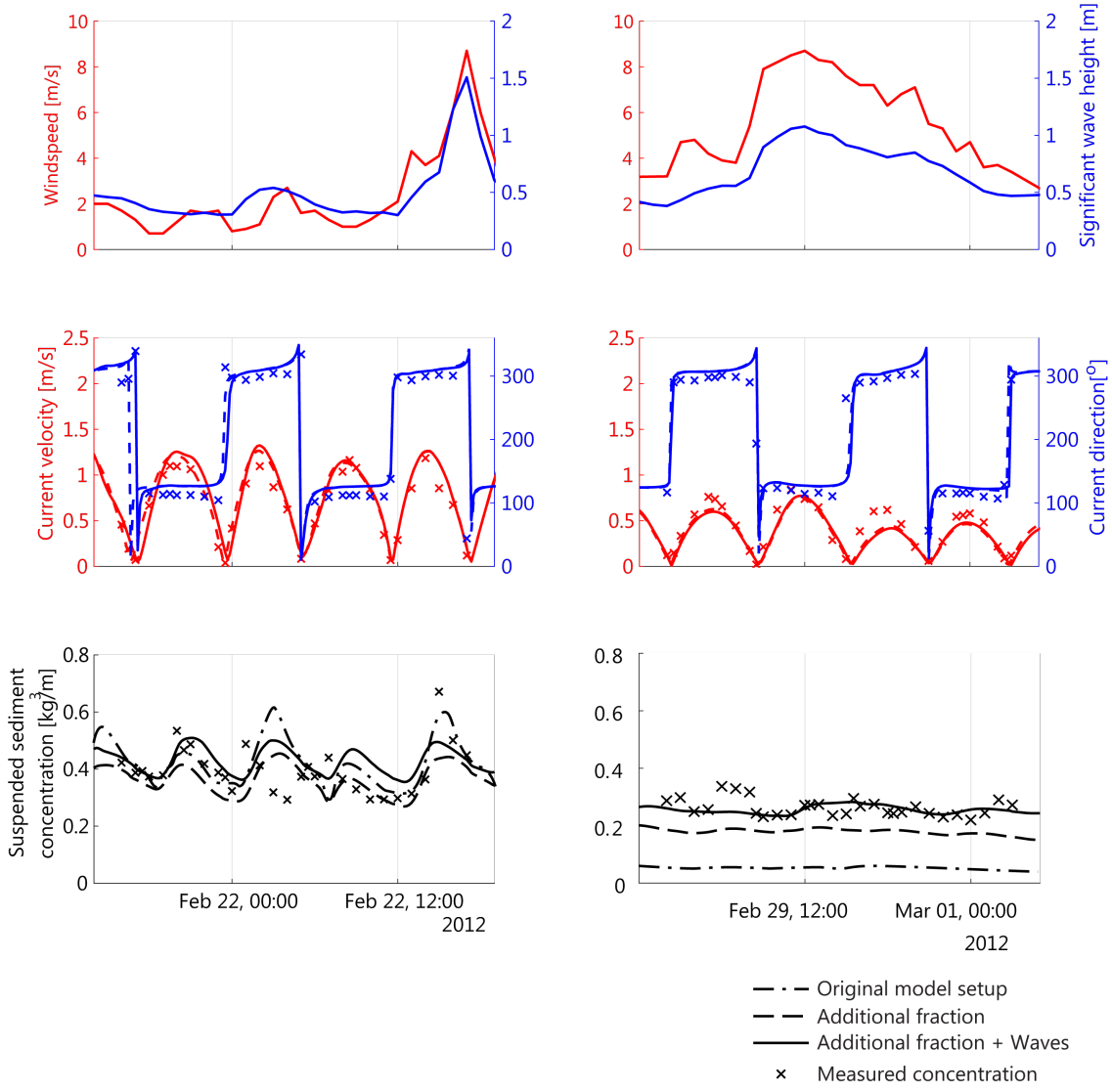

Figure 3.4: Calculated and measured quantities at station N7. Top panels show the measured wind-speeds and calculated waveheights form the model. The middle panels show the influence of waves on current velocities and direction, which is very small. Bottom panels show the overall sediment concentration for the initial model setup (−.−), the inclusion of an additional cohesive fraction (−−) and the combined effect of wind-induced waves (−).

3.2.3. Bedcomposition

The bed of the TBM is composed of the 5 sediment fractions (*e.g.* 16, 45, 90, 180 μm and a cohesive fraction (see Section 3.2.2))). Initially, a spatially varying bed composition from the JRM was adopted, which was compiled from bed surface samples from earlier studies (Yao, 2016). The TBM was further updated with more recent bed surface samples obtained in 2012 at Tongzhou Bay (CCCC Third Harbor Consultants Co. Ltd, 2012), (see section A). Preliminary tests of both old and new bed compositions showed significant spatially differences in calculated suspended sediment concentration. This made it difficult to decisively analyze differences in the suspended sediment concentration due to the total amount of varieties governing the sediment concentration and transport. Therefore, a simplified bed composition was compiled in which each

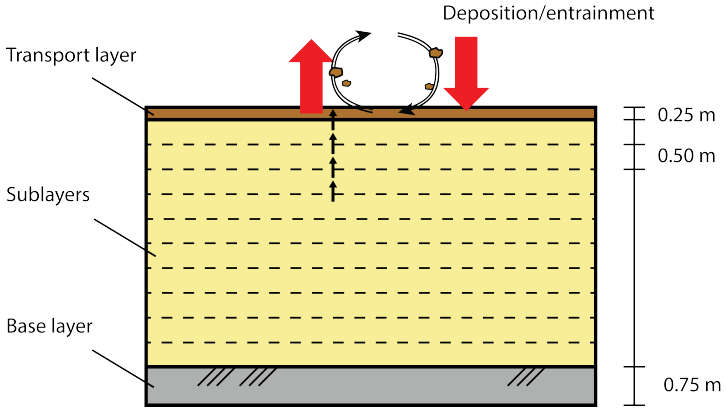

Figure 3.5: Schematic depiction of the bed stratigraphy as defined in the TBM

fraction makes up 25% of the total bed layer. In order to provide sufficient material of the added cohesive fraction, a sensitivity analysis was performed into the thickness of the cohesive fraction layer. This showed that an initial thickness of 0.02 m over the whole TBM domain gave acceptable results (see section C.2). This thickness was subtracted from the 180 fraction, giving it a final thickness of 1.48 m.

The bed stratigraphy of the TBM was structured similar to the JRM, consisting of a vertical homogeneous active layer with a thickness of 6 m. This layer consisted of a transport layer of 0.25 m, which is constantly active by sedimentation and erosion. A total of 10 sublayers are defined, each with a thickness of 0.5 m and will become active once the layer above requires more material (*e.g.* erosion). Below this is a base layer of 0.75 m. Additional simulations confirmed this thickness to be sufficient for continuous erosion during a simulation of 3 morphologic years (Yao, 2016)

3.3. Model validation methods

The performance of the model is validated through qualitative and quantitative assessments between the calculated and measured values at several monitoring locations at Tongzhou bay. This approach is similar to verification methods as used by Yao (2016) and makes it possible to quantitatively compare the two models performance.

The qualitative assessment of the model consist of the visual comparison of the calculated and measured values through time series plots. These relative short-term measurements were retrieved during spring-neap tidal conditions at 14 mooring stations and 6 tidal gauges at Tongzhou bay (see Appendix A) (CCCC Third Harbor Consultants Co. Ltd, 2012). The quantitative assessment compares the calculated and measured values through statistical quantities. For the case of coupled hydrodynamic-ecosystem models, (Allen et al., 2007) suggest the use of the Nash-Sutcliffe Model Efficiency coefficient, ME (Nash and Sutcliffe, 1970) and the bias expressed in percentages, PB. Similar as applied in Yao (2016), both parameters include the effect of measurements errors in the definition. The model efficiency coefficient is the ratio of the variance in the calculated values and the measured ones. It quantifies if the modeled values vary more or less with the measured values and is a measure how accurate the model predictions are relative to the mean of the observed data. Including the effect of a possible error in the measurements, the definition is as follows:

$$ME = 1 - \frac{\Sigma(|m-p| - \Delta m)^2}{\Sigma(m-\bar{m})^2} \tag{3.1}$$

where m is the measured value; p is the predicted or calculated value by the model; $\bar{m}$ is the mean measured value; δm is the error in the measurements. The absolute value between the measured and calculated value minus the error in the measured value, cannot be negative. In that case, the whole term becomes zero. The value of ME are classified based on the performance the model represent. This classes ranges from: excellent ($ME > 0.65$), very good ($0.5 > ME > 0.65$), good ($0.2 > ME > 0.5$) and poor ($ME < 0.2$).

The bias of the model is an overall error relative to the expected values and is expressed in percentages. Including the error margin, the definition is as follows:

$$PB = \frac{\Sigma[(m-p) \pm \Delta m]}{\Sigma m} * 100 \tag{3.2}$$

where the numerator can either be $(m-p)-\Delta m$ in case of $(m-p)<0$ and $(m-p)+\Delta m$ if $(m-p)>0$. The absolute value of the percentage bias are also classified in four classes: excellent ($|PB|<10\%$), very good ($20\%<|PB|<20\%$), good ($20\%<|PB|<40\%$) and poor ($|PB|>40\%$).

3.4. Ecotope classification method

The goal of this study is to asses the impact of different reclamation strategies on the ecosystem at Tongzhou Bay. In order to couple the results of the model with potential occurrence of species habitat, use will be made of an ecotope map. An ecotope is the smallest spatial landscape unit in which relative homogeneous biotic and abiotic features are present. An ecotope map is often used as a tool in determining maintenance and development policies for natural habitats (Bouma et al., 2005) The usage of an ecotope map allows to quantify the possible occurrence and changes in ecological value for a certain ecosystem.

3.4.1. ZES.1 methode

In order to quantify certain ecotopes in the Tongzhou Bay system, use will be made of the ZES.1 method, as described by Bouma et al. (2005). This method is part of a system of characterizations of open waters in the Netherlands (*RijksWateren Ecotopen Stelsels (RWES)* in Dutch), in which the ZES.1 specifically looks at saline ecosystems. The method is a tool to outline the potential occurrence of certain habitat based on abiotic features.

By selecting relevant abiotic features and defining certain classes and corresponding boundaries, individual regions can be determined which describe relative homogeneous characteristics and therefore the occurrence of a certain habitat. This classification is based on the dominance of certain processes on the occurrence of a habitat and regarding the quality and availability of required data. Combining these regions into a map gives an overview of the location and types of habitats that could occur within a open water system.

It has to be noted that this method only describes a potential niche for the possibility of occurrence of a certain habitat. Therefore, the method does not describe what habitat could be found in reality. Ecotope maps should be validated with specific locally retrieved data if said habitat truly occurs. Generally, the data is retrieved from measurements or other existing charts. Additionally, data simulated by hydrodynamic models can be used, such as flow velocities and salinity (Ysebaert et al., 2016). However, the performance and error of the model will have an impact on the maps validity. It is assumed that the ZES.1 salt water classification method is also applicable to the Jiangsu open coast.

3.4.2. Feature classes and class bounds

Feature classes are hierarchically ordered on the influence each class has on the occurrence of certain habitat. As such, the most dominant processes are treated first during classification of ecotopes. The ZES.1 describes multiple feature classes. In this study, the following feature classes for Tongzhou Bay will be determined in similar order:

1. Salinity and salinity variance.
2. Substrate 1 (hard, soft)
3. Depth 1 (sublittoral, littoral or supralittoral zone)
4. Hydrodynamic conditions
5. Depth 2 (subdivision of the littoral zone, dryfall duration)

Salinity and salinity variance The ecological effect of salinity is the most determining feature, as species that occur in salt environments cannot prevail in fresh water ecosystem and vice versa. The magnitude and variance in salinity occurs due to fresh water discharges into salt seawater. This process of mixing of the two different water densities varies seasonly, as during higher rainfall and therefore discharge. At the Jiangsu coast, several agricultural rivers outflow at the Jiangsu coast. However, this effect is small and is often not included in hydrodynamic modeling studies (Tao et al., 2011; Yao, 2016; Su et al., 2015). Also the influence of the Yangtze river is confined to the estuary mouth. Salinity measurement taken at several mooringstations in 2012 (CCCC Third Harbor Consultants Co. Ltd, 2012) show an average salinity of 31 ppt with small derivation in more shallow regions. Therefore, it is assumed that the spatio-temporal variance is small throughout Tongzhou Bay region.

Hard of soft substrate Ecologically, hard or soft substrate describes the possibility if the area provides a 2D or 3D habitat. Species living at hard regions such as pebble coasts or gravel shores are confined to a 2D habitat, unable to access the soil. At mudflats or sandy beaches, shelter and food can be provided not just on the surface but also within the bedsoil. The Jiangsu coast does not contain any natural hard or rock formation coasts and is mostly fine sand or silty. Therefore this feature class is also deemed constant at the Tongzhou domain and is set as soft.

Depth 1 The class is divided into sublittoral (permanently inundated), littoral (inundated during every tide) or supralittoral zone (sporadic inundated due to spring tide or storm events). This division is based on potential foodsources and the difference in foraging techinques by differt types of species within an ecosystem. For instance, shore birds prefer deeper tidal channels for foraging and the higher elevated mudflats to brood (Bouma et al., 2005; Ma et al., 2010). The class bounds are based on the averaged water levels during a tidal cycle. Sublittoral zone is defined as the area that is still inundated during low water at springtide ($d < MLWS$), with d the local water depth. The littoral zone is defined as the inundated area between low water at springtide and mean high water during neaptide ($MLWS < d < MHWN$). The supralittoral zone is the area above mean high water during neap tide ($d > MHWN$). The depth classification can be further sub-divided. However, the dominance of local hydrodynamics play a more important role.

Hydrodynamic conditions The hydrodynamic conditions have a governing effect on the occurrence of certain habitat. In case of soft substrate systems, during high dynamic conditions, species need use more energy to remaining on the bed or have to move further into the soil. During low dynamic conditions, flora and fauna can develop with more ease and increases brood and foraging areas. However, hydrodynamics also have an indirect effect on species. Due to the low velocities and fluxes, mixing and the supply of new food will decline, especially if the local population density is high. High dynamic conditions can cause a higher sediment transport, which indirectly has a negative effect on the growth and availability of food. According to the ZES.1 method for soft regions, the assessment of the hydrodynamic feature should be done based on the maximum linear flow velocity during an averaged spring tide and the maximum orbital velocity, due to prevailing waves (Bouma et al., 2005). In this study, the effect of waves and orbital velocities near the bed are assumed small and the classification will only be based on the maximum linear flow velocities. The classification is based on high or low hydrodynamic conditions. Threshold value for this classification is set on the theoretical/physical value of $0.8 m/s$. This value is suggested by multiple studies on the occurrence of large sand dunes on the bed or mayor bed adaptations at the Dutch Waddensee and Westernscheldt (Bouma et al., 2005).

Depth 2 The littoral zones can be further divided into shallow or deeper depth subclasses. The Tongzhou Bay region mainly classifies as shallow conditions with a depth up to $d < 20m$. Therefore, only the sublittoral is further classified into shallow and deep sublittoral zones. The benchmark between shallow and deep sublittoral zones is described as 5 m below mean low water during spring tide (*e.g.* $d = MLWS - 5m$) Ysebaert et al. (2016). The littoral zone can be further classified based on the dryfall time during a tidal cycle. The inundation period plays an important role in the availability of shelter and the amount of time species can forage. Some species which live in the bed cannot survive if some areas have not been inundated sufficiently long enough. The class bounds are set on 25% and 75% of a tidal cycle, indicating high, mid and low littoral (*e.g.* $t_{dryfall} > 75\%, 25\% > t_{dryfall} > 75\%$ and $t_{dryfall} < 25\%$ respectively). These bounds are based on biomass data measured at the Westernscheldt and other saline open water systems in the Netherlands (Bouma et al., 2005).

Final sub-feature, described by the ZES.1, is the inundation frequency during a full year. However, in this study only model simulations of several months of morphological time are considered and is therefore not included.

The ZES.1 method also prescribes the inclusion of certain eco-elements, which are areas that deflect from the normal feature classes and allow for alternative habitat at that location Bouma et al. (2005). Examples are sea grass fields, oyster reefs, shipwrecks etc. For deriving an ecotope map for the Tongzhou Bay region, these eco-elements are not included. Full overview of the defined feature classes and corresponding class boundaries are shown in Figure3.6. The applied color scale

Finally, these features can be visualized by a spatially varying map. By combining these features following the hierarchical structure, a final ecotope map can be created (Figure 3.7). In this study only littoral and hydrodynamic classification will be made. Figure3.6 also shows the assigned color for each ecotope, as will be used in the full ecotope maps.

Salinity					low varying salinity		
Substrate					soft substrate		
Hydrodynamics			>0.8 m/s; <0.8 m/s		high		low
Depth	Supralittoral						
	Littoral	Dryfall	>60 %	High-range			
			>25 %	Mid-range			
			>4 %	Low-range			
	Sublittoral		<MLWS-5m	Shallow			
			<MLWS-5m	Deep			

Figure 3.6: Overview of ecotope classification and corresponding color scales

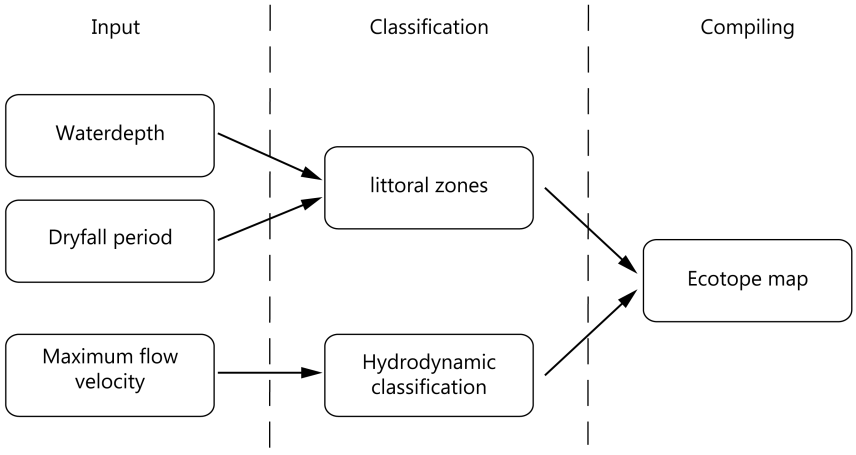

Figure 3.7: Schematic view of the procedure of creating an ecomap. Input comes from resutls as calculated by the model

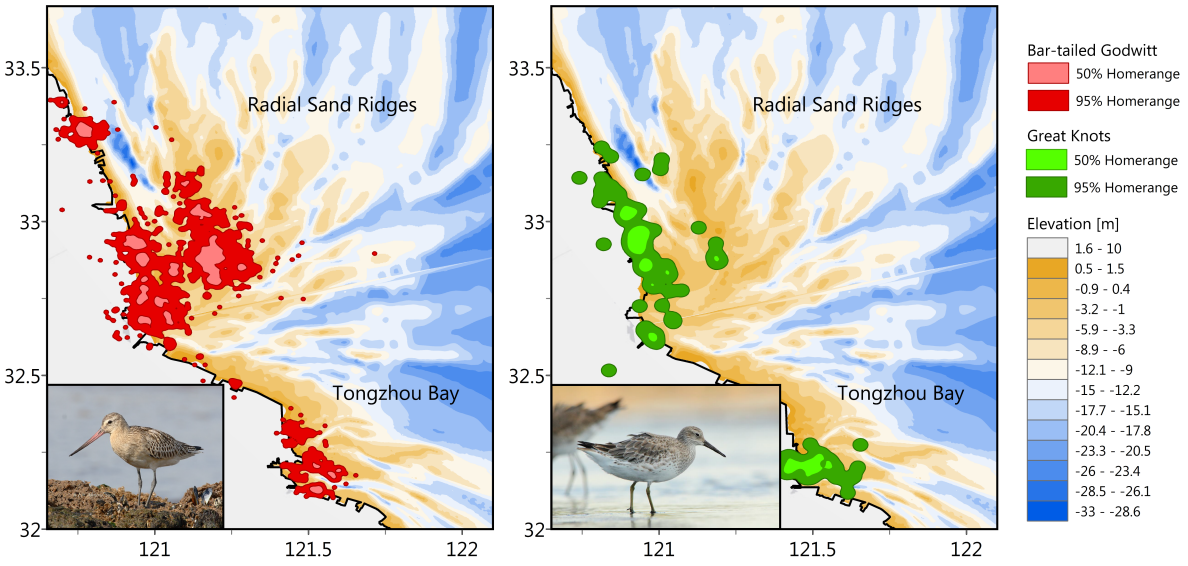

Figure 3.8: Homerange of two migratory bird species: Bar-tailed Godwit and Great Knots. Data was collected by satellite tracking from May 2015 to September 2017. Data is retrieved and made available by Chan et al. (2018).

3.4.3. Ecotope verification

An ecotope map shows the possible occurrence of certain habitat, based on abiotic features. However, these maps require to be validated in order to check whether certain habitat truly occur in reality. This can be done with multiple siting data from the field, such as floral and faunal species within the ecosystem. For this study, the validation will be done with siting data of two migratory bird species, namely the Bar-Tailed Godwit and the Great Knot . These species are part of approximately 30 other shorebird species that reside at the Jiangsu coast and serve as a first indication of the habitat preferences of all these shorebirds (Peng et al., 2017; Piersma et al., 2017; Barter, 2002). This data was acquired through tagging and satellite-tracking of several specimens during May 2015 to September 2017. Figure 3.8 show the corresponding home-range of these two species at the Jiangsu coast. The great knot show the largest density of homerange more closer to the coast. The Bar-tailed Godwit shows an overall larger homerange, covering large part of the intertidal mudflats at Dongsha as well. This corresponds well with the overall understanding of these species preferences, with the BTG being classified as a 'tide-followers' and GK preferring higher mudflat areas (Piersma et al., 2017).

4

Model results

In order to obtain confidence in the ability of the model to represents the flow and transport characteristics at Tongzhou Bay, the model results will be visual and statistical validated. A selection of relevant validated model results are then further elaborated. A morphologic development of 8 years is simulated. These model results are further used to create an ecotopemap of the initial and predicted state of Tongzhou Bay following the ZES.1 classification method. In this stage, no further reclamation or anthropogenic impacts are included, thereby serving as a reference case for further testing of alternative scenarios in the following chapter.

4.1. Model performance

4.1.1. Visual validation

The final model setup, as described in section 3.2 is verified with short-term measurements during spring (22 to 23 February 2012) and neap tide (29 February to 1 March 2012) at 14 mooring stations and 6 tidal gauges (Figure 2.1). The predicted water levels are validated separately from the current velocities and suspended sediment concentrations, as the measured data from the 6 mooring stations differ in location and sample frequency.

Figure 4.1 shows the predicted and measured water levels at three tidal gauges, namely Lengjiasha (LJS), Sanshahong (SSH) and Xiaomiaohong (XMH). These are located at the LJS shoal and the upper reaches of the SSH and XMH tidal channels, respectively. Predicted water levels show a good conformation with measured values, with a slight under prediction at high water during both spring and neap tides. This disagreement could be caused by inaccuracy in the bathymetry, since the model is set-up with data retrieved during October 2010 instead of the 2012 measurements. Also grid resolution could play a role. The phase of rising and lowering tide seems to be reproduced quite well.

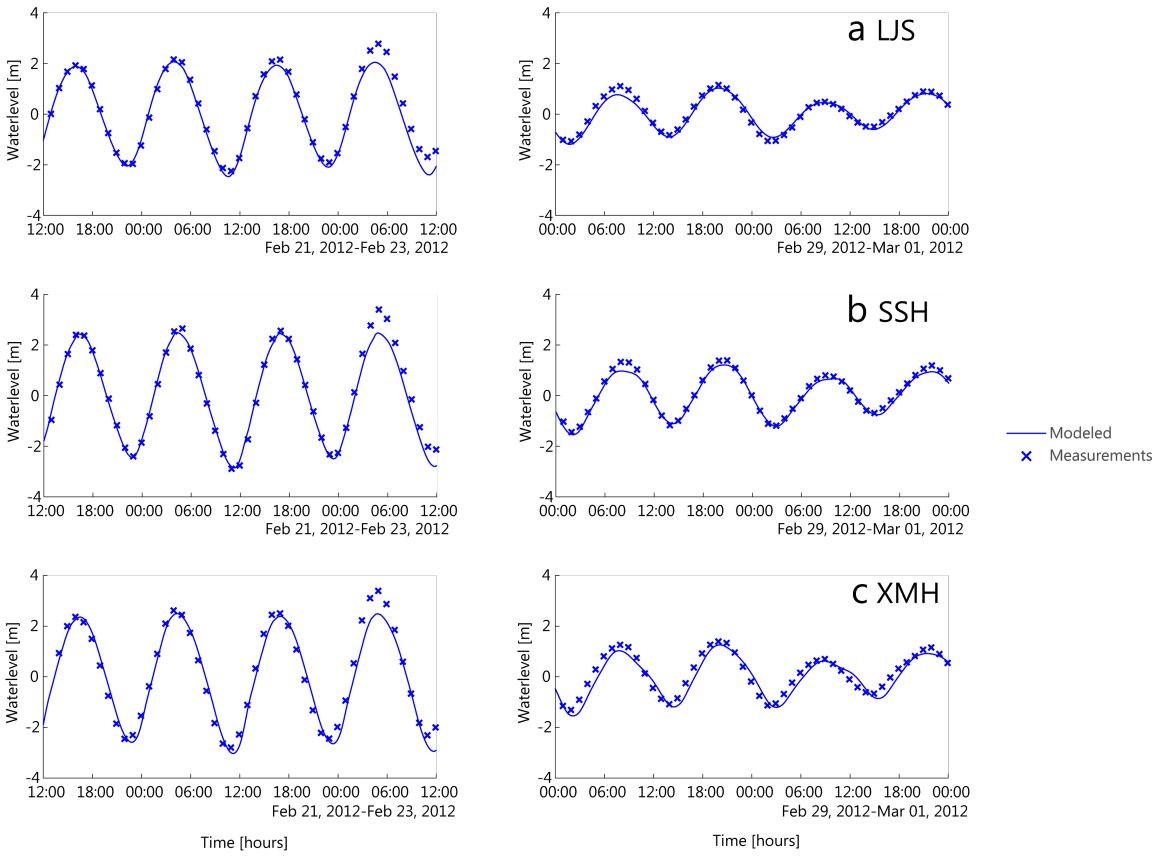

Figure 4.1: Calculated and measured waterlevels at Lengjiasha shoal (a), Sanshahong channel (b) and Xiaomiaohong channel (c)

Figure 4.2 shows the calculated and measured current velocities and directions and the suspended sediment concentrations at three different stations. These stations are located up the Xiaomiaohong channel (N1), at the entrance of the Sanshahong channel (N7) and at shallower waters at the Lengjiasha shoal (N10). The calculated current velocity and directions, generally approximate the measurements quite well. During springtide, the overall peak velocities range between $1 \sim 1.5\ m/s$. The model shows some slightly higher peak velocities during flood tide compared to ebb. This peak flow asymmetry suggest a flood dominant regime inside the channels. This is important for overall transport of fines, as stronger fluxes during flood will gradually move fines up the channel. During neap tide, peak velocities are lower and range from $0.5 \sim 1\ m/s$. The model shows an underestimation of $\pm\ 0.1\ m/s$ at several monitoring locations. This could be caused by the mentioned inaccuracy in bathymetry of the model and is most apparent for more shallow stations. The calculated phase of flow reversal during flood and ebb tide coincide with the measured patterns. The calculated current direction also shows a confirming results compared to the measurements with small deviations

The calculated suspended sediment concentrations are shown separately for each fraction and with the summation of all the fractions. Overall, the model shows similar trends in the development of the concentrations over time as the measurements. However, both during spring and neap conditions, the actual concentration can be over or under predicted, within $100 \sim 200\ mg/L$. The calculated and measured concentrations all show a concentration during both spring and neap tide of more or less $300\ mg/L$. Previous studies including measurement and numerical modeling, suggest similar concentrations at southern RSR and Tongzhou Bay (Chen, 2013; Yao, 2016; Xu et al., 2016; Xing et al., 2012). Both the calculated and measured concentrations show a less dynamic and slightly declining trend during neap tide. A closer examination of the concentrations of each fraction show that the 16 μm fraction show a higher dependency on flow conditions compared to the added cohesive fraction. Similar behavior can be observed from the measurements. However, during neap tide, the 16 μm fraction and coarser fractions are not entrained. The calculated cohesive fraction concentration remains in suspension and makes up most part of the total concentration. Compared

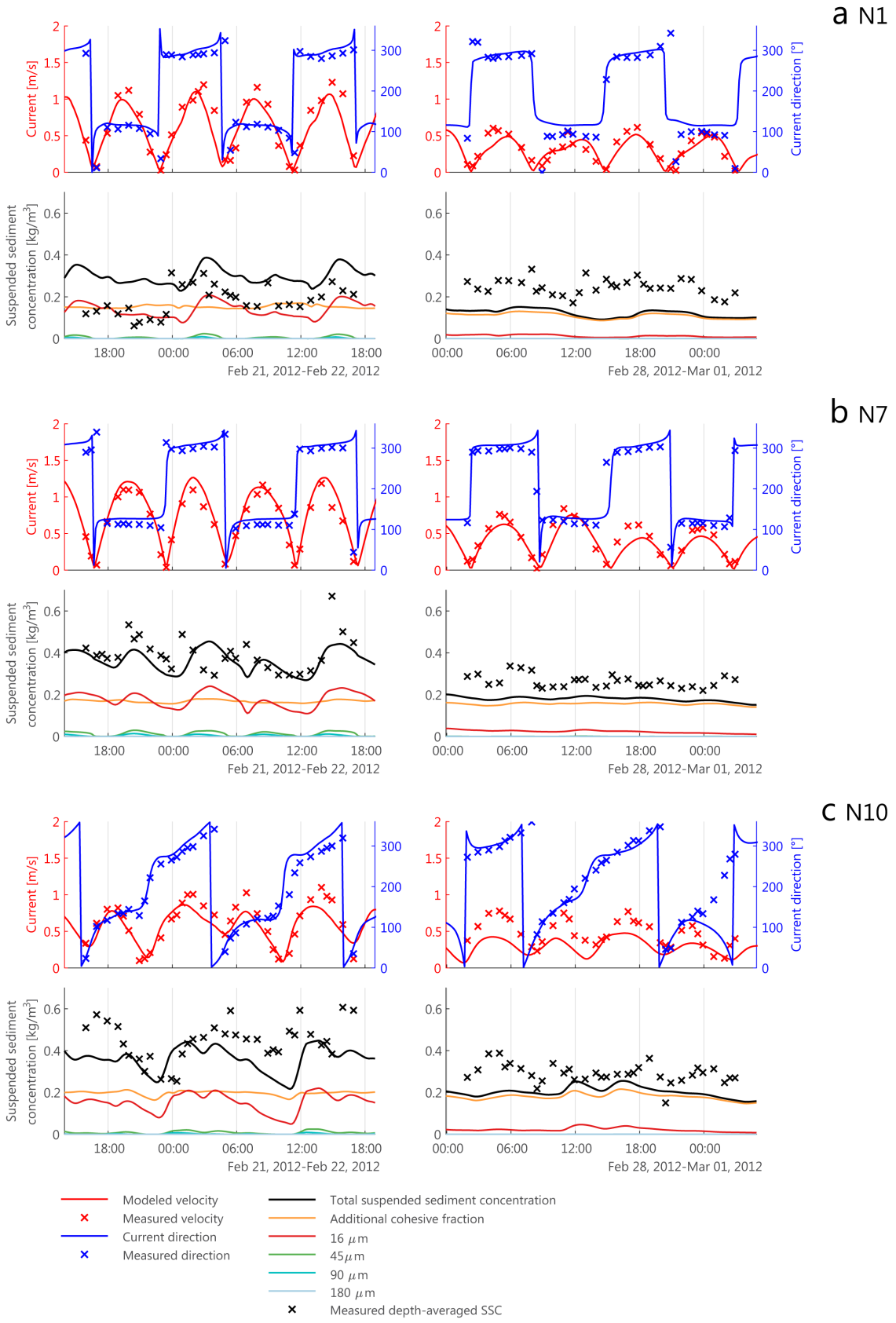

Figure 4.2: Calculated and measured current velocities, direction and suspended sediment concentration at monitoring stations N1 (a), N7 (b) and N10 (c), located at the upper Xiaomiaohong inlet, Sanshahong inlet and the Lengjiasha shoal, respectively. The left figures correspond to spring tidal conditions, the right figure to neap tide

to the measurements, the model show an under prediction of the concentration and is less dynamic at some stations.

4.1.2. Statistical validation

Beside the visual validation, the model results are evaluated by two statistical parameters, namely the Model Efficiency ME coefficient and the overall bias $|PB|$. Figure 4.3 shows the ME and $|PB|$ for the calculated water levels at the 6 tidal gauges. With an efficiency of $ME > 0.65$ the model shows an excellent performance on calculating water levels. Xiaomiaohong station shows a slightly less accurate performance. This could be due to bathymetry inconsistencies at the upper reaches of XMH. The model shows similar results for the percentage bias, scoring very good for all the stations and good for the Xiaomiaohong and Datang station (i.e. $|PB| < 20\%; < 40\%$, respectively).

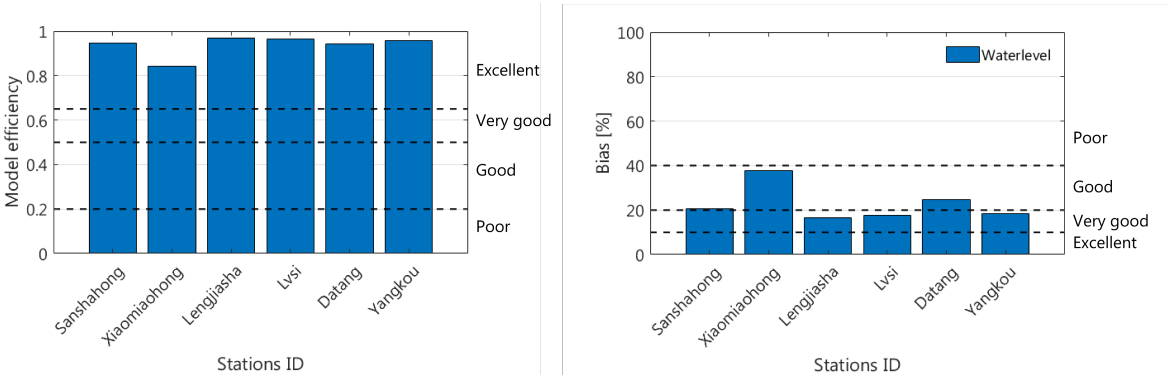

Figure 4.3: Model Efficiency and Percentage Bias for the calculated waterlevels at the 6 tidal gauges

The same statistical validation is performed for the current velocities and sediment concentrations at the 14 mooring stations. Figure 4.4 show the ME coefficient of current velocity, current direction and SSC.

The overall ME coefficients on current velocities are relatively high with an 'excellent' score (i.e. $ME >$ 0.65). Station N6 diverges from this trend and scores considerably 'poor' ($ME >$ -2). This negative ME reflects the observed mean is a better predictor than the model prediction. This is mostly due to significant low velocities measured during ebb (peak flow of $< 0.3\ m/s$), which suggest inconsistencies in bathymetry or error in measurements compared to other locations(see section A.2). Stations N10, N12 and N13 are situated at the Lengjiasha shoal in more shallow water. Validation of the predicted values for current velocity show a slightly less performance, scoring as 'good' ($0.2 > ME > 0.5$). This is mainly due the velocity being less bidirectional compared to the other stations. Also, wind-induced waves have a larger effect on the hydrodynamics in these shallow regions compared to other regions.

The majority of ME coefficients on current direction range from a 'very good' to 'excellent' score (i.e. ME > 0.5). Compared to ME coefficient for current velocities, the model performance on current direction is less compared to velocity. Closer examination of the calculated and measured results reveal that this lower performance is due to the relative large errors with a small shift in phase. For instance, when the calculated directions lags behind the measured result with 30 minutes, this results in an error of 150 degrees (see Figure4.2).

The model performance on the calculated suspended sediment concentrations varies with the station locations. In the upper reaches of the Xiaomiaohong channel (i.e. N1 and N2) the model performance is 'poor' (ME = -0.2 ~ -0.5). In this case, the model overestimates the concentrations compared to the measured values. This can also be observed in the percentage bias, ranging from $20\% < |PB| < 40\%$. Same observations can be made at the station N6, N8. The model performance at middle reaches of the channel show better performance with ME coefficients scoring 'very good' to excellent' (i.e. N3, N4 in the XMH channel and N7 and N9). Causes for this missmatch in measured and calculated values could be due to neglecting hydrodynamic processes, such as waves or large scale residual fluxes. Also, the simplified bed composition could play a role as the model is given a limited spinup time.

Figure 4.5 shows the percentage bias of the model at the 14 stations. Overall the model shows 'excellent' to 'very good' scores (i.e. $|PB| < 20\%$). As discussed earlier, exception is the poor score in current velocities at the N6 station ($|PB| = 100\%$).

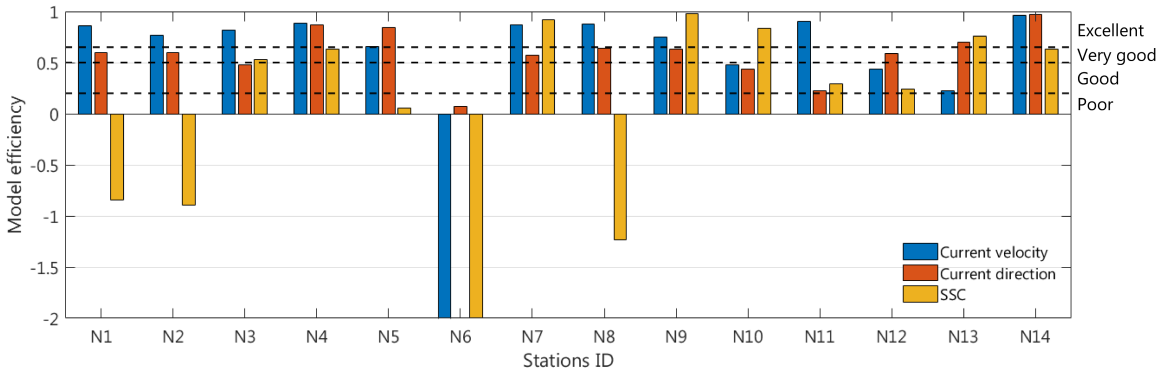

Figure 4.4: Model Efficiency for the calculated current velocity, direction and suspended sediment concentration at the 14 mooring stations

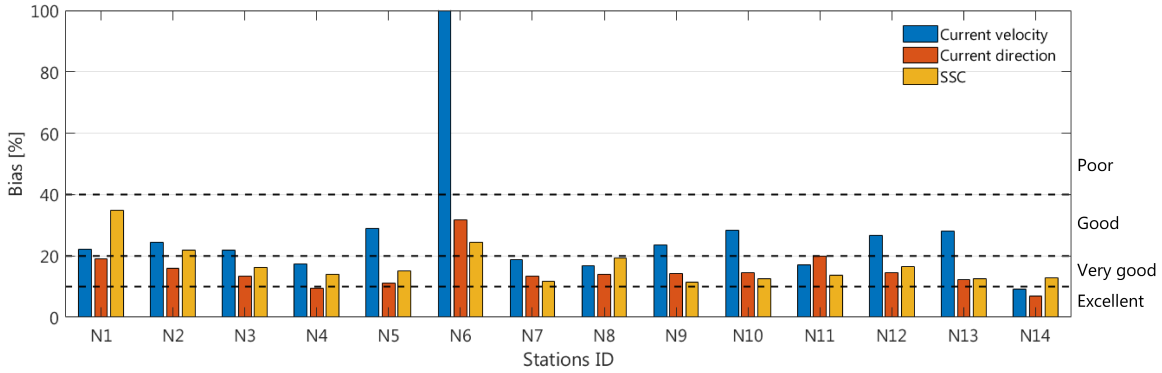

Figure 4.5: Percentage Bias for the calculated current velocity, direction and suspended sediment concentration at the 14 mooring stations

4.1.3. Siltation and morphological acceleration factor verification

As mentioned in section 3.2.1, to efficiently model siltation over large timescales, a morphological multiplication factor was included. The model was set-up to run from 8 January to 8 March 2014 with a *morfac* = 24, which means a morphological development of 4 year. This time frame corresponds with the completion of the first phase of the Yaosha reclamation around 2013 and 2017. Figure 4.6 shows the calculated bedlevel changes after 4 years of development. Severe erosion occurs inside the tidal channels, indicating scouring of the bed. Generally, siltation takes place at higher elevations and around edges of the tidal flats, such as the southside of Yaosha, the southside of Lengjiasha and the smaller formations between the main tidal channels. Also, siltation can be observed at the center of Yaosha and along the southside of the elevated work road. However, in between these two siltation zones in the enclosed area, the model shows local erosion up to $1 \sim 2$ m. The strong erosion close to the west side of the offshore reclamation, suggest the formation of a new tidal channel. This could be caused by the sharp corners of the reclamation and the focusing of retreating ebb tidal volumes. Similar pattern can be seen inside the harbor basin. General siltation patterns at Tongzhou bay will be further treated in section 4.2.

Calculated bedlevel changes are verified with elevation data retrieved with remote-sensing. Due to the lack of high-resolution surveyed elevation data of the Yaosha shoal for the initial 2014 situation, only a qualitative comparison can be made of the calculated bedlevel and morphodynamic features for the 2017 situation. Also, qualitative comparison is done through visual observations during a fieldvisit of the site. Figure 4.7 compares the calculated and measured elevation for the 2017 situation. Similar patterns can be observed in the measured elevation data, such as the formation of a tidal channel at the left side of the reclamation. However, the model predicted the location of this channel more towards the left. This is likely caused by the relative coarse grid resolution of the model. The calculated backfilling of the area between the higher ridge on the shoal and the newly constructed elevated road is similar to the measured data. However, the model tends

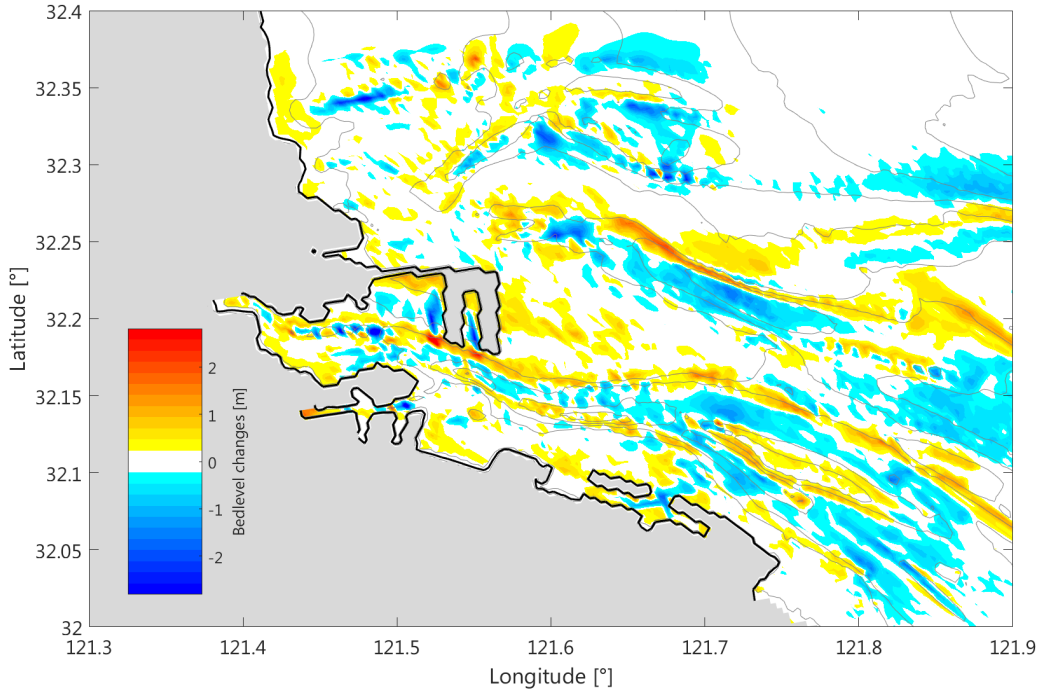

Figure 4.6: Predicted siltation patterns at the current extend of the Tonghzou bay reclamations after 4 morphological years, indicating siltation (red colors) and erosion (blue)

to over-predict the final elevation. This could be due to not including processes that play an important role in siltation at higher elevations, such as the effect of longterm consolidation of the top layer and vegetation.

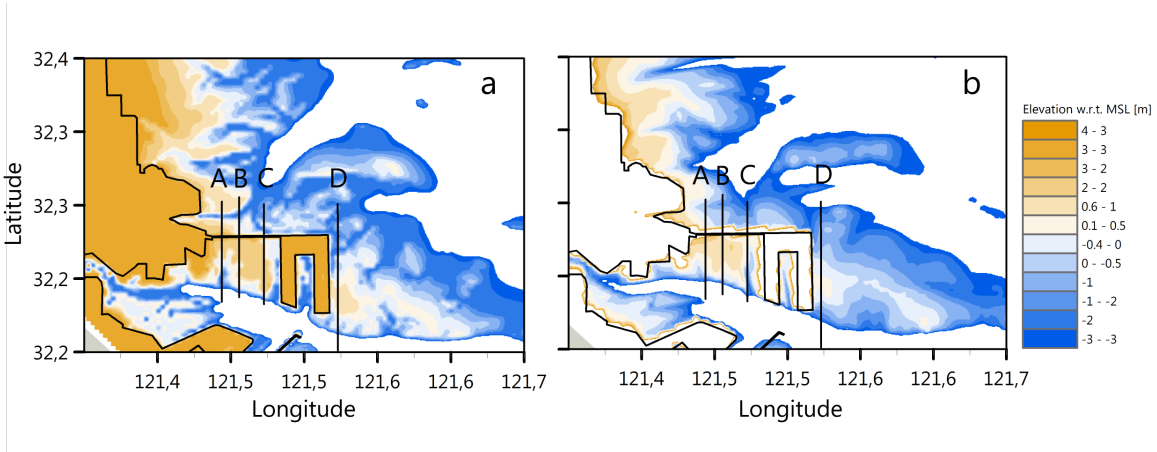

Figure 4.7: Surveyed (a) and modeled (b) bed elevation above MLWS at the recent reclamation at Tongzhou Bay. Indicated are the sampled cross-sections (A,B,C,D) at which both elevations are compared (see Figure 4.8)

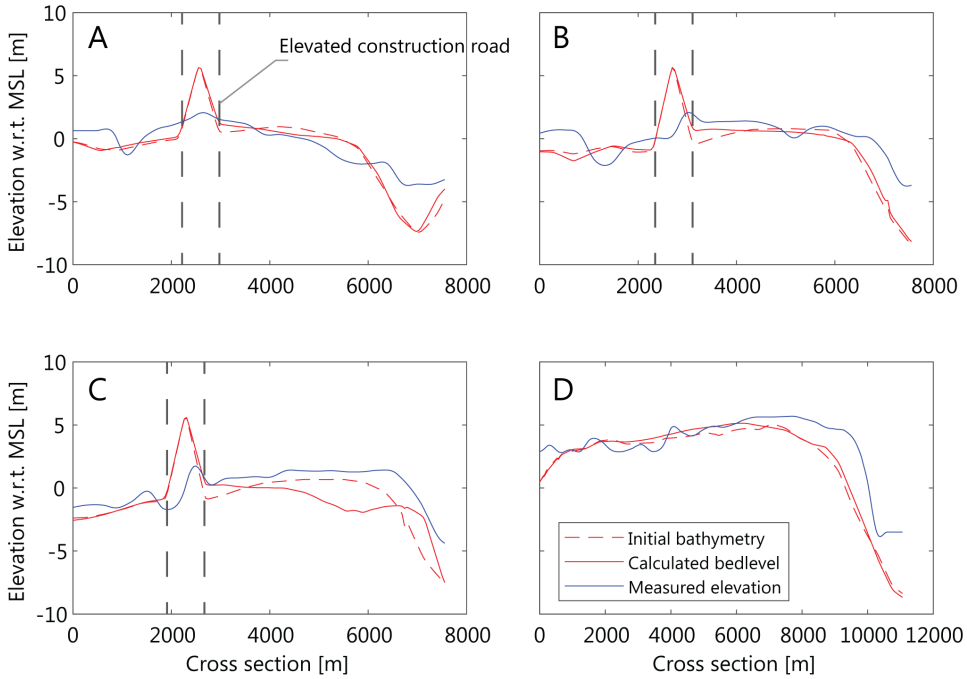

Figure 4.8: Calculated and measured bed level change after 4 years of morphological time at several cross sections at the current extend of the reclamations at Tongzhou bay

Additionally, several cross-sections were retrieved for the initial and calculated bed elevation after a period of 4 years. These are referenced with the surveyed elevation at 2017, as shown in Figure 4.8. It can be seen that overall siltation rates are small. As suggested by Figure 4.6, siltation mostly takes place at the edge of the shoal and at the area between higher regions of the shoal and the new constructed work road. More diverging erosion results can be seen in cross-section C where the model predicts the formation of a deeper channel.

4.2. Model results on Tongzhou Bay

The verification of the model results with measured values at several monitoring locations, provides sufficient confidence in the models ability to reproduce local hydrodynamics and sediment transport. Several significant hydrodynamic and transport characteristics for the development of the Tongzhou Bay region and its ecosystem are closer examined in this section.

4.2.1. Tidal characteristics

Calculated maximum waterlevels are selected over 4 consecutive spring-neap cycles to determine the mean, spring and neap tidal ranges for the 6 monitoring locations inside the model domain. The simulated tidal signal is a semi-diurnal tide, with spring-neap variation of a fortnight period. These values are shown in Table 4.1. The calculated tidal ranges increases from south to north and from offshore towards near shore monitoring locations (Figure 4.9). Other studies found similar values by examining several tidal gauges, with values of 6.2, 4.5 and 3 m at Yangkou and 5.2, 3.9 and 2.6 m at Lüsishayang for spring, mean and neap tidal range, respectively Kang (2015).

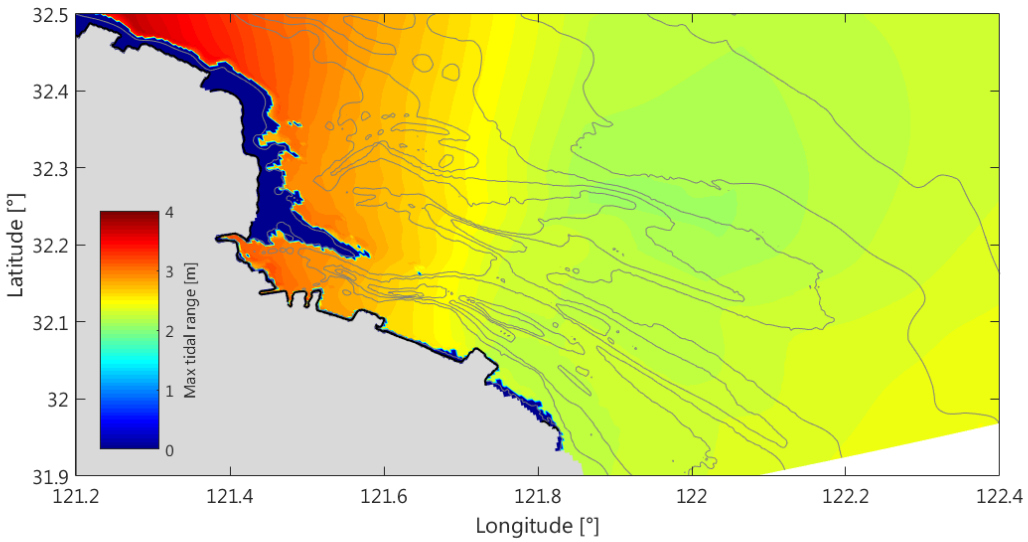

Figure 4.9: Calculated maximum tidal range during a full spring-neap cylce at the Tongzhou Bay domian

Monitoring location	spring mean tidal range m
Lusishayang	5.54
Datang	5.15
Lengjiasha	4.87
Sanshahong	5.77
Xiaomiaohong	5.97
Yangkou	6.02

Table 4.1: Spring, neap and mean tidal ranges as calculated by the model at 6 monitoring locations

The mean current patterns are assessed by determining the mean current velocity over the whole computational domain of Tongzhou Bay over 4 consecutive spring-neap cycles with a temporal resolution of 1 hour. Figure 4.10 shows the mean current fluxes and magnitude. It can be seen large scale tidal flux enters form the southern boundary towards the north, following the Lanshayang channel. At Tongzhou Bay, the main tidal wave comes in through the three main tidal channels; Xiaomiahong, Sanshahong and smaller channel formation at the north end of the Tongzhou domain. It can be seen that part of the residual tidal current through the Sanshahong channel splits of by crossing over the more deeper parts of the Lengjiasha shoal and merges with the large scale current into the Lanshayang channel. The remaining flux continues up the Sanshahong channel until it collides with the flux form the upper tidal channels. The tidal volumes of the Xiaomiaohong and upper tidal channel eventually meet over the Yaosha shoal. Mean currents show an overall northward pattern through the Xiaomiaohong channel over the Yaohsa shoal during a tidal cycle. Another observation can be made on the upper side of the Xiaomiaohong channel, where a tidal flux is directed towards the south, joining with the incoming flux from the channel entrance and crossing over into the Sanshahong channel.

4.2.2. Net sediment transport

Similar net transport fluxes were retrieved by averaging suspended transport over 4 consecutive spring-neap cycles with a 1 hour interval. Figure 4.11 show the mean depth-averaged suspended transport for the sum-

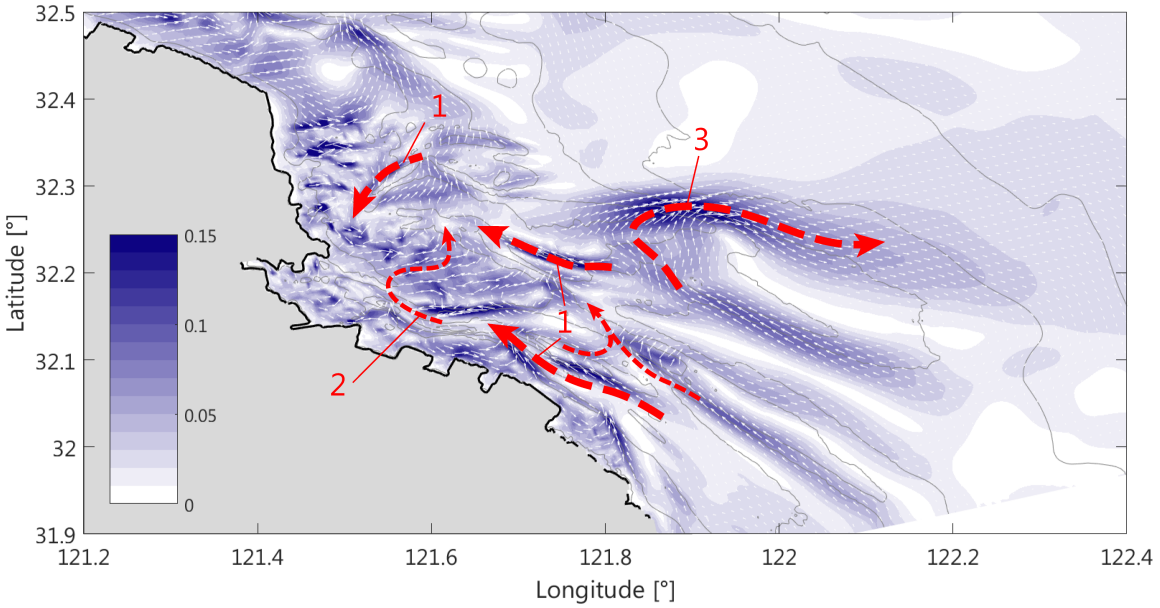

Figure 4.10: Calculated mean current patterns and the magnitude locations at Tongzhou Bay. Mean residual patterns are indicateed with red dashed lines. Overall pattern can be seen to be transported into the main tidal channel, namely Xiaomiaohong, Sanshahong and the upper channel (1). An overall mean current is found in a South-North direction of the Yaosha shoal of the two tidal volumes from Xiaomiaohong and the upper channel (2). This indicates the overall tidal flux in a South-North direction. A strong residual tidal flux is found over the Lengjiasha shoal, where the main tidal volume bypasses the Sanshahong channel.

mation of all sediment fractions. It was found that the net bedload transport was 10 orders smaller than the net suspended transport and was therefore neglected for the total net transport. Similar transport patterns can be seen compared to net tidal volumes. Mean suspended transport is directed through the channels, confirming a net import of fines through the tidal channels. Inside the Sanshahong channel, the suspended transport flux becomes segregated as well. A large part of the suspended material crosses over the lower parts of the Lengjiasha shoal and a smaller part is transported up the Sanshahong channel. Similar patterns to the mean tidal currents can be found at the Yaosha shoal. Compared with the net transport through the channels, the net flux over Yaosha is several times smaller. This northwrad flux over the Yaosha shoal would suggest the supply of sediment mainly comes from the Xiaomiaohong channel.

The net transport of sediment was further examined by defining several smaller zones along the computational grid to match the main topographic features at the domain (*e.g.* tidal channels, Yaosha and Lengjiasha shoal). Cumulative suspended and bed transports were monitored on each zone boundary during a single spring-neap tidal cycle, in order to get better insight in cumulative sediment sources and sinks. Figure 4.12 shows the zones boundaries and the corresponding transports.

Several features can again be recognized. Most of the sediment material is being supplied by the main tidal channels, showing an inward flux at all the southern boundaries. The distinct bypass pattern over the deeper parts of the Lengjiasha shoal can be recognized as well. Most of the cumulative volumes are transported in a south-north direction, showing a flux over the Yaosha shoal. At the northside of the Tongzhou Bay domain, an influx of material occurs at the nearshore zone. However, more offshore this shifts towards an outflux. The net sediments budgets of each zone was calculated by the summation of all the cumulative transports after a single spring-neap tidal cycle and are presented in Table 4.2. Almost every zone at the Tongzhou Bay domain show a trend of deposition, with the largest volumes at the south and eastside of Yaosha shoal. Most of this deposition occurs at the tidal flats or nearshore areas. Remarkable erosion locations are the northside of Yaosha. This is mostly due to the scouring inside the Sanshahong channel, which is also included in this zone. Further elaboration on the siltation patterns is done in the next section

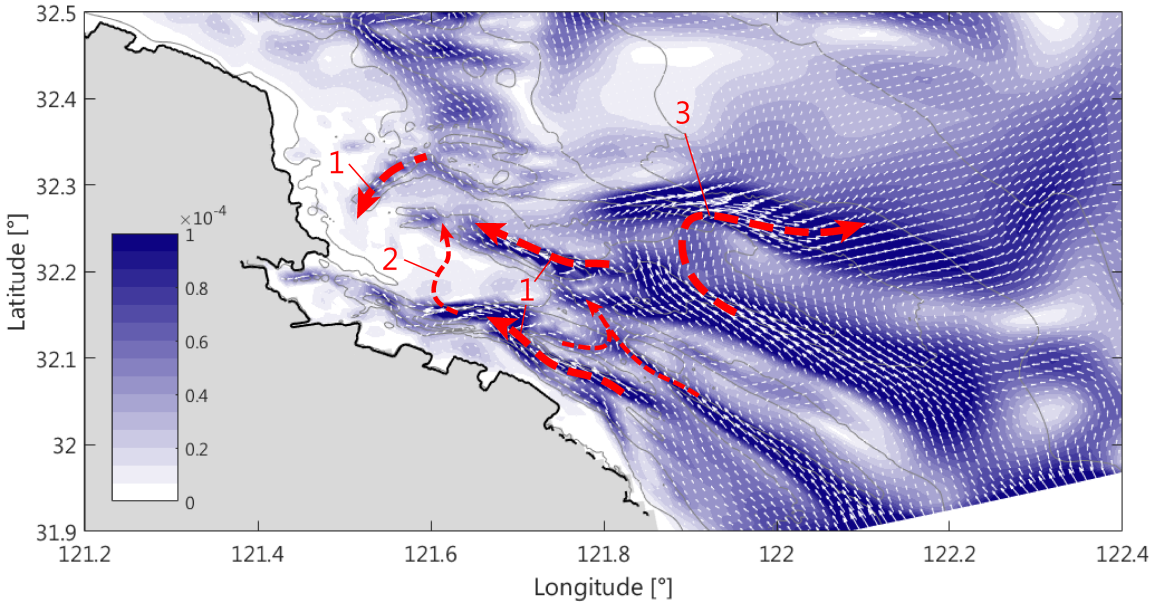

Figure 4.11: Calculated depth-averaged suspended sediment transport for all defined fractions over a full spring-neap tidal cycle at Tongzhou Bay domain. Similar transport patterns can be observed as with mean tidal fluxes, such as the main import of fines through the tidal channels (1), a bypass transport flux over the Yaosha shoal (2) and a large bypass over the more submerged parts of the Lengjiasha shoal. The model shows that this bypass eventually links up with the larger transport flux at deeper waters.

Sector	Location	Cumulative transport budget [tons]	
I	Norhtern upper tidal flats	+7.32e4	Deposition
II	Upper tidal channel north	+30.58e4	Deposition
III	Upper tidal channel south	+38.18e4	Deposition
IV	Yaosha north	−5.48e4	Erosion
V	Upper reach Xiaomiaohong	+8.16e4	Deposition
VI	Yaosha south	+33.41e4	Deposition
VII	Yaosha east	+106.43e4	Deposition
VIII	Lengjiasha	−10.43e4	Erosion

Table 4.2: Calculated deposition or erosion budget for the 6 sectors indicated in Figure 4.12 over a single spring-neap tidal cycle and consists of the summation of all sediment fractions

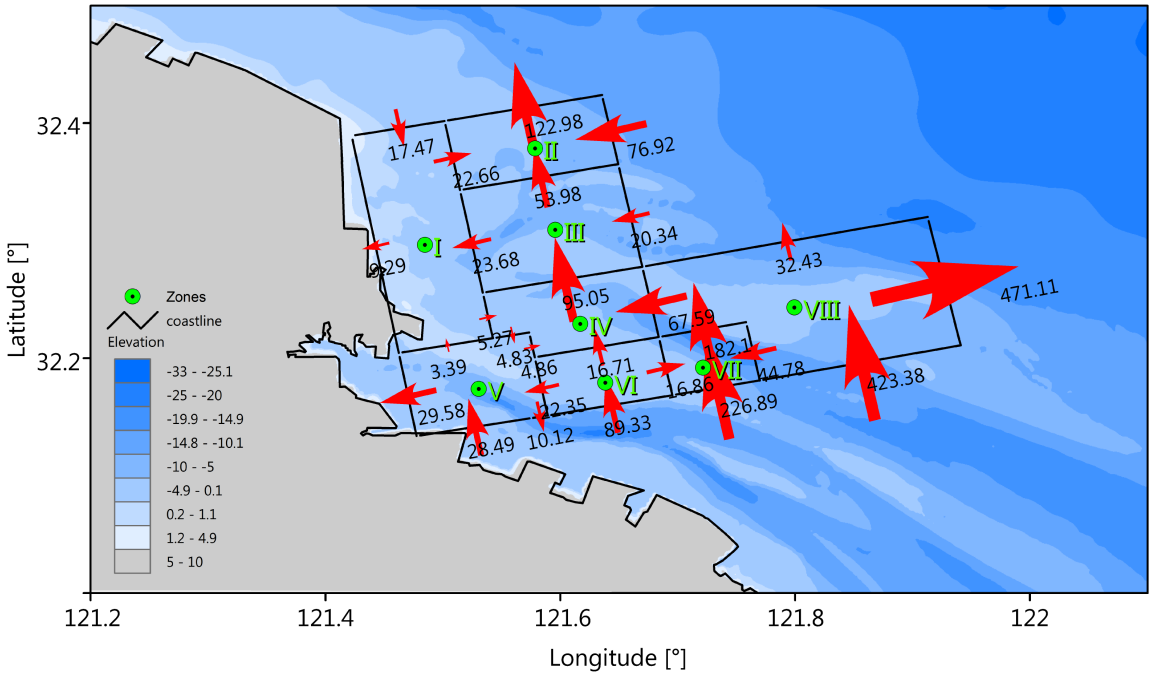

Figure 4.12: Transport zones at the Tongzhou domain and cumulative sediment fluxes in 1.0e4 ton. Indicated are the cumulative transports at each interface between the zones. The total mass balance for the Yaosha shoal and nearshore areas are performed and indicated with the yellow roman numerals

4.2.3. Siltation patterns

Deposition and erosion patterns were further examined by setting up the model to run for 8 morphological years (*morfac = 48*) without further reclamation activities. The results are shown in Figure 4.13 together with the initial bathymetry. Most of the siltation occur at the shoals and the upper coastal zones, whereas siltation mostly occur inside the main tidal channels, meaning a constant scouring of the tidal channel. A clear pattern can be observed with siltation on the edges of the southern Yaosha shoal and at the Hengsha and Wulongsha shoal. Both north and south passage around the Wulongsha shoal show strong ecrosion.

The model results shows the highest siltation rates at the southsides of the intertidal areas. This would suggest a southward migration of the Yaosha shoal. The Lengjiasha shoal shows similar patterns, where strong siltation takes place on the southwest and northeast ridges. With heavy erosion of the adjacent tidal channels, these intertidal rigdes at Yaosha and Lengjiasha becoming more steep. Similar results were found at intensive monitoring of the nearshore mudflats at Xiyang channel in the northern RSR (Gong et al., 2017).

4.3. Ecotopemap for Tongzhou Bay

Previous model results are used to construct an ecotope map of Tongzhou Bay through the ecotope classification as described in section 3.4. From required data it was determined that the system already can be described as a saline environment as the salinity show no large variations and no significant freshwater discharges are present. Further, it was determined that the bed consist of soft substrate, allowing benthos to live in and on top the bed. The classification of littoral and hydrodynamic classification will be done separately and are combined to create a full ecotope map. This will be done for the initial state and after 8 years of morphological development. No further reclamations were included with respect to the situation of 2012. The development of ecotopes can be determined by comparing these change in ecotope area over time.

4.3.1. Littoral classification

The littoral zones are described by the general water depth and the dryfall time over a full spring-neap tidal cycle. The waterdepth is deduced from the initial bathymetry of the model, as shown in Figure 4.14a. The classification is based on the supralittoral ($> MHWN$), littoral ($MLWS < d < MHWN$) and sublittoral zones ($z_b < MLWS$). Subsequently, the sublittoral is further divided into shallow or deep regions (*e.g.* $MLWS - 5 <$

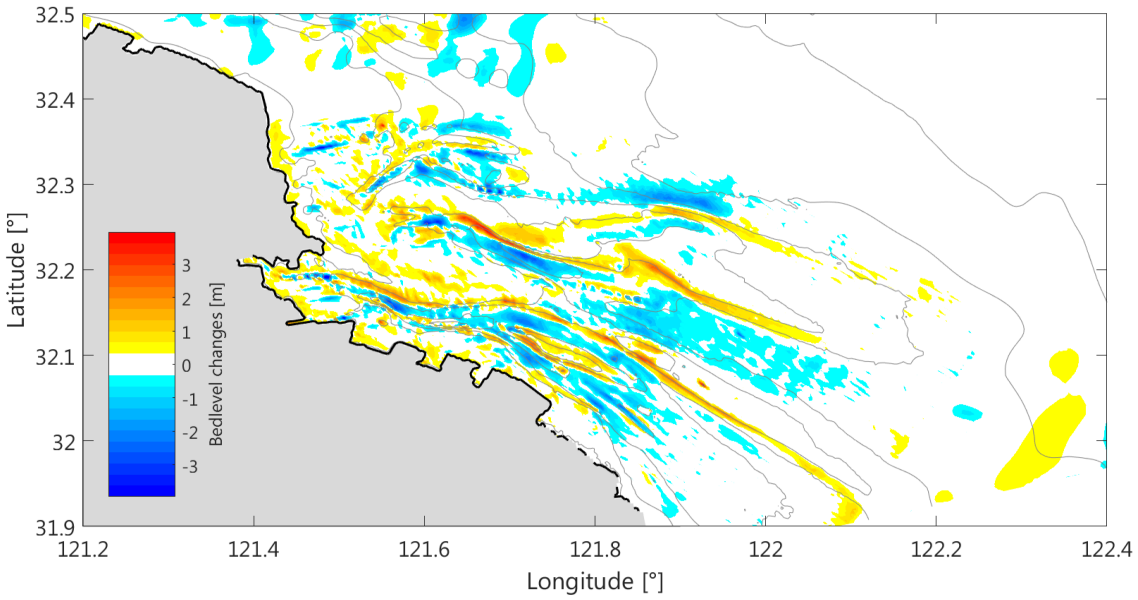

Figure 4.13: Total siltation for 8 years of morphological development without further reclamations. The initial bathymetry is indicated with contour lines

$d < MLWS$ and $d < MLWS-5$, respectively). The littoral zone is further classified by means of the percentage of dryfall time over a full tidal cycle, indicating high, mid and low littoral (*e.g.* $t_{dryfall} > 75\%, 25\% > t_{dryfall} > 75\%$ and $t_{dryfall} > 25\%$ respectively). This is determined by the calculated water depths with the threshold value of 0.2 m during a full spring-neap tidal cycle. The results are shown in Figure 4.14b. It can be seen that the southern Yaosha shoal and the adjacent Rudong coast generally show a dryfall time of 25 to 75% for a full spring neap cycle. Areas with higher dryfall durations are mostly close to the coastline and consist of small areas of the open coast, indicating that during $MHWS$, nearly the whole extend of the Tongzhou bay mudflats become inundated.

Finally, the full littoral classification is made by combining the previous subdivisions, as shown in Figure 4.15. It can be seen that most of the Yaosha shoal and the adjacent northern coast is within the littoral class boundaries. The Lengjiasha shoal and other nearshore regions are within the shallow sublittoral zone, suggesting the constant inundation and therefore tidal fluxes and transport over the shoal. The deeper sections of the Xiaomiaohong and Lengjiasha channels are mostly in the deep sublittoral zone. Only the more elevated region on the southern end of Yaosha are within the higher littoral zone, having longer dryfall durations.

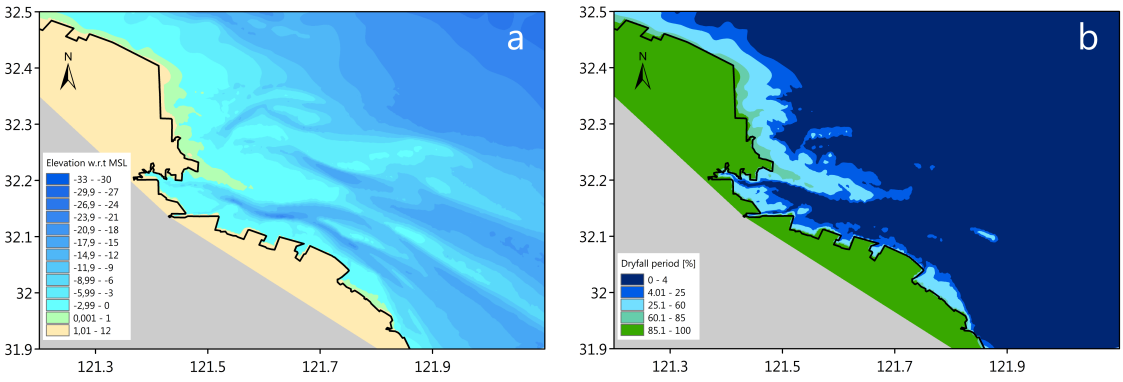

Figure 4.14: Bathymetry (a) and dryfall period in percentage of the total duration of a tidal cycle (b), determined by the ZES.1 method (Bouma et al., 2005).

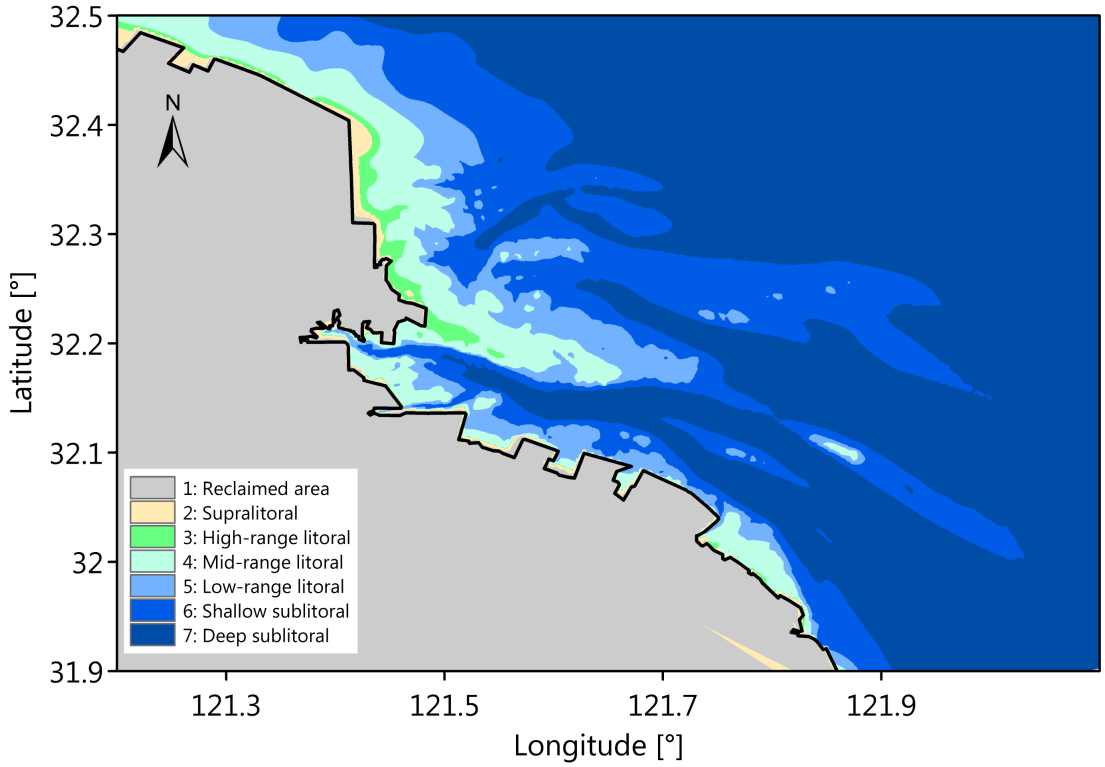

Figure 4.15: Littoral classification of Tongzhou Bay according to the ZES.1 method.

4.3.2. Hydrodynamic classification

The hydrodynamic classification is based on the maximum tidal current velocity, produced by the model. This is classified into high, or low-dynamic, based on the threshold value of 0.8 m/s (see section 3.4). The results are shown in Figure 4.16. It can be seen that the Yaosha and Lengjiasha shoal show low-dynamic conditions, except lower elevated regions at the eastern end of the shoal where overflow occur.

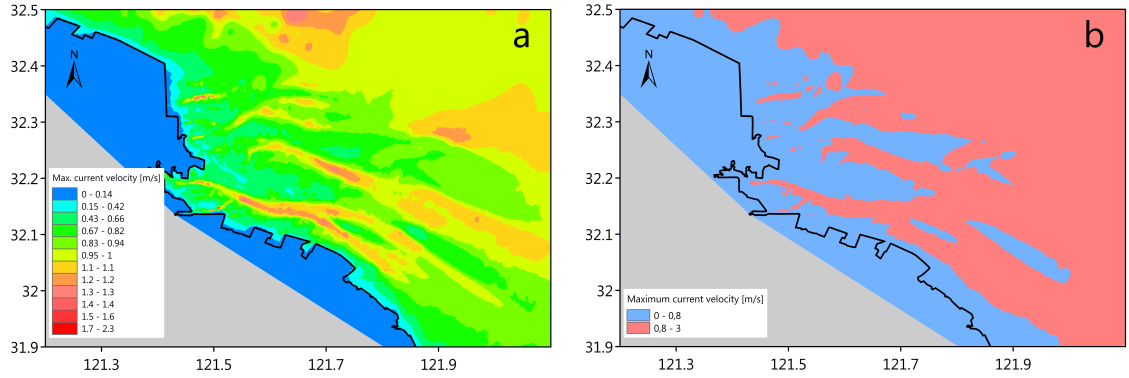

Figure 4.16: Classification of high and low-dynamic conditions based on the maximum current velocity during a spring-neap tidalcycle

4.3.3. Initial ecotope map

The littoral and hydrodynamic features are combined to construct a preliminary ecotope map of the Tongzhou bay, as shown in Figure 4.17. The main color scale is indicating the littoral zones, whereas the hydrodynamic low and high conditions are shown in lower or darker shades. It can be seen that the hydrodynamic conditions roughly coincide with the overall elevations of the region. It can be seen that the Yaosha shoal mainly

consists of littoral ecotope, ranging from low-range at the outer edges up to high-range and supralittoral close to the current seawall.

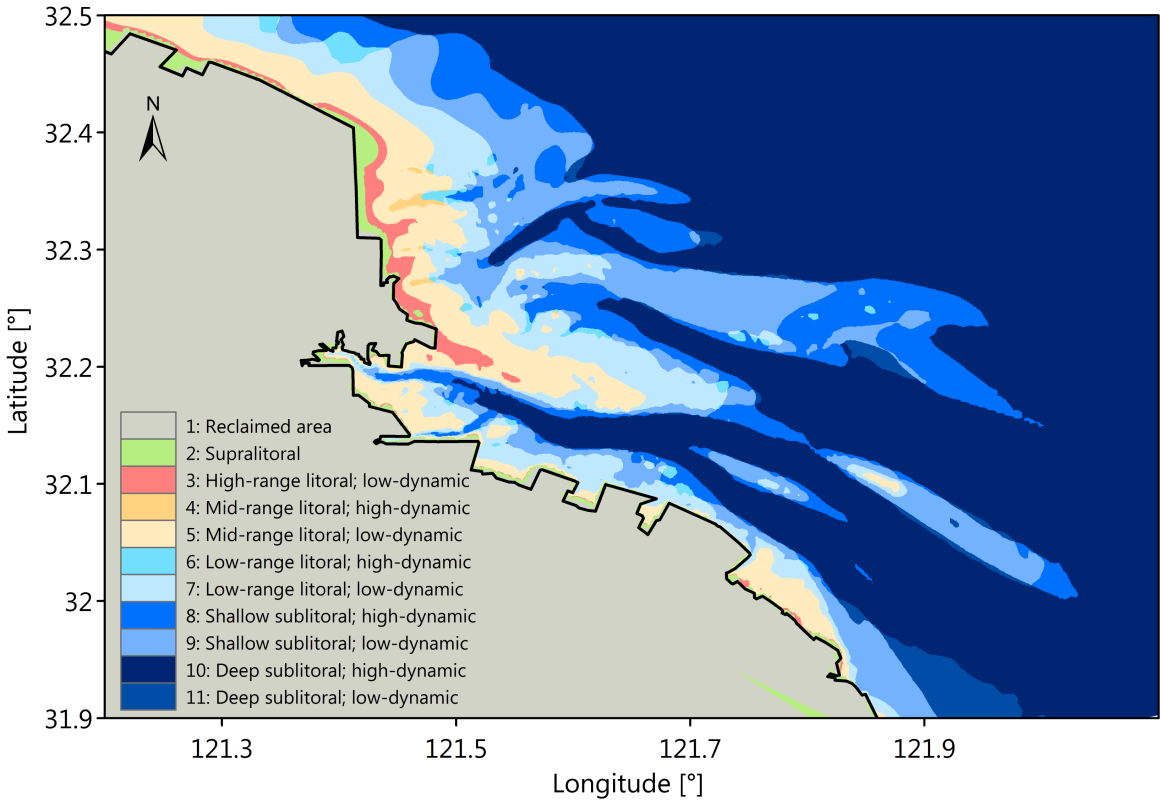

Figure 4.17: Full ecotope map of Tongzhou Bay for the situation of 2012, through the combination of the littoral and hydrodynamic classification. It shows the intertidal flat area can be classified into supralittoral and littoral zones. The tidal channel are mostly classified into the sublittoral zones. The hydrodynamic classification into high and low dynamic conditions follow this littoral classification closely, as lower dynamic conditions occur at the supralittoral and littoral zones. The tidal channels are mostly classified as high-dynamic conditions

4.3.4. Ecotope validation

As mentioned in section 3.4, in order to draw conclusions on the possible occurrence of certain ecosystem, an ecotope map needs to be validated with field measurements of certain habitat. Two sets of sighting data were made available of two shorebird species at the Jiangsu coast; the Bar-tailed Godwitt (BTG) and the Great Knot (GK). Figure 4.18 shows the 95%, 90% and the 50% home-range of these two shorebird species with the derived ecotope map of Tongzhou Bay for the 2012 situation. A close coincidence of these species can be observed with mid and low-littoral zones (*e.g.* being inundated 25 to even 100% during a spring-neap tidal cycle).

Figure 4.19 shows the total percentage of corresponding ecotope zones based on the 90% homerange of both the BTG and GK. Most of the species prefer the mid-range littoral zone (30 sim40%). Second highest ecotopes are the low-range littoral and shalow sublittoral zones (16 ~ 19%). This is supported by other findings on the brood and forage preferences of these two shorebird species and their dependency on higher elevated tidal flats (Peng et al., 2017; Bouma et al., 2005; Piersma et al., 2017) (see section 2.5). The BTG is characterized as 'tide-followers' moving up and down the mudflat with the tide. The high coincidence with the mid-range littoral shows confirming results for this species. In contrast to the BTG, the GK show a higher occurrence at reclaimed regions. This can be understood as the GK also prefers more elevated regions for nestbuilding and breeding.

Hence, based on the correlation between shorebird behavior/sighting data and the constructed ecotopemap, the mid- and low-range littoral ecotope indicate the most preferable conditions for suitable habitat for both the BTG and GK populations. Individual preferences also show confirming results, such as high dependency of the BTG on intertidal mudflat and GK's preference of higher elevated regions. However, several

important abiotic and biotic parameters have not been considered in the creation of this map. For instance, species which are lower in the food chain and serve as food sources for the observed shorebirds species not necessarily rely on the same ecotope type and require different conditions in order to thrive as a population (Ma et al., 2010). Also the role of vegetation both affect hydrodynamic as well as shorebird populations. On the one hand, *Spartina antiflora* will reduces overall flow velocities during inundation and increase siltation rates (Gong et al., 2017; Wang et al., 2005; Yin et al., 2017). On the other hand, this also limits the space for nestbuilding over open mudflat area (Peng et al., 2017). Therefore, these validation results only serve as an first indication for the performance of alternative port configurations.

In order to include the relative importances of each ecotope in further evaluation on alternative port configurations, a weight factor can be defined as shown in Table 4.3. This weight factor consists of the averaged percentage of occurrence of the two shorebirds species with each ecotope. With a high coincidence of the sighting data with mid- and low-range littoral and shallow sublittoral zones, these types have a high factor.

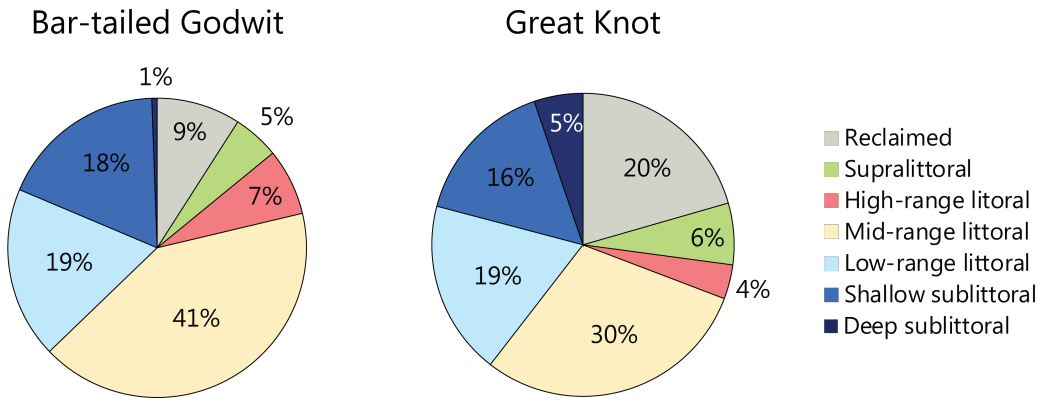

Figure 4.19: Corresponding ecotope type with the 90 % homerange of the Bar-tailed Godwit and Great Knot. The two species mainly reside at the mid-range littoral zone. The BGT, show a similar percentage for lower range littoral zones. This is in conformation with their 'tide-following forage pattern (Piersma et al., 2017). Other preferred areas are high-range littoral and reclaimed zones, which are more suitable for nestbuilding and breeding.

	Reclaimed area	Supralittoral	High-range littoral	Mid-range littoral	Low-range littoral	Shallow sublittoral	Deep sublittoral
Weight factor, f_{eco}	0.15	0.06	0.05	0.36	0.19	0.17	0.03

Table 4.3: Weight factor for each ecotope significance based on the coincides with the homerange of the Bar-Tailed Godwit and Great Knot at Tongzhou Bay

4.3.5. Unhindered ecotope development

In order to asses the alternative port designs, the model was setup to simulate 4 and 8 years of morphological development assuming no further reclamations or anthropogenic impacts. During these periods, bed elevation and local hydrodynamics will adapt, thereby increasing or decreasing in corresponding ecotope area. These changes in ecotope area represent the natural unhindered ecotope development and will serve as a reference case. Figure 4.21 shows the ecotope map for the initial situation in 2012 and predicted situation in 2020 of Tongzhou Bay. Most significant changes are the increase in supralittoral and the high-range littoral zones, due to continues siltation at these zones. New tidal channels are formed over the intertidal mudflat zones and the main old channels become more scoured.

To make this more insightful, these areas are compared in Figure 4.20. Supralittoral ecotope show a clear growing development, with gradual increase from 11.84e-4 to 18.47e-4 hec. Within the littoral zones, the high hydrodynamic regions show a general decrease, which is mainly attributed to the siltation of smaller channels and northern nearshore areas at the Yaosha shoal. The low-dynamic littoral regions generally show a gradual increase, with high-, mid- and low-range littoral zones growing 1500, 35.550 and 28.580 hec respectively. The relative smaller growth of the high-range littoral is mainly caused by rapid transition of new acquired high-range littoral to supralittoral zones. Sublittoral zones show opposite behavior, increasing in high dynamic

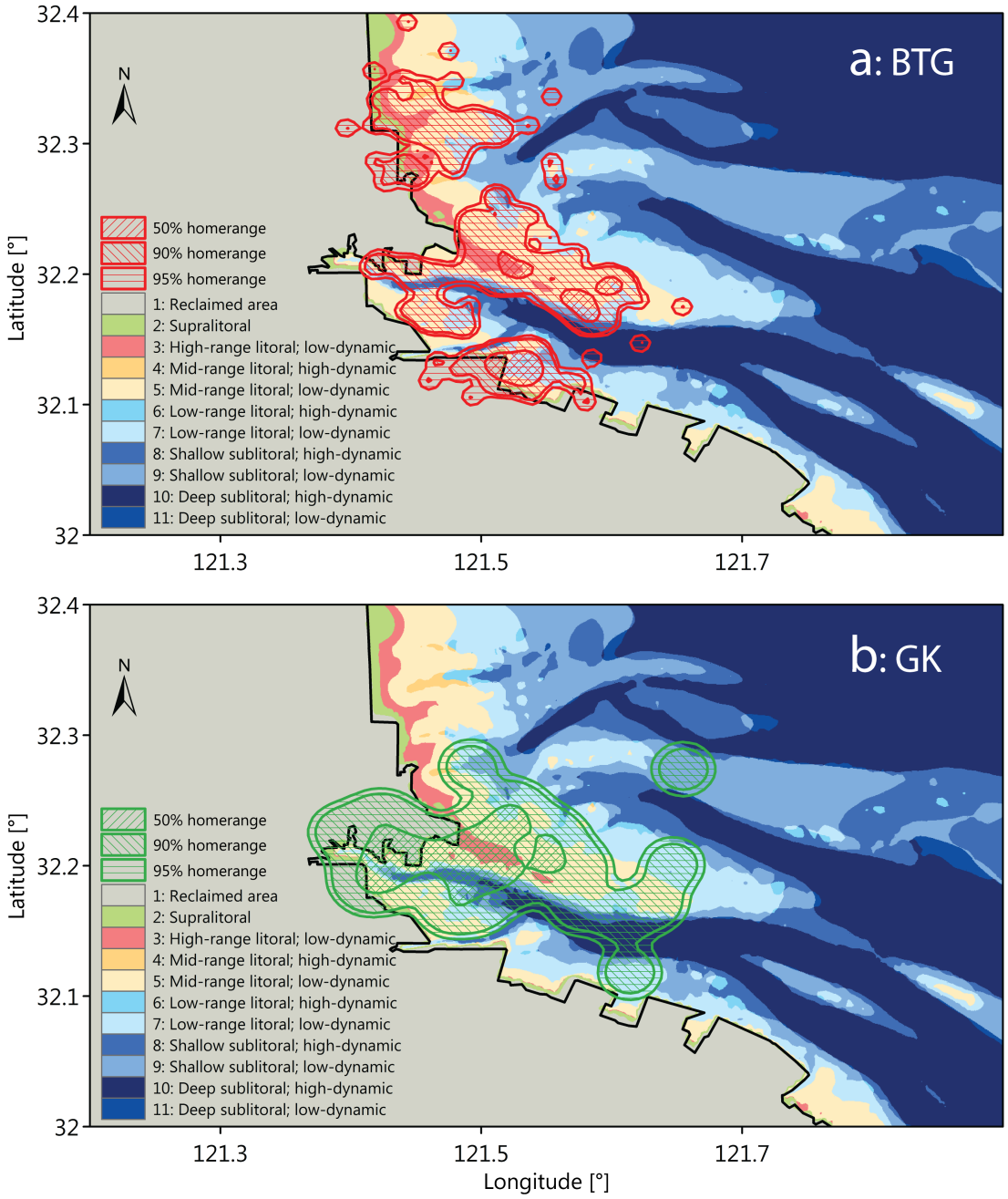

Figure 4.18: Full ecotope map of Tongzhou Bay for reference case at 2012. This ecotope map is be referenced with observations of the shore-bird species, the Bar-tailed Godwitt. It can be seen that the higher elevated littoral zones show most correlation with the observation, suggesting the preference of this species to high- and mid-littoral zones with weak hydrodynamic conditions. Similar to the Bar-tailed Godwitt, this species presumably gives preference to high- and mid-littoral zones with weak hydrodynamic conditions

regions and a decreased in low-dynamics conditions. This signifies the scouring of the main tidal channel Xiaomiaohong and Sanshahong with high dynamics over a tidal cycle. This trend also includes the formation of new ebb tidal channels at the nearshore regions north of Yaosha. This can be explained as the focusing of ebb tidal volumes during falling tide.

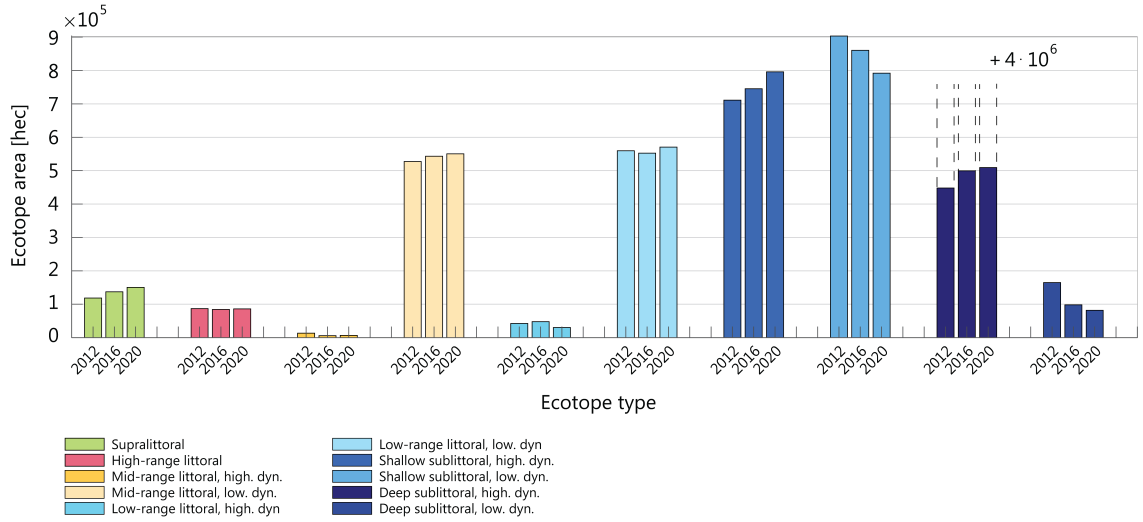

Figure 4.20: Development in total ecotopes area for the reference case, assuming no additional reclamation at Tongzhou Bay. The deep sublittoral zone are subtracted with $4\dot{1}0^6$ in order not to scale the vertical axes.

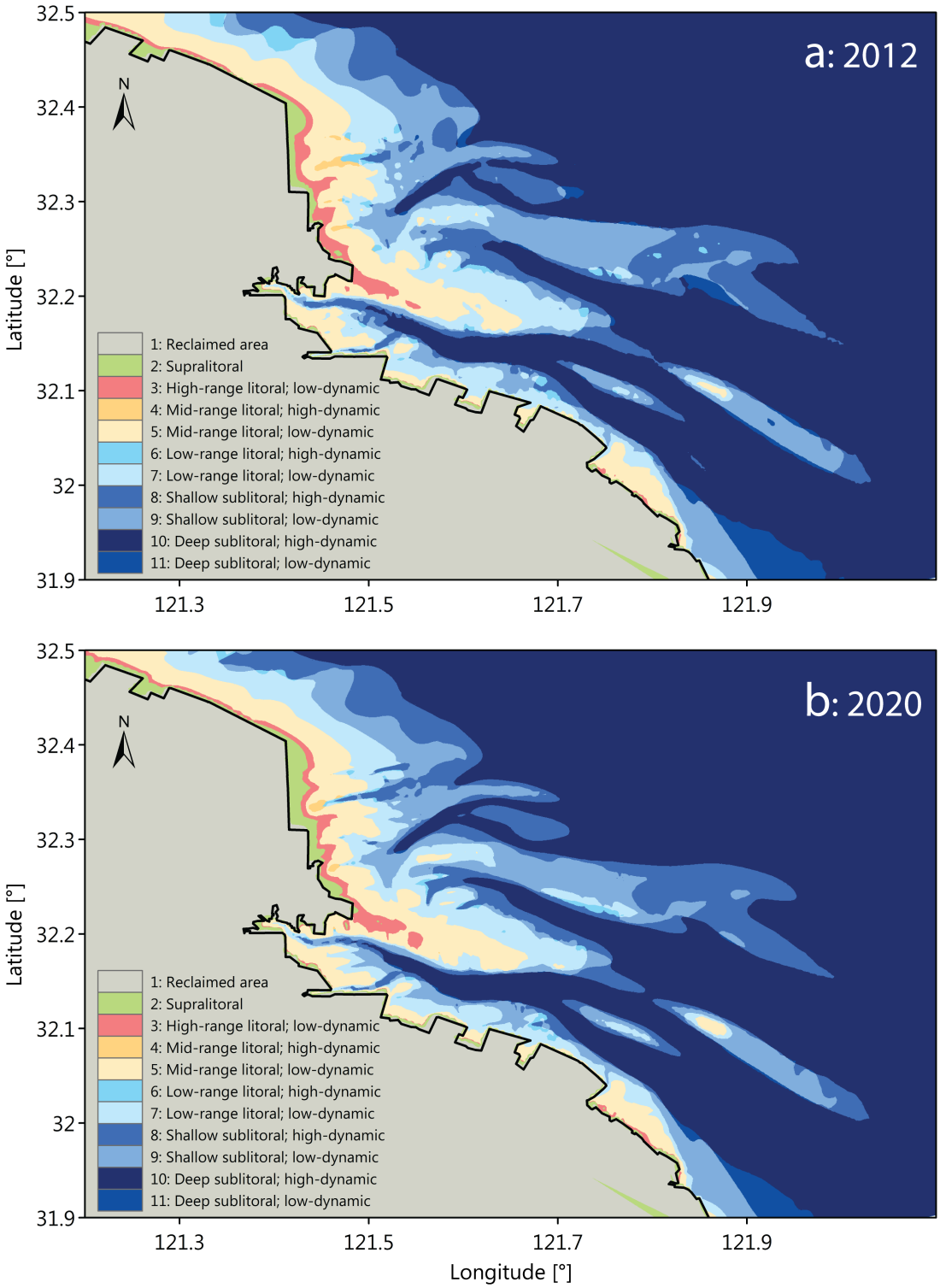

Figure 4.21: Calculated unhindered ecotope development from 2012 (a) to 2020 (b).

5

Alternative port designs

In previous chapter, a better understanding was obtained in the dynamics and development of Tongzhou Bay. By use of an ecotope map, the ecosystem of Tongzhou Bay was quantified and the natural development was predicted. With this insight, several alternative port reclamations can be designed and simulated within the model. This chapter elaborates on the design process and the set requirements for these alternatives It continues by showing results of a representative configuration.

5.1. Design process

The design of alternative reclamation strategies follows the common design cycle often followed in engineering projects, which is divided in several steps; analysis, synthesis, simulation and evaluation (Figure 5.1). This design cycle can be done over multiple iterations, working in a coarse to fine approach. To save computational time, the first iteration cycle was evaluated based on short-term hydrodynamic response on the various scenarios (not shown here). Large increase in flow velocities and bed-shear stresses were used as indicator whether more siltation was to be expected in a full morphodynamic simulation. Form these first results, a total of 7 final scenarios were selected and simulated.

Analysis The analysis focuses on the exploration of the design space in which the solution has to be created. From the analysis step, several design criteria are formulated at which an alternative design needs to fulfill and will be evaluated. In this thesis, the scope of the design space will be restricted to ecological and basic port utility criteria. Previous chapters elaborated on the driving processes in the morphological development of Tongzhou Bay and local ecosystems. The results of these sections serve as an analysis of the design space of alternative port designs. Form this gained insight, the following criteria for the alternative configurations are formulated:

1. The configuration should preserve existing high-value ecotopes. In previous results, high-value ecotopes were quantified based on sighting data of two shorebird species. In order to not further endanger these species and their habitat, initial high-value ecotope area should be preserved as much as possible.

2. The configuration should enhance the growth of high-value ecotopes. Aside the preservation of the high-value ecotopes, alternative port configurations should be designed to increase growth of valuable ecotopes with respect to the natural development.

3. The configuration should provide potential area for future port exploitation. With an large economic demand for new port facilities, larger reclamations offers more berthing capacity, larger terminals and better logistics. However, this means the reclamation of valuable habitat at shoals. Other port functionality requirements, such as local hydrodynamics around the port layout and siltation rates are not included in this study.

Synthesis The synthesis aims at designing several alternatives that fit within the design space and satisfy the criteria. The alternative designs are based on the proposed Tongzhou Bay port outline (Nantong Port

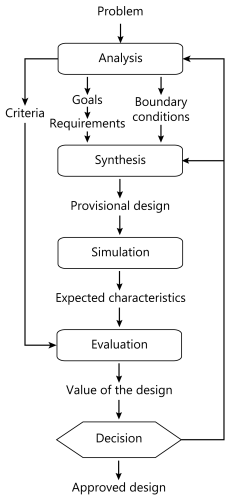

Figure 5.1: Common design cycle as used in engineering projects

Authority, 2013). Guiding principles is the utilization of natural processes, as proposed by the 'Building with Nature' approach (de Vriend et al., 2014a; van Slobbe et al., 2013).

The preservation of high-value ecotopes is achieved by planning the reclamations around these zones. . Results on unhindered ecotope development showed the transition from lower ecotopes (*e.g.* shallow sublittoral) to low-range littoral and subsequently higher elevated littoral zones. In order to enhance this transition, the design should promote high siltation rates at these regions. Previous model results showed the mean current and sediment flux are directed landward though the tidal channels and subsequently over the intertidal shoals. Different configurations were designed, aimed at optimizing this siltation and enhance the growth in valuable ecotopes.

All variants were designed to include a significant area for potential port development, although it is significantly smaller to the original proposed port reclamation. These designs take into account sufficient space for terminal and logistics activities, as well as connection to major tidal channels as approach channels. Judging from the different configurations, it can be assumed some alternatives would offer better hydrodynamic conditions, such as lower tidal velocities and sheltering from dominant wind and wave direction. However, this is not further included in the overall evaluation.

Simulation and evaluation Alternative designs are subsequently simulated, by adding the design in the validated model setup. Finally, the performance of each scenario is evaluated, based on the set criteria in the analysis. This is done by first determining the relative performance of each scenario for a the criteria. Table 5.1 shows the set criteria and corresponding procedure to evaluate the performance. In order to capture the relative importances of an ecotope type to preferred shorebirds habitat, a weight factor was introduced (see section 4.3.4). Therefore, the preservation and development of more high-value ecotopes results in a better performance. Subsequently, these relative performance values are than assigned a score, from worst to best performance, ranging from $0 \sim 6$ respectively. Some alternatives initially lead to a loss of valuable ecotopes, but could result in a higher siltation rates and subsequent growth of valuable ecotopes. This makes it possible that a certain configuration score low on preserving valuable ecotopes, but obtain a higher score in developing new ecotope area over time. Final evaluation will be further discussed in section 6.2.

5.2. Alternative reclamation scenarios

Previous findings on existing ecotopes indicated the importance of the intertidal mudlfats at Yaosha shoal. The full extent of the original proposed Tongzhou Bay port (Nantong Port Authority, 2013) will result in the total reclamation of these high-value mudflat areas and inevitable loss of habitat (Figure 5.2). As such, several smaller alternative configurations for the Tongzhou Bay port were designed based on the original port design. These contain alterations in overall shape, extent and combination of different port terminals within the original port planning. Since the main interest is the development of the Tonghzou Bay system as a whole,

Criteria	Scoring procedure
Preserve initial ecotope	$Y_{preseverd} = \sum \left(\widetilde{Y}_{preserved,n} \cdot f_{eco,n} \right)$
Enhance ecotope growth	$Y_{growth} = \sum \left(\widetilde{Y}_{growth,n} \cdot f_{eco,n} \right)$
Provide potential port area	$Y_{port} = \left(A_{port} / A_{port,max} \right)$

Table 5.1: Procedure for determining performance scores for each criteria. Here, $\widetilde{Y}_{growth,n} = g_n / g_{max,n}$, g_n = relative growth w.r.t. the reference case for each ecotope n, $f_{eco,n}$ = ecotope weight factor and $\widetilde{Y}_{preseved,n} = q_n / q_{max,n}$, q_n = initial preserved ecotope area w.r.t. the reference case for each ecotope

smaller port basins are not considered within the configurations.

Two reclamation strategies are explored, namely the partial reclamation of the Yaosha shoal and Lengjiasha shoal.

The Yaosha shoal holds most of the valuable ecotopes (*e.g.* mid- and low-range littoral)(Figure 4.17). Therefore, full reclamation as in the original design is not preferable. To asses if reclamation of the Yaosha shoal could benefit the development of valuable ecotopes, several alternative designs were made based on the original reclamation contours. A total of 4 scenarios were conceived as shown in Figure 5.2 ($v2$, $v10$, $v9$ and $v11$). Only part of the Yaosha shoal is reclaimed in order to preserve as much of the original high-value ecotopes as possible. The reclamations are adjacent to either the XMH channels (*e.g.* $v11$ and $v2$) or the upper SSH channel ($v2$, $v9$ and $v10$), allowing large berthing areas on the natural tidal channels. Some of the variants are designed to look into the effect of connecting the reclamation with the mainland ($v10$, $v11$) or keeping it open for tidal flow to pass around the reclamation.

The second set of alternatives are designed to investigate the effect of reclaiming the Lengjiasha shoal. Multiple configurations were examined, which are also based on the original port design contours. During preliminary assessment on short-term hydrodynamic results, it was found that by extending the end of the original extend of the terminal on the Lengjiasha shoal, a low hydrodynamic zone is created on the seaward side of the reclamation. Finally, 3 scenarios were selected for a full morphodynamic simulation and are further assessed (Figure 5.2) ($v7$, $v8$ and $v12$). These are designed as offshore reclamations of either south or north side of Lengjiasha shoal. Initially, no significant high-value ecotope zones are present at this region. It is therefore interesting if these offshore configurations are effective in trapping sediments, thereby promoting siltation and growth of these ecotope at these shallow areas.

5.3. Scenario results

Instead of treating all individual results, this section will elaborate on the siltation results and ecotope map creation of a single representative configuration. First, the calculated siltation patterns are elaborated. Next, an ecotopemap is constructed for the initial and final situation for the alternative reclamation.

5.3.1. Effect on siltation

As a representative design, the selected alternative port configuration consists of an offshore partial reclamation at the north side of the Yaosha shoal (v9). Guiding principle of the design is trapping sediments over the Yaosha shoal, by blocking tidal current and sediment fluxes (as found in section 4.2) at the northside of the shoal. Furthermore, this design looks into the effect of keeping a open connection with the mainland in order to allow ebb tidal volumes to leave the shoal via two routes; the southside of the shoal and northwards through the preserved opening between the reclamation and the coastline.

Figure 5.3 show the calculated siltation at Tongzhou Bay after 8 years of morphologic development for the reference case and port configuration $v9$. The siltation patterns in case of port configuration $v9$ show strong siltation at the edges of the shoals and indeed at the enclosed section of the Yaosha shoal. Comparing these patterns with the predicted siltation for the reference case confirms the positive effect of this configuration on trapping additional sediments at the backside of the Yaosha shoal. Similar to the reference case, heavy erosion takes place at the main tidal channels. However, strong erosion patterns can also be observed at the shoal itself. This can be understood as the the result of concentrated ebbtidal flow. In this configuration, the northside of the Yaosha shoal is reclaimed and the tidal volume is restricted to retreat during ebbtide. As a result, the return flow during falling tide becomes more focused and slowly forms new creeks and channels through the new acquired mudflats. Figure 5.4 show the mean tidal current patterns at Tongzhou bay for

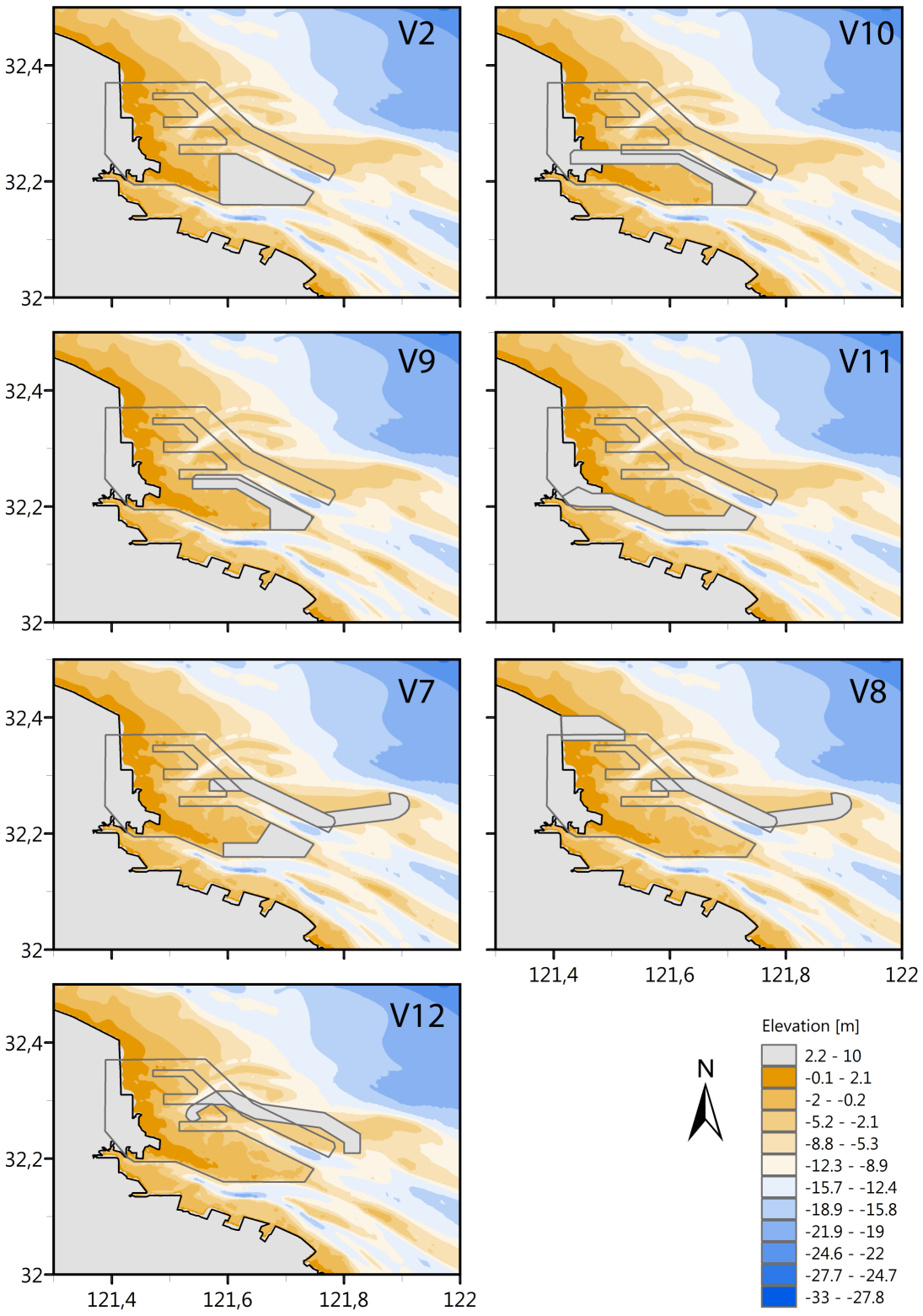

Figure 5.2: 7 final selected alternative port designs for the Tongzhou Bay port after several iterative design cycles. Indicated is the original port design as proposed by the Nantong Port Authority (2013)

configuration $v9$. Similar tidal fluxes can be identified as in the reference case, such as the net influx of tidal waters at the entrances of the main tidal channels and a bypass current over the Lengjiasha shoal. Additionally, a strong outward flux is present at the Yaosha shoal, close to the reclamation, indicating a newly formed ebb tidal channel.

5.3.2. Effect on ecotopemap

Previous results show the effect of the alternative reclamation on the mean tidal current and siltation patterns. As a result of this adaptation, the extent and development of ecotope areas will change as well. In order to examine this effect, an ecotope map is constructed following the same procedure as for the reference case. Figure 5.5 shows the ecotope maps for the initial situation and after 8 years of development in the case of configuration $v9$.

The initial ecotope map shows similar features with respect to the ecotope map of the reference case. Aside the reclamation of the northside, most of the high-value ecotopes (*e.g.* mid- and high-range littoral zones) are preserved. After 8 years of morphodynamic development, the siltation at the backside of the Yaosha shoal can also be recognized in the transition of low-range littoral to mid-range. Some of these areas are even developed further into high-range or supralittoral, indicating the lower rate of inundation over time at these regions. The formation of the ebb tidal channels can be seen as well. The initial low-range littoral area at the south side of the shoal, is stretched northward due to the continuous scouring and new tidal channels are formed. Aside the scouring, these regions also shift from low-dynamic into high-dynamic regions, signifying the higher flow velocities over a spring-neap tidal cycle. Opposite effect can be seen at the Lengjiasha shoal, were the shallow sublittoral zone shifts from a high- to low-dynamic conditions. Apparently, the reclamation of the northside of Yaosha also leads to lower mean velocities in the adjacent Sanshahong channel and higher dynamic conditions along the Xiaomiaohong channel.

Further comparison in ecotope development with the reference case and other configurations is discussed in section 6.2. A full overview of all ecotope maps for each configurations can be found in Appendix D.

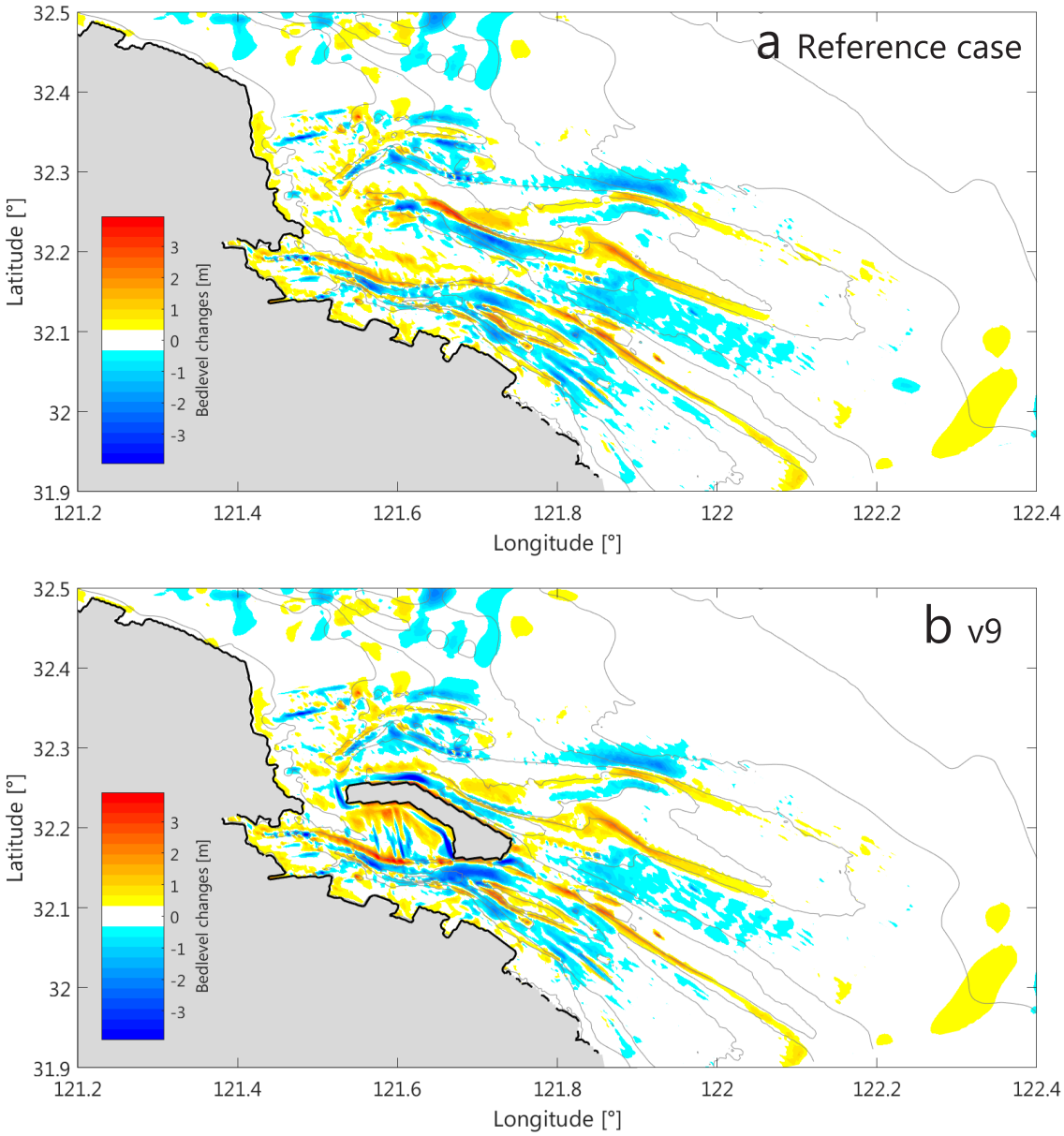

Figure 5.3: Siltation patterns for 8 years of morphological development at Tongzhou Bay for the reference case with no further reclamations (a) and port configuration $v9$ (b)

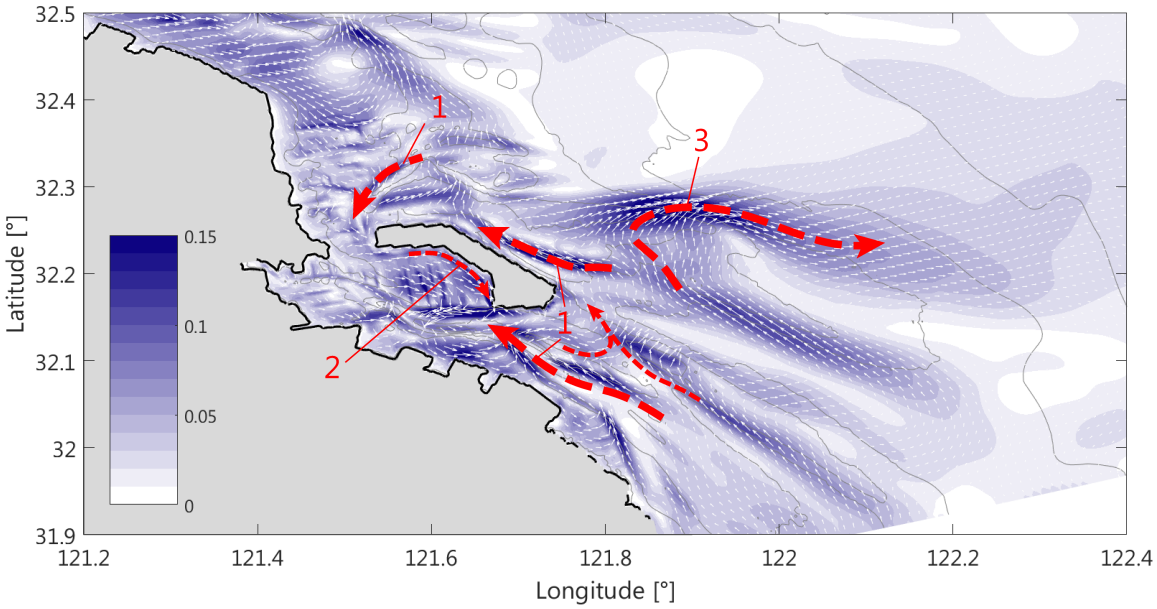

Figure 5.4: Mean tidal currents at Tongzhou Bay for configuration $v9$. Similar to the reference case, the model shows inward fluxes at the entrance of the main channels (1) the large bypass over the Lengjiasha shoal (3). Additionally, a strong return flux can be recognized attached to the inner edge of the reclamation (2), indicating the focusing of the ebbtidal volumes and the formation of an ebbtidal channel

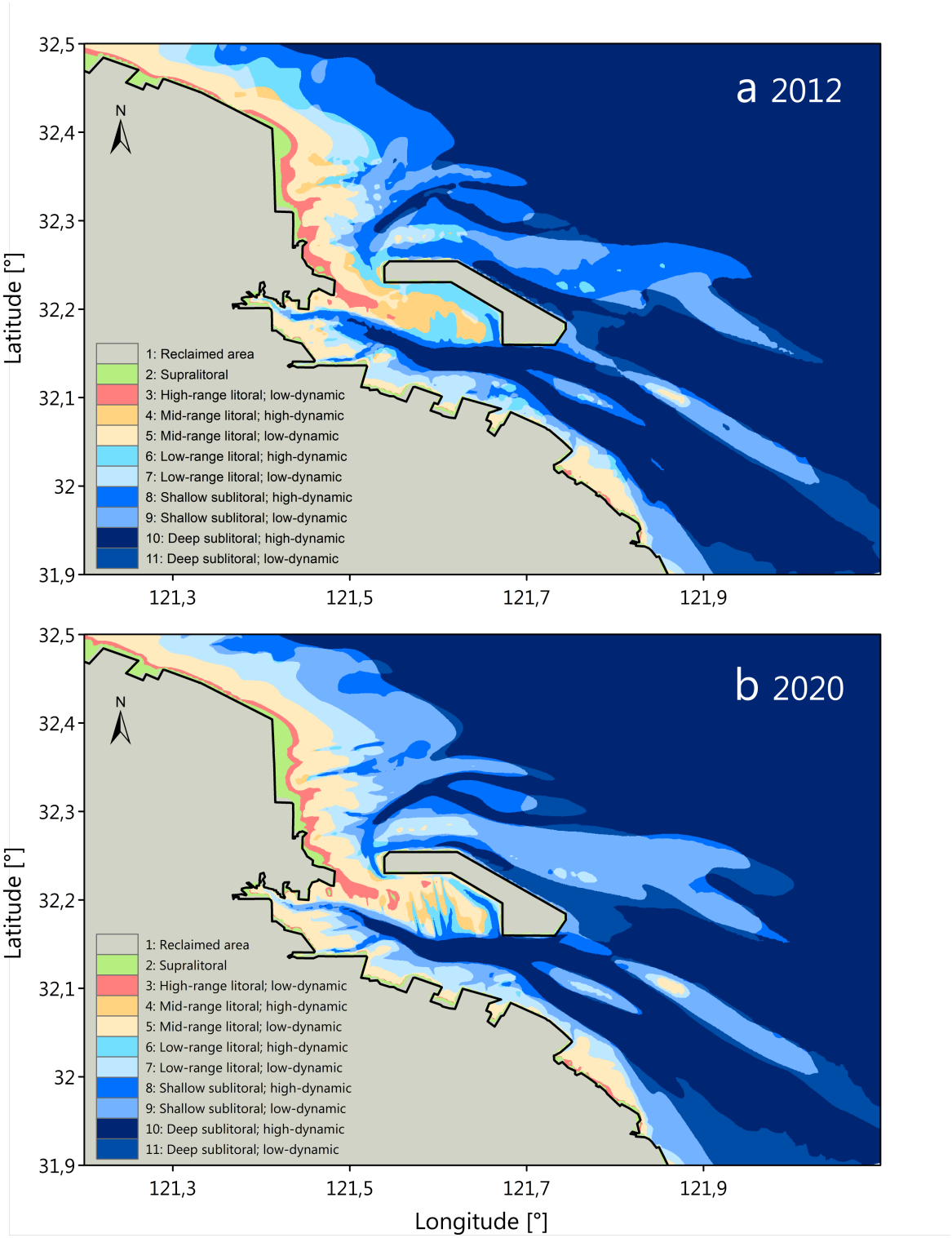

Figure 5.5: Initial ecotope map (a) and after 8 years of development (b) for configuration v9

6

Discussion

This study used the previous developed numerical model as described by Yao (2016). Based on literature and data analysis extra fraction was added and several simplification were made which have effect on sediment transport. In this chapter, calculated results are reflected upon and observed behavior is further interpreted. Calculated ecotope development is examined and each alternative design is evaluated.

6.1. Tongzhou bay characteristics

The calculated transport and siltation patterns have been crucial in the understanding of Tongzhou Bay dynamics and determining ecotope development. Previous model results showed several characteristic properties in tidal currents and transport. In this section the calculated current, transport and siltation patterns are interpreted and further evaluated.

6.1.1. Residual current and transport

The main current and transport patterns were elaborated in section 4.2. The model showed that a residual flow can be found in the XMH and SSH channels. Since the model is not explicitly setup with residual currents, the net landward flux of tidal volume and sediments is generated by local flow asymmetries. Closer examination of this residual flow is done by taking a closer look at the calculated current velocity and depth-averaged suspended sediment transport through the major tidal channels. Here, the flow pattern is mostly bidirectional. This signal can be made visible by changing the coordinate system relative to the flow direction and neglecting the several order smaller perpendicular flow component. Figure 6.1 shows the tidal current and sediment transport for N1 and N2 inside Xiaomiaohong and N7 inside Sanshahong channel.

The current transition from ebb to flood or in reverse direction, occurs approximately at low water or high respectively, indicating the tidal wave having a standing character. The current velocity at stations N2 and N7, show a skewed signal with the transition from ebb to flood, or low water slack (LWS) being shorter than from flood to ebb, or high water slack (HWS). This tidal asymmetry is typical for 'flood dominant' regime and signifies the net landward transport of fines. As the flow transition from flood to ebb flow is longer, sediments that are being picked up during flood have more time to settle. Therefore, less particles are in suspension and are being transported during ebb. This results in a net import of fines through the tidal channels. The opposite is true for station N1, where the low water slack is longer than the high water slack, indicating a 'ebb-dominant' regime and an export of fines.

Aside the asymmetry in slack water duration, the tidal current signal shows an small difference in peak tidal velocity, where flood tide is somewhat larger than ebb peak velocity. Cause of this peak velocity could be generated by the smaller cross-sectional area during flood, where the flow has to increase in order to have the same discharge. This is relevant for sediment transport as higher velocities mean higher transport rates during flood than ebb tide. In combination with the difference in flood/ebb duration, suspended particles are being transported over a longer distance during flood that during ebb, showing a net import of sediments. Similar patterns in peak velocity asymmetry was found by (Huang et al., 2015; Wang et al., 2012b; Zhang et al., 2013).

However, these results only depict the averaged current-induced sediment concentrations. In case of wind-waves, more entrainment on the shoals will occur. Also influence of residual currents, such as wave-

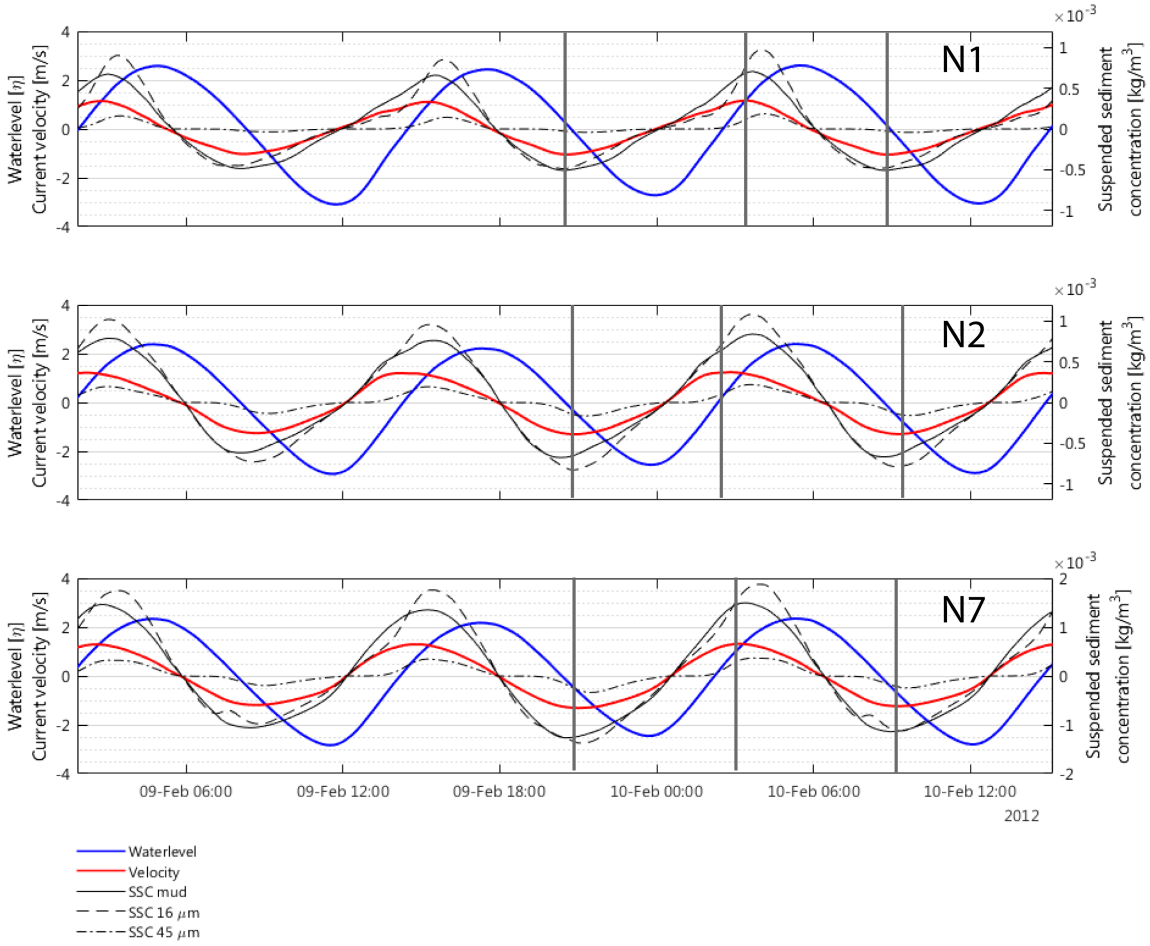

Figure 6.1: Asymmetry signal in waterlevel, current velocity and sediment transport at three locations. Indicated are 3 sediment fracions, namely mud(−), 16 μm (−−), and 45 μm(−.−) fraction at 3 stations at Tongzhou. other fractions show same but stronger pattern as 45/mum and are not shown here

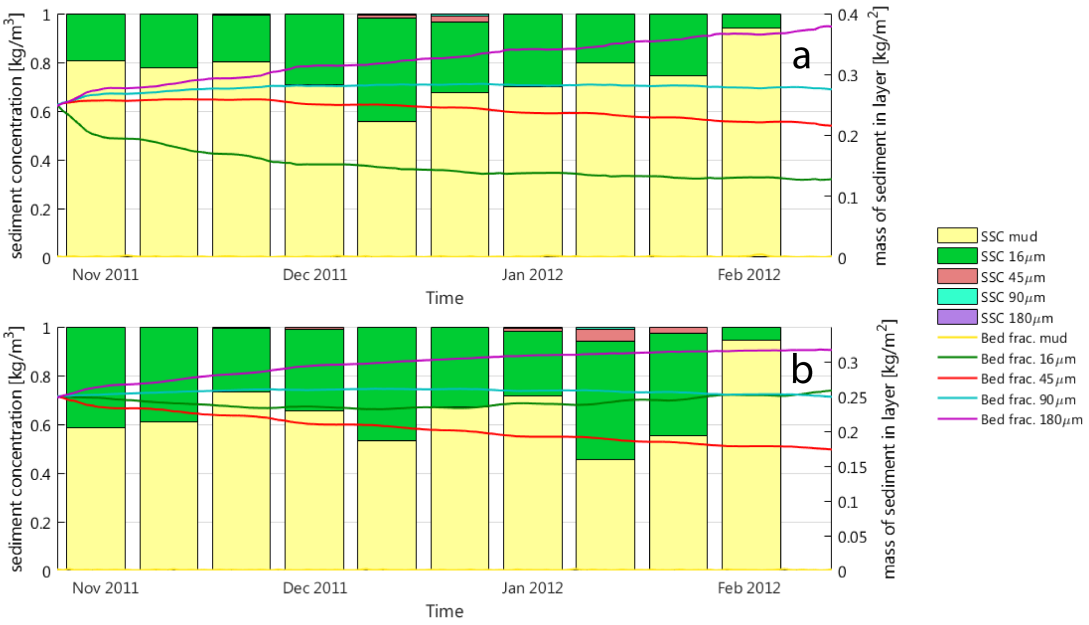

Figure 6.2: Composition of the suspended concentration and the development of each fraction within the bedlayer inside the Xiaomiaohong channel (a) and on the Lengjiasha shoal (b)

induced residual current Xu et al. (2014) are not included in the model.

6.1.2. Added cohesive fraction

In section 3.2.2, an additional mud fraction was introduced in order to match the smaller suspended grainsize and measured concentration. The parameters were chosen as such that the fraction was very easy to entrain, reminiscent to fluid mud layers as described by Shi et al. (2016); Yang et al. (2016). Model verification gave a better approximation of the suspended sediment concentration. As a result, this fraction takes up most of the suspended transport calculated by the model and does not show significant siltation at the Tongzhou domain.

Figure 6.2 shows the contribution of each fraction on the total suspended sediment concentration inside the Xiaomiaohong channel and at the Lengjiasha shoal. The available mass of each fraction inside the bedlayer is shown was well. It can be seen that the newly added mud fraction and 16 μm fraction make up most of the suspended concentration for both inside the tidal channels and on top of the shoals. However, the bedlayer composition show a different trend over time. In the tidal channels, strong hydrodynamics cause a higher transport capacity and small particles are being entrained more easily. As a result, the bedlayer is becoming more coarse over time. The opposite can be seen at the Lengjiasha shoal where most of this fine material is deposited, making the overall bedcomposition finer. This corresponds with other studies at the average grain size difference found over the Tongzhou domain (Gong et al., 2017; Xu et al., 2016). More on the sorting of bedlayer sediment in the following section.

6.1.3. Sorting of bedsediments

Most of the morphological development occurs as siltation at the shoals and scouring inside the main channels. The calculated siltation is further looked into by examining the bed composition at the end of 8 years of morphological development. Figure 6.3 show the average grainsize of the total bed. Initially, this consists of 25% for each fraction, except the 180 μm and mud fraction which are 0.2% and 24.8 % respectively. This initial composition gives an average grainsize of $\pm$ 82 μm. After 8 years of morphological development, the bed composition at the intertidal shoals has become finer and the bed inside the channels coarser. Previous examination of the suspended sediment concentration showed that the finer particles make up most of the calculated transport and are therefore deposited at the higher elevation such as the intertidal shoals. The coarse fractions are eroded less, and make up less of the overall transport through the channels. At the end of

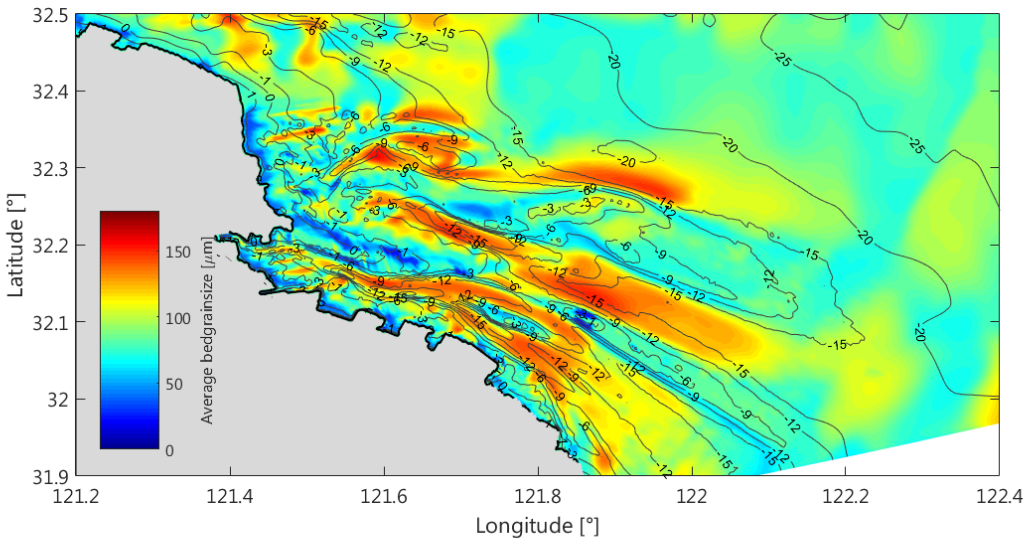

Figure 6.3: Calculated average grainsize inside the bedlayer after 8 years of morphological development

simulation, the average grainsize inside the channels varies form 120~150 μm an on the shoals from 10~80 μm.

6.1.4. P-A relation

The model is set-up with a measured bed topography and hydrodynamic boundary conditions. Due to this setup, the model will adjust this initial set bathymery to the hydrodynamic forcing to find a new dynamic equilibrium. As a result, the predicted morphodynamic change could be related to this adjustment instead of realistic siltation behavior.

In order to get a reference on the calculated morphodynamic behavior, the relation between bathymetry and the hydrodynamic forcing is examined by means of the empirical relation between the channel flow cross sectional area, A and the tidal prism, P. For similar tidal basins properties, such as tidal features, sediment availability and sediment types, the theoretical PA-relation remains constant (Stive et al., 2011) Subsequently, the $P-A$ relation as calculated by the model is referenced with previous studies on similar tidal inlets along the East China Sea and Tongzhou Bay (Gao and Collins, 1994).

Along the Xiaomiaohong and Sanshahong tidal channels, a total of 24 consecutive cross-sectional areas were defined. The reference case, which represents the situation in 2012, simulated a period of 2,5 months morphological time with one hour output interval. Figure 6.4 shows the relation of the calculated tidal prism and cross-sectional area at the tidal channels (*e.g.* XMH, SSH and Northern inlet). The calculated prism suggest a relation with the corresponding cross-sectional areas inside the tidal channel. Drawing the best fitted regression line, yields the expression for this empirical relation of $A_e = 3.0\text{e}{-5} \cdot P^{1.0208}$, with a regression value of $R^2 = 0.88$. Gao (1988) performed measurements at 11 tidal inlets situated on the ECS and found similar values. Zhang (1995) expanded this with measurements at 15 tidal inlets along the Yellow and Bohai sea. Both best regression expressions are shown in Figure 6.4 as well.

As these values are not verified with field measurements, this comparison at least gives a reference on the relation between the tidal volumes and the channels depth as calculated by the model. It is therefore deemed the model does not show large initial unrealistic adjustments to reach a new dynamic equilibrium.

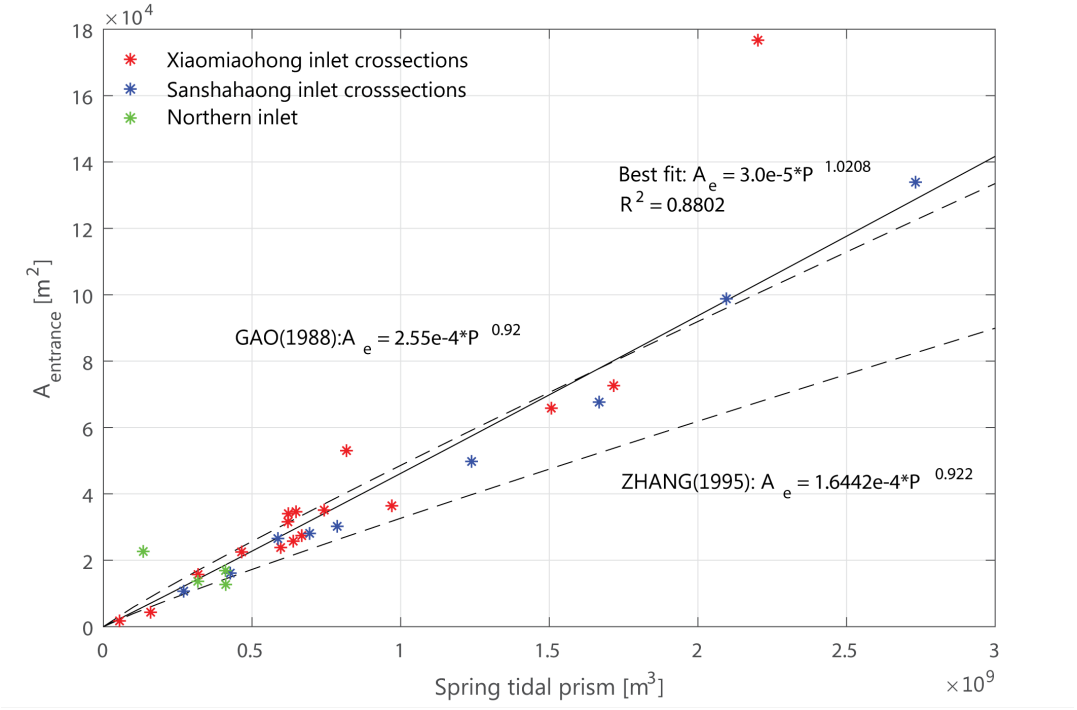

Figure 6.4: PA-relation of several intersections along the three main tidal channels at Tongzhou bay. Smaller tidal channels, such as the northern inlet support smaller tidal volumes and have smaller cross-sectional areas. Therefore, these can be found closer to the origin. Main channels of Xiaomiaohong and Sanshahong have larger volumes.

6.2. Ecotope development

In chapter 5, alternative port configurations and design criteria were described. With the calculated morphodynamic development, the ecotope zones change as well. To asses the relative performance of each variant, the development of these ecotopes is determined and compared with the reference case. For simplicity, the hydrodynamic classification is included in the littoral classes, resulting in 6 final ecotope types (*e.g.* supralittoral, high-, mid-, low-range littoral, shallow and deep sublittoral).

Figure 6.5 shows the development during 8 years for each ecotope area and configuration. All configurations show a strong increase in supralittoral zone. It can be seen that the initial supralittoral area is already larger than the reference case. This is due to class boundaries and the relative coarse schematisation in the model. Reclamations are schematized in the model as higher elevated areas (+8 MSL). As a result, some of the area in this steep increase is classefied within the boundaries of the supralittoral class. It is therefore deemed that this initial increase in supralittoral ecotope is not caused by morphodynamic development and will not be included. The high-, mid- and low-range littoral zones for each configuration, also show an initial difference relative to the reference case. This due to the location of the port reclamation and therefore initial loss of ecotope area. For instance, configuration $v11$ shows a large decrease in high- and mid-range littoral, as most of the extend of this reclamation is at these ecotope zones at the southside of Yaosha (see Figure 5.2). Several scenarios show an strong shift in the initial sublittoral (shallow and deep). This is most notable for configuration $v7$ and $v8$. Within these configurations, the southside of the Lengjiasha shoal is reclaimed and the adjacent tidal channel is flattened. Most of these regions are classified within shallow sublittoral zone, which are reduced significantly with respect to the reference case. The flattening of the tidal channel in these configurations also lead to a strong increase in deep sublittoral.

Aside the difference in initial ecotope area, differences in growth rate between different configurations can be recognized as well. This is further examined by comparing the cumulative growth in ecotope for each configuration, as shown in Figure 6.6. Again, the hydrodynamic classification is combined with the littoral classification, resulting in 6 total ecotopes.

Examining the results of overall ecotope area, growth and individual ecotope maps (see Appendix D),

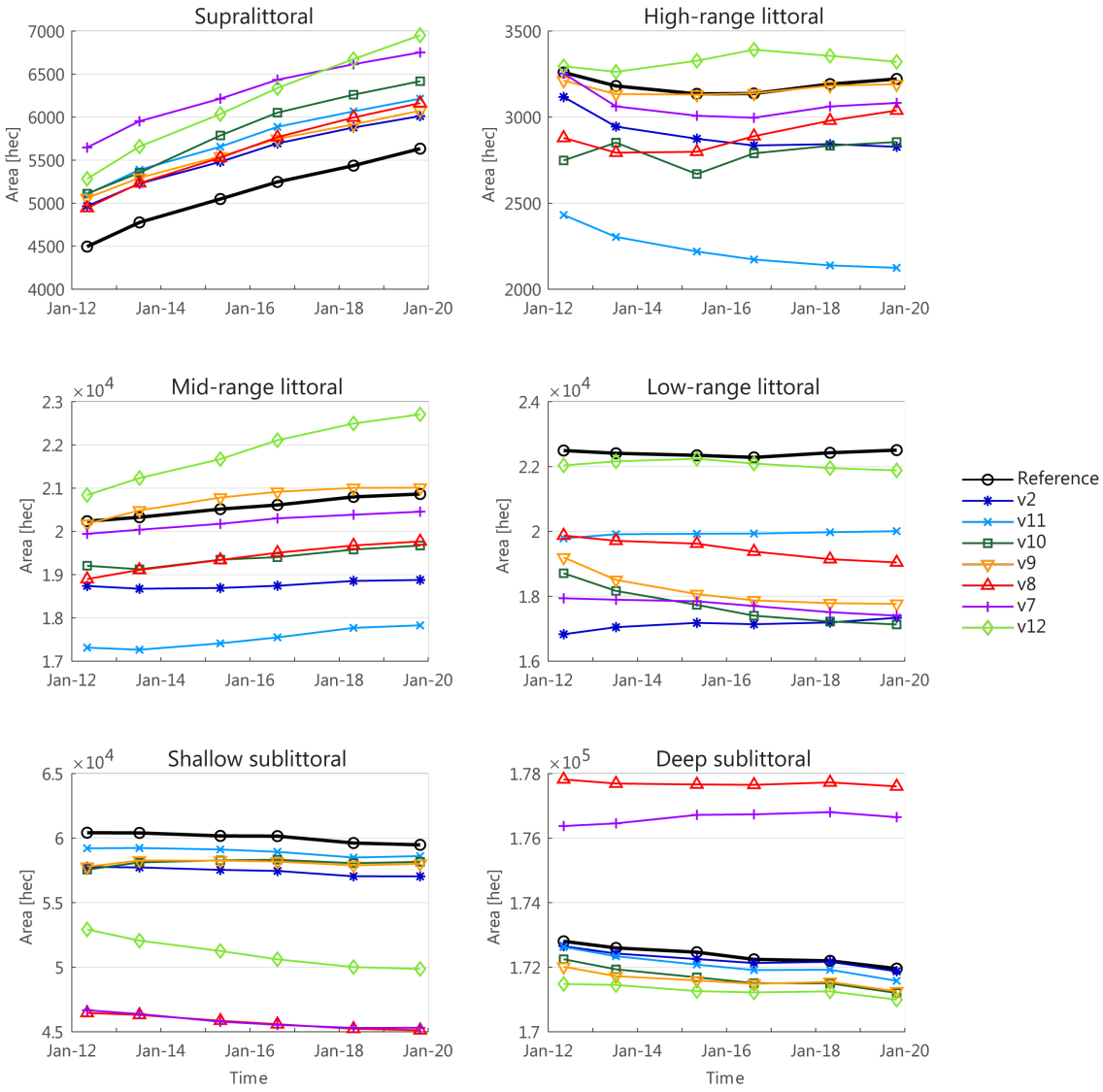

Figure 6.5: Initial ecotope areas and development for all scenarios after 8 years of morphologic development. The reclamation of sections of Tongzhou bay lead to the initial loss of several ecotopes. Following this reclamation, development of these ecotopes show a varying response relative to the reference case

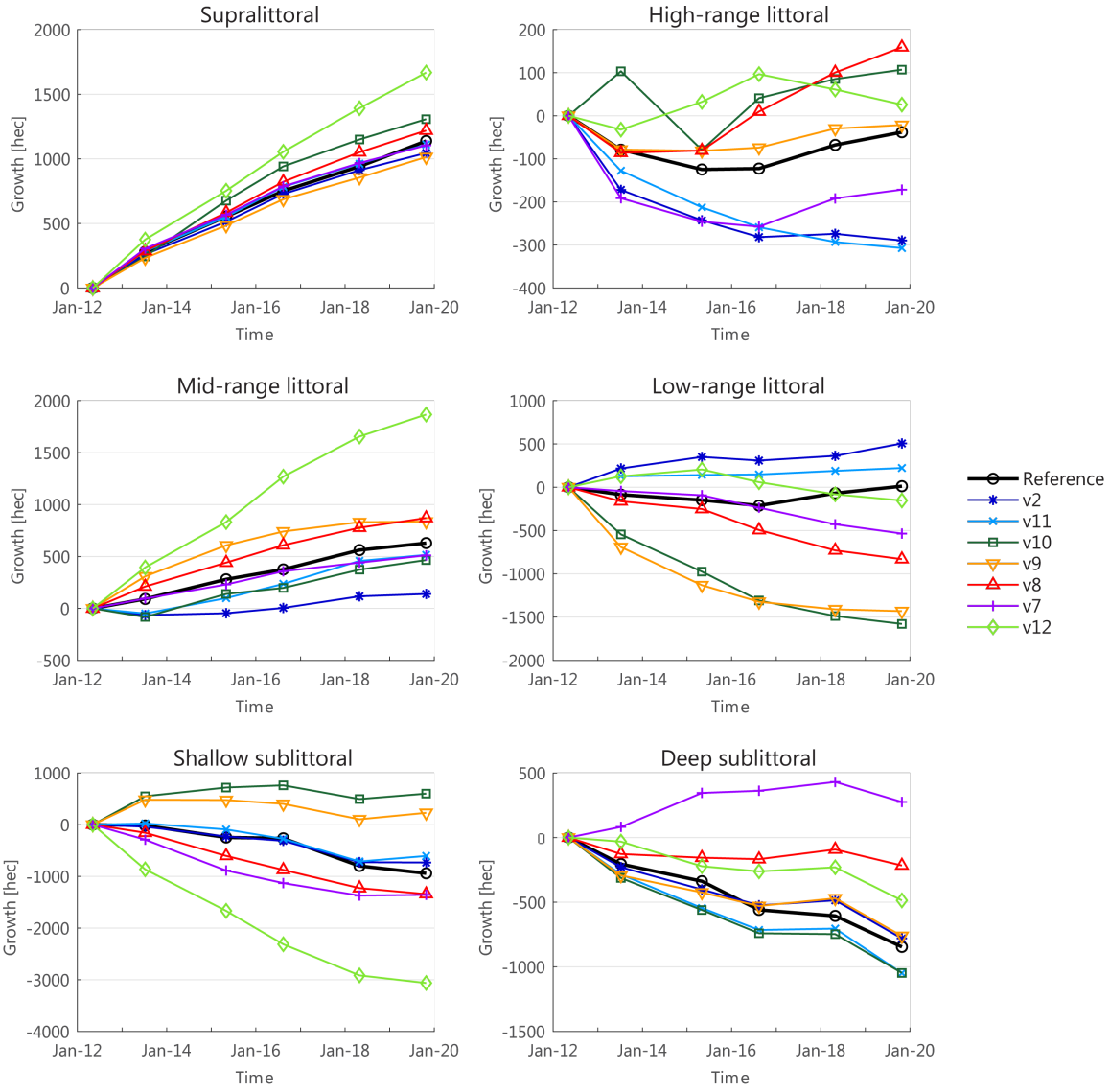

Figure 6.6: Cumulative growth/decline in area for each ecotope type for all scenarios after 8 years of morphologic development

several observations can be made:

1. The continuous supply of fine material and calm hydrodynamic conditions on top of the mudflats lead to the steady increase of supralittoral (only inundated during extreme waterlevels) and high- and mid-range littoral (inundated during 25 ~ 40% of a tidal cycle) zones. Each littoral zone supplies the higher elevated zone. Turning point of this trend occurs at the shallow sublittoral, which supplies both the low-range littoral and the deep sublittoral. This division in transitioning of ecotopes indicating the scouring of the channels and (horizontal and vertical) growth of higher littoral zones.

2. Most sediment is supplied through the Xiaomiaohong channel at the south side of Yaosha. By reclaiming the south side of Yaosha ($v11$), the northward transport from the Xiaomiaohong channel is blocked. This results in lower siltation rates at the higher elevated littoral zones relative to the reference case and a lower growth in ecotopes at the Yaosha shoal.

3. By reclaiming the northside of Yaosha ($v9$, $v10$), tidal flow and transport can still reach the Yaosha shoal and is blocked at the backside of the mudflat. This leads to higher siltation rates and development of higher elevated ecotopes, relative to the reference case. Since flow cannot exit over the shoal, deep ebbtidal channels are formed due to the focusing of ebb-tidal flows. In case of an open connection with the mainland (v9), less deep and dynamic channels are formed. This is due to the possibility of high water volumes leaving the Yaosha shoal through multiple sides, thereby causing lower velocities and lower scouring of these regions.

4. Reclaiming of north- or southside of Yaosha with a closed connection with the mainland, leads to reduced velocities inside the adjacent tidal channels. This can be explained as the reclamation reduces the floodplain area and therefore the capacity for tidal volumes. These lower velocities result in less scouring of the channels and a decline in deep sublittoral area over time. The reclamation of Lengjiasha causes the flow within the Sanshahong channel to be canalized and deep sublittoral ecotopes increases.

5. By reclaiming the southside of the Lengjiasha shoal, low dynamic conditions occur at the seaward side of the reclamation. However, siltation rates do not increase. By blocking the north side of the shoal, transport is blocked in a similar way as at the Yaosha shoal and siltation rates increase. This leads to the overall best performing scenario in terms of conserving and enhance natural growth of valuable ecotopes.

6.3. Scenario evaluation

A total of 6 alternative port reclamations were designed based on 3 criteria for ecologic and port utility requirements. These criteria were based on the preservation of high-value ecotopes, stimulation of the accretion of these high-value ecotopes and create potential port construction area. With previous results on the extent and development of these ecotopes, each scenario can be evaluated. Each scenario receives a score based on their performance.

Table 6.1 shows the performance matrix, based on the relative performance per criteria. In order to combine the individual performances, each variant is assigned a relative score. Finally, these scores are added together to form the final score for each scenario. As such, scenario $v12$ has the highest score (14), followed by scenario $v7$, $v2$ and $v8$. Scenario $v12$, performs best on preserving ecotope and stimulates the growth of these ecotopes. Due to the reclamation of the Lengjiasha shoal, all initial high-value ectope is preserved and overall dynamics are low, thereby enhancing the growth of mid- and low-range littoral. The offshore reclamation however does not score very high for potential port development, as the area is smaller than other scenarios and overall connectivity with the mainland is difficult.

Scenario	v2	v11	v10	v9	v8	v7	v12
Growth of high-value ecotope	-0.009	0.024	-0.448	-0.380	-0.197	-0.277	0.185
Preservation of high-value ecotope	0.775	0.768	0.793	0.822	0.769	0.777	0.834
Potential port development area	0.694	0.521	0.585	0.451	0.925	1	0.565
Assigned score	4	5	0	1	3	2	6
	2	0	4	5	1	3	6
	4	1	3	0	5	6	2
Total score	10	6	7	6	9	11	14

Table 6.1: Performance matrix and overall assigned score for each scenario. Total score is the summation of the indivdual variant score on each set requirement in the design cycle

7

Conclusions

7.1. Conclusions

In order to conclude on the findings of this thesis, the previous formulated research sub-questions and main question are stated again and will be answered accordingly.

Which processes are governing for flow and transport characteristics at Tongzhou Bay?

In order to identify the driving processes at Tongzhou Bay, use was made of the Jiangsu Regional Model as described by Yao (2016), which proved to be an effective tool in modeling tidal patterns and sediment transport at the Tongzhou bay domain. Validation of the model showed good confrontation between calculated and measured tidal features. Also sediment concentration during spring tide was reproduced quite well. However, the model calculated significantly lower concentrations during neap tide. Several causes were explored, namely the inclusion of an additional cohesive fraction with easy-entrainable properties and the effect of severe measured wind conditions, indicating the precedence of wind-induced waves during neap tide. Preliminary model results showed better concentrations during both spring and neap tide. The effect of waves increased this concentration even more leading to overall better results. During spring tide, overall sediment concentrations are mainly governed by tidal currents, whether during neap tide, the effect of waves can become more significant.

During a spring-neap tidal cycle, the model shows a net residual flow through the main tidal channels. Closer examination of this net flow pattern showed this is mainly caused due to local depth-induced flow asymmetry, consisting of slack water and peak flow asymmetry. Mean tidal volumes through the Xiaomiaohong channel are directed landward and eventually over the Yaosha shoal, where they collide with the tidal volumes from the Sanshahong channel and northern inlet. The mean sediment transport follows these current pattern quite closely. At the Yaosha shoal, the sediment is mostly supplied by the Xiaomiaohong channel and is transported over the shoal in south-north direction. During low currents, these sediments are deposited at the intertidal mudflat area, such as the Yaosha shoal and upper reaches around the tidal channels. Severe erosion, mainly occurs inside the main tidal channels. This is mostly due to the high bidirectional flow inside the channels.

What types of ecosystem exist at Tongzhou Bay?

An ecotope map was developed for Tongzhou Bay, applying ZES.1 method, as described by Bouma et al. (2005). This method can be used to quantitatively asses the potential occurrence on certain ecosystems based on abiotic characteristics, as provided by the model. Most of the offshore depths and tidal channels can be classified in to deep and shallow sublittoral, representing low regions that are always inundated during a spring-neap tidal cycle. High hydrodynamics conditions mostly occur in these regions. The tidal flats are classified into the low, mid and high-range littoral zones, determined by the rate of inundation of the regions. High and low hydrodynamic condition alternate at these regions, depending on the local tidal current. Upper reaches around the mainland are classified into supralittoral regions, which do not become inundated during an average spring-neap cycle. Verification of this map was based on the homerange of two satellite-tracked

migratory bird species, showing a significant coincidence with mid- and low-range littoral zones. This was further confirmed by literature on the brood and forage behaviors of these shorebirds species. High littoral zones are more suitable for nestbuilding and brooding as these regions are less often inundated. Mid and low-range littoral zones provide preferable foraging grounds. As such, the mid and low-range littoral zones are deemed most valuable ecotopes for the support of these two species.

What is the state of development of these ecosystems without anthropogenic influence ?

The calculated siltation rates at the higher-elevated mudflats lead to the continuous growth of the supralittoral and littoral zones. Similarly, low-range littoral is transfered to mid-range littoral. Most of the development takes place at the Yaosha shoal, where most of the siltation occurs. Heavy scouring of the tidal channels, lead to an increase in high-dynamic sublittoral. The shallow sublittoral zone loses relatively the most acreage as it is transfered to either low-range littoral due to siltation or deep sublittoral due to scouring.

What is the impact of alternative port reclamations on this ecosystem development ?

The construction of the original Tongzhou Bay port design would lead to the loss of nearly all high-value ecotopes at the Tonghzou bay. Several alternative port configurations were designed, which aimed at satisfying 2 ecological and one port criteria. These included preserving as much of the initial ecotope areas as possible, enhance growth of these areas with respect to the reference case and providing potential area for future port development. These alternative configurations were iteratively designed in a coarse to fine approach.

In order to enhance growth of ecotope area, the alternative designs aimed at increasing the siltation rates over the intertidal mudflats. Previous model results showed the main sediment flux is directed over the Yaosha shoal in a south-north direction. By partly reclaiming the southside of the shoal, this flux is blocked from flowing over the intertidal area and lower ecotope development was found. By reclaiming the northside of the Yaosha shoal, this flux is blocked on the backside of Yaosha, effectively capturing the supplied sediments and increasing ecotope development at the Yaosha shoal. Additional impacts were the focusing of ebb tidal volumes due to the limited routes of leaving the intertidal area. Strong erosion occurred over the mudflat and new channels were formed. By making reclamations offshore, multiple openings remain for the volumes to leave, leading to lower erosion rates. Similar patterns are found at the Lengjiasha shoal. Construction of Lengjiasha showed the canalization of the Sanshahong channel and the creation of more deep sublittoral zones and overall higher dynamics. A calm region was modeled behind an extended variant of the Lengjiasha reclamation. This does not lead to siltation as sediment is also blocked from the south side. The reclamation of the northside of the Lengjiasha shoal leads to similar results found at the Yaosha shoal.

Finally, the main research question is answered:

Could the reclamation of alternative port configurations for the Tongzhou Bay port benefit the development of valuable ecosystems at Tongzhou Bay?

Gaining a better understanding of the governing processes on the natural development of Tongzhou Bay can effectively be used in the design of alternative port reclamations. The use of a ecotopemap, showed the Yaosha shoal to be of high value. The original plans for the development of Tongzhou Bay lead to the certain loss of this habitat. Moreover, these large scale reclamations will affect the governing processes in the natural development of these areas. Several partial reclamation scenarios were iteratively designed that aims at using these processes in order to enhance the natrual growht potential habitat. It is found that by capturing sediment transports over the Yaosha shoal, higher siltation volumes and ecotope growth can be accomplished. However, alternating in flow patterns could still weaken this effect. Partial reclamation of more offshore regions, such as the Lengjiasha shoal, showed better results as it leaves the vital Yaosha shoal unaltered and reduces local hydrodynamics. This resulted in the optimum evaluated scenario, as it preservers most of the initial high-value ecosystem and enhances natural growth. However, port development at more offshore regions implies large difficulties in port operations and logistics with hinterland and industries.

7.2. Recommendations

From the conclusions drawn in the previous section, several recommendations are made for future endeavors.

The model only incorporates limited amount of processes that are present at Tongzhou Bay. For instance, large-scale residual currents that also drive sediments are not included. At a more local scale, processes that influence siltation and depositions, such as consolidation and vegetations effects were also not included. As these are crucial for typical mudflat accretion, it has to be determined how large this effect is on longterm natural development.

The Tongzhou Bay Model uses a larger model at its boundaries with 'online' nesting. This makes the model somewhat inefficient, as this procedure does not allow for multiple processing. Because of this, the simulation was restricted to 8 years of development, with the use of a morphological acceleration factor. This simplification could have unrealistic affected the presented siltation patterns and has to be examined in more depth. A more efficient model would lead to shorter runtimes and is more preferable for simulating longer timescales

The method of quantifying the ecosystem at Tongzhou Bay uses the ZES.1 method. This only shows a potential nich for the occurrence of certain habitat. The method requires to be verified with real life data in order to check whether the classification give reliable results. In this thesis, this is done based on two shorebird populations. Therefore, the constructed ecotopemaps should be validated with more species throughout the whole ecosystem.

This study provided a more insight in the driving processes for the morphological development of Tongzhou Bay. This should be used as input for designing more port configurations, based on multiple criteria from other disciplines as well. Including different needs and requirements increases the value of the design and can lead to more feasible options that could provide for ecosystem as well.

Bibliography

Allen, J., Somerfield, P., and Gilbert, F. (2007). Quantifying uncertainty in high-resolution coupled hydrodynamic-ecosystem models. *Journal of Marine Systems*, 64(1-4):3–14.

Baptist, M. J., van Eekelen, E., Dankers, P. J. T., Grasmeijer, B., van Kessel, T., and van Maren, D. S. (2017). Working with nature in Wadden sea ports. *Australasian Coasts & Ports 2017: Working with Nature*, page 40.

Barter, M. (2002). Shorebirds of the Yellow Sea: Importance, threats and conservation status. Technical Report 9, International Wader Studies 12, Canberra, Australia.

BirdLife International (2018). Great news for shorebirds! China to halt coastal land reclamation. https://www.birdlife.org/worldwide/news/great-news-shorebirds-china-halt-coastal-land-reclamation.

Borsje, B. W., van Wesenbeeck, B. K., Dekker, F., Paalvast, P., Bouma, T. J., van Katwijk, M. M., and de Vries, M. B. (2011). How ecological engineering can serve in coastal protection. *Ecological Engineering*, 37(2):113–122.

Bouma, H., de Jong, D., Twisk, F., and Wolfstein, K. (2005). Zoute wateren EcotopenStelsel (ZES.1). Voor het in kaart brengen van het potentiële voorkomen van levensgemeenschappen in zoute en brakke rijkswateren. Technical Report Rapport RIKZ/2005.024, Ministerie van Verkeer en Waterstaat.

Cai, F., Su, X., Liu, J., Li, B., and Lei, G. (2009). Coastal erosion in China under the condition of global climate change and measures for its prevention. *Progress in Natural Science*, 19(4):415–426.

Cai, F., van Vliet, J., Verburg, P. H., and Pu, L. (2017). Land use change and farmer behavior in reclaimed land in the middle Jiangsu coast, China. *Ocean & Coastal Management*, 137:107–117.

CCCC Third Harbor Consultants Co. Ltd (2012). Hydrological Analysis Report of Tongzhou Qianwan planning. Technical report, CCCC Third Harbor Consultants Co. Ltd, Shanghai, China.

Chan, Y.-C., Peng, H.-B., and Piersma, T. (2018). Personal communications.

Chen, K. (2013). Study on Characteristics of Flow and Sediment for Xiaomiaohong Tide Inlet in Radial Sand Ridges. *Applied Mechanics and Materials*, 405-408:1385–1389.

Chen, K. and Wang, Y. h. (2009). Effects of coastline changes on tide system of Yellow Sea off Jiangsu Coast, China. *China Ocean Engineering*, 23(4):741–750.

Chen, K. and Yu, L. (2011). The research of hydrodynamic mechanism of morphology revolution of the Xiaomiaohong tidal channel in radial sand ridges, Jiangsu Province, China. In *Proc. of 6th Int. Conf. on Asian and Pacific Coasts*, Hong Kong, China.

Chen, K., Zheng, J., Zhang, C., Wang, N., and Zhou, C. (2017). The evolution characteristics of main waterways and their control mechanism in the radial sand ridges of the southern Yellow Sea. *Acta Oceanologica Sinica*, 36(3):91–98.

Chen, L. and Zhang, Y. (2011). Analysis of the evolution on tidal flat and their reasons in Dongsha based on remote sensing. In *Proc. of Int. Conf. Spatial Data Mining and Geographical Knowledge Services*, Fuzhou, China. IEEE.

Chen, Y., Xie, D., Zhang, C., and Qian, X. (2013). Estimation of long-term wave statistics in the East China Sea. *Journal of Coastal Research*, 65:177–182.

China Daily (2017). Growing Jiangsu hub exploits proximity, relation to Shanghai. http://www.chinadaily.com.cn/cndy/2017-05/19/content_29409603.htm.

China Daily (2018). Reclaiming land to be restricted. http://english.gov.cn/news/top_news/2018/01/18/content_281476017712430

Cong, X. and Zhu, W. (2017). Research on the Influence of Reclamation on Water and Sediment Environment Offshore. *Journal of Water Resources and Ocean Science*, 6(4):55–60.

Cui, B. (2017). Impact of Large-scale Reclamation on Coastal Wetlands and Implications for Ecological Restoration, Compensation, and Sustainable Exploitation Framework. *S & T and Society*.

de Vriend, H. J., van Koningsveld, M., and Aarninkhof, S. (2014a). 'Building with nature': the new Dutch approach to coastal and river works. *Proceedings of the Institution of Civil Engineers - Civil Engineering*, 167(1):18–24.

de Vriend, H. J., van Koningsveld, M., Aarninkhof, S. G., de Vries, M. B., and Baptist, M. J. (2014b). Sustainable hydraulic engineering through building with nature. *Journal of Hydro-environment Research*, 9(2):159–171.

Deltares (2014). Delft3d-WAVE User Manual. Technical Report 3.05.

Deltares (2018). Delft3d-FLOW User Manual. Technical Report 3.15.

Deng, B., Wu, H., Yang, S., and Zhang, J. (2017). Longshore suspended sediment transport and its implications for submarine erosion off the Yangtze River Estuary. *Estuarine, Coastal and Shelf Science*, 190:1–10.

Ding, X. R., Kang, Y. Y., Ge, X. P., Li, Q., and Zhang, T. T. (2011). Tidal flat evolution analysis using remote sensing on Tiaozini flat of the radial sand ridges. *Journal of Hohai University (Natural Sciences)*, 39(2).

Economic Daily (2017). Jiangsu coastal cities rely on ecological advantages. http://district.ce.cn/zg/201709/19/t20170919_26100967.shtml.

Encyclopedia, B. (2018). Tongzhou Bay.

Fan, C., Li, R., Dai, L., Li, C., and Liang, L. (2015). Effects of tidal flat reclamation on wave field in Jiangsu coast. *Port & Waterway Engineering*, 12(No. 510):16–22.

Fan, D. (2012). Open-Coast Tidal Flats. In Davis, R. A. and Dalrymple, R. W., editors, *Principles of Tidal Sedimentology*, pages 187–229. Springer Netherlands, Dordrecht.

Fan, D., Wu, Y., Zhang, Y., Burr, G., Huo, M., and Li, J. (2017). South Flank of the Yangtze Delta: Past, present, and future. *Marine Geology*, 392:78–93.

Forst, M. F. (2009). The convergence of Integrated Coastal Zone Management and the ecosystems approach. *Ocean & Coastal Management*, 52(6):294–306.

Fredsøe, J. (1984). Turbulent Boundary Layer in Wave-current Motion. *Journal of Hydraulic Engineering*, 110(8):1103–1120.

Gao, M., Xu, L., and Li, G. (2009). The study of scoring and silting evolution of radiative sand ridge field of the south Yellow Sea in support of DEM. *Marine Science Bulletin*, 28(4):168–176.

Gao, S. (1988). P-A relationships of tidal inlets along the East China Sea coast. *Marine Sciences*, 1.

Gao, S. and Collins, M. (1994). Tidal Inlet Equilibrium, in Relation to Cross-sectional Area and Sediment Transport Patterns. *Estuarine, Coastal and Shelf Science*, 38(2):157–172.

Gong, Z., Jin, C., Zhang, C., Zhou, Z., Zhang, Q., and Li, H. (2017). Temporal and spatial morphological variations along a cross-shore intertidal profile, Jiangsu, China. *Continental Shelf Research*, 144:1–9.

Gong, Z., Wang, Z., Stive, M. J. F., Zhang, C., and Chu, A. (2012). Process-Based Morphodynamic Modeling of a Schematized Mudflat Dominated by a Long-Shore Tidal Current at the Central Jiangsu Coast, China. *Journal of Coastal Research*, 285:1381–1392.

Gu, Y., Gong, M.-j., and Li, H. (2014). Application of Remote Sensing Axis Line Method in Xiaomiaohong Creek. *Indonesian Journal of Electrical Engineering and Computer Science*, 12(5):3323–3330.

He, H. and Xu, Y. (2016). Wind-wave hindcast in the Yellow Sea and the Bohai Sea from the year 1988 to 2002. *Acta Oceanologica Sinica*, 35(3):46–53.

He, H. and Zhou, R. (2016). Spatial-temporal variation of land use based on landscape patterns in the coastal zone of Yancheng, Jiangsu. *Resources and Environment in the Yangtze Basin*, 25(8):1191 – 1199.

Hu, Z., Stive, M. J. F., Zitman, T., Ye, Q., Wang, Z., Luijendijk, A., Gong, Z., and Suzuki, T. (2011). Interaction between hydrodynamics and salt marsh dynamics: An example from Jiangsu Coast. In *Proc. of 6th Int. Conf. on Asian and Pacific Coasts*, Hong Kong, China.

Huang, L. and Liu, B. (2017). Entrance layout and sedimentation reduction measures of the first and second basin in Tongzhou Bay Port. *China Harbour Engineering*, 37(4):29 – 34.

Huang, L. and Zhang, W. (2017). Layout scheme of the first and second harbor basin in Tongzhou Bay Port. *China Harbour Engineering*, 37(4):39 – 43.

Huang, Z., Liu, H., Zhang, J., and Ding, Q. (2015). Construction condition analysis of Xiaomiaohong waterway artificial deep-water channel at radial sand ridges in North Jiangsu. *Port & Waterway Engineering*, 12(510).

Huo, W., Zhang, W., and Chen, P. S.-L. (2018). Recent development of Chinese port cooperation strategies. *Research in Transportation Business & Management*, 26:67–75.

Hwang, J. H., Van, S. P., Choi, B.-J., Chang, Y. S., and Kim, Y. H. (2014). The physical processes in the Yellow Sea. *Ocean & Coastal Management*, 102:449–457.

Jiangsu Yangkou Port Co., Ltd. (2018). China Yangkou Port Portal. http://www.ntykg.com/site/kfgh/ztgh/622636114220.shtml.

Kang, Y. (2015). Maximum tidal range analysis of radial sand ridges in the southern Yellow Sea. *Indian Journal of Geo-Marine Sciences*, 44(7):971–976.

Kang, Y. Y. (2017). Personal communications.

Le Hir, P., Roberts, W., Cazaillet, O., Christie, M., Bassoullet, P., and Bacher, C. (2000). Characterization of interitdal flat hydrodynamics. *Continental Shelf Research*, 20:1433–1459.

Lee, H. and Chough, S. (1989). Sediment distribution, dispersal and budget in the Yellow Sea. *Marine Geology*, 87(2-4):195–205.

Li, C., Zhang, J., and Deng, B. (2001). Holocene regression and the tidal radial sand ridge system formation in the Jiangsu coastal zone, east China. *Marine Geology*, 173(1):97–120.

Li, P., Yang, S. L., Milliman, J. D., Xu, K. H., Qin, W. H., Wu, C. S., Chen, Y. P., and Shi, B. W. (2012). Spatial, Temporal, and Human-Induced Variations in Suspended Sediment Concentration in the Surface Waters of the Yangtze Estuary and Adjacent Coastal Areas. *Estuaries and Coasts*, 35(5):1316–1327.

Li, X., Zhang, L., Ji, C., Liu, H., and Huang, Q. (2014). Spatiotemporal changes of Jiangsu coastline: A remote sensing and GIS approach. *Geographical Research*, 33(3):414–426.

Liang, S.-k., Pearson, S., Wu, W., Ma, Y.-j., Qiao, L.-l., Wang, X. H., Li, J.-m., and Wang, X.-l. (2015). Research and integrated coastal zone management in rapidly developing estuarine harbours: A review to inform sustainment of functions in Jiaozhou Bay, China. *Ocean & Coastal Management*, 116:470–477.

Liu, J., Li, A., Xu, K., Velozzi, D., Yang, Z., Milliman, J., and DeMaster, D. (2006). Sedimentary features of the Yangtze River-derived along-shelf clinoform deposit in the East China Sea. *Continental Shelf Research*, 26(17-18):2141–2156.

Liu, J., Xu, K., Li, A., Milliman, J., Velozzi, D., Xiao, S., and Yang, Z. (2007). Flux and fate of Yangtze River sediment delivered to the East China Sea. *Geomorphology*, 85(3-4):208–224.

Liu, X., Gao, S., and Wang, Y. (2011). Modeling profile shape evolution for accreting tidal flats composed of mud and sand: A case study of the central Jiangsu coast, China. *Continental Shelf Research*, 31(16):1750–1760.

Liu, Z., Huang, Y., and Zhang, Q. (1989). Tidal current ridges in the southwestern Yellow Sea. *Journal of Sedimentary Research*, 59(3):432437.

Lu, P. and Dou, X. (2011). Hydrodynamic research and application of the radial sand rigdes in South Yellow Sea, China. In *Proc. of 6th Int. Conf. on Asian and Pacific Coasts*, pages 43 – 52, Hong Kong, China.

Ma, Z., Cai, Y., Li, B., and Chen, J. (2010). Managing Wetland Habitats for Waterbirds: An International Perspective. *Wetlands*, 30(1):15–27.

Murray, N. J., Ma, Z., and Fuller, R. A. (2015). Tidal flats of the Yellow Sea: A review of ecosystem status and anthropogenic threats: Status of Yellow Sea tidal flats. *Austral Ecology*, 40(4):472–481.

Nantong Port Authority (2013). The tidal current numerical model of Tongzhou Bay port area and sediment deposition calculation. Technical report, Nantong Port Tongzhou Bay Port Planning Special Project Research.

Nantong Port Group Co., Ltd. (2017). Nantong Port Group Co., Ltd.

Nash, J. and Sutcliffe, J. (1970). River flow forecasting through conceptual models part I — A discussion of principles. *Journal of Hydrology*, 10(3):282–290.

National Bureau of Statistics (2016). China Statistical Yearbook 2016.

National Bureau of Statistics (2017). Statistical Communiqué of the People 's Republic of China on National Economic and Social Development. Technical report, National Bureau of Statistics of China.

Partheniades, E. (1965). Erosion and Deposition of Cohesive Soils. *Journal of the Hydraulics Division*, 91(1):105 – 139.

Peng, H.-B., Anderson, G. Q. A., Chang, Q., Choi, C.-Y., Chowdhury, S. U., Clark, N. A., Gan, X., Hearn, R. D., Li, J., Lappo, E. G., Liu, W., Ma, Z., Melville, D. S., Phillips, J. F., Syroechkovskiy, E. E., Tong, M., Wang, S., Zhang, L., and ZöCkler, C. (2017). The intertidal wetlands of southern Jiangsu Province, China – globally important for Spoon-billed Sandpipers and other threatened waterbirds, but facing multiple serious threats. *Bird Conservation International*, 27(03):305–322.

PIANC (2011). 'Working with Nature'. PIANC Position Paper, PIANC.

Piersma, T., Chan, Y.-C., Mu, T., Hassell, C. J., David S., D. S., Peng, H.-B., Ma, Z., Zhang, Z., and Wilcove, D. S. (2017). Loss of habitat leads to loss of birds: reflections on the Jiangsu, China, coastal development plans. *Wader Study*, 124(2).

Piersma, T., Lok, T., Chen, Y., Hassell, C. J., Yang, H.-Y., Boyle, A., Slaymaker, M., Chan, Y.-C., Melville, D. S., Zhang, Z.-W., and Ma, Z. (2016). Simultaneous declines in summer survival of three shorebird species signals a flyway at risk. *Journal of Applied Ecology*, 53(2):479–490.

Roberts, W., Le Hir, P., and Whitehouse, R. J. S. (2000). Investigation using simple mathematical models of the effect of tidal currents and waves on the profile shape of intertidal mudflats. *Continental Shelf Research*, 20(10):1079–1097.

Roelvink, J. (2006). Coastal morphodynamic evolution techniques. *Coastal Engineering*, 53(2-3):277–287.

Shepard, F. P. (1954). Nomenclature Based on Sand-silt-clay Ratios. *SEPM Journal of Sedimentary Research*, Vol. 24.

Shi, B., Wang, Y. P., Wang, L. H., Li, P., Gao, J., Xing, F., and Chen, J. D. (2016). Great differences in the critical erosion threshold between surface and subsurface sediments: A field investigation of an intertidal mudflat, Jiangsu, China. *Estuarine, Coastal and Shelf Science*.

Shi, Z. and Chen, J. (1996). Morphodynamics and sediment dynamics on intertidal mudflats in China (1961-1994). *Continental Shelf Research*, 16(15):1909–1926.

Song, D., Wang, X. H., Zhu, X., and Bao, X. (2013). Modeling studies of the far-field effects of tidal flat reclamation on tidal dynamics in the East China Seas. *Estuarine, Coastal and Shelf Science*, 133:147–160.

Stive, M., Ji, L., Brouwer, R. L., Van de Kreeke, C., and Ranasinghe, R. (2011). Empirical relationship between inlet cross-sectional area and tidal prism: A re-evaluation. *Coastal Engineering Proceedings*, 1(32):86.

Su, M. (2016). *Progradation and erosion of a fine-grained, tidally dominated delta: A case study of the Jiangsu coast*. PhD thesis, TU Delft, Delft University of Technology, Delft. OCLC: 6893251766.

Su, M., Yao, P., Wang, Z. B., Zhang, C. K., and Stive, M. J. (2017a). Exploratory morphodynamic hindcast of the evolution of the abandoned Yellow River delta, 1578–1855ce. *Marine Geology*, 383:99–119.

Su, M., Yao, P., Wang, Z. B., Zhang, C. K., and Stive, M. J. (2017b). Exploratory morphodynamic modeling of the evolution of the Jiangsu coast, China, since 1855: Contributions of old Yellow River-derived sediment. *Marine Geology*, 390:306–320.

Su, M., Yao, P., Wang, Z. B., Zhang, C. K., and Stive, M. J. F. (2015). Tidal Wave Propagation in the Yellow Sea. *Coastal Engineering Journal*, 57(03):1550008.

Sun, C., Liu, Y., Zhao, S., Li, H., and Sun, J. (2017). Saltmarshes Response to Human Activities on a Prograding Coast Revealed by a Dual-Scale Time-Series Strategy. *Estuaries and Coasts*, 40(2):522–539.

Sun, Z., Wang, F., Yin, Y., Li, G., Ge, S., and Xu, Q. (2014). Sedimentary environment evolution of Lanshayang tidal channel within the radial sand ridges, Southern Yellow Sea. *Journal of Nanjing University (natural sciences)*, 50(5):553 – 563.

Swaine, M. D. (2015). Chinese views and commentary on the 'One Belt, One Road'initiative. *China Leadership Monitor*, 47(2):3.

Tao, J., Zhang, C. K., and Yao, J. (2011). Effect of large-scale reclamation of tidal flats on tides and tidal currents in offshore areas of Jiangsu Province. *Journal of Hohai University (Natural Sciences)*, 39(2):225–230.

Tian, B., Wu, W., Yang, Z., and Zhou, Y. (2016). Drivers, trends, and potential impacts of long-term coastal reclamation in China from 1985 to 2010. *Estuarine, Coastal and Shelf Science*, 170:83–90.

UNESCO World Heritage Centre (2017). The Coast of the Bohai Gulf and the Yellow Sea of China.

USGS (2018). EarthExplorer.

van Maren, D., Oost, A., Wang, Z., and Vos, P. (2016). The effect of land reclamations and sediment extraction on the suspended sediment concentration in the Ems Estuary. *Marine Geology*, 376:147–157.

van Rijn, L. C. (1993). *Principles of sediment transport in rivers, estuaries and coastal seas, Part 1*. Number 1006. Aqua publications, Amsterdam.

van Rijn, L. C. (2007a). Unified View of Sediment Transport by Currents and Waves. I: Initiation of Motion, Bed Roughness, and Bed-Load Transport. *Journal of Hydraulic Engineering*, 133(6):649–667.

van Rijn, L. C. (2007b). Unified View of Sediment Transport by Currents and Waves. II: Suspended Transport. *Journal of Hydraulic Engineering*, 133(6):668–689.

van Rijn, L. C. (2007c). Unified View of Sediment Transport by Currents and Waves. III: Graded Beds. *Journal of Hydraulic Engineering*, 133(7):761–775.

van Slobbe, E., de Vriend, H. J., Aarninkhof, S., Lulofs, K., de Vries, M., and Dircke, P. (2013). Building with Nature: in search of resilient storm surge protection strategies. *Natural Hazards*, 66(3):1461–1480.

Wang, A., Gao, S., Jia, J., and Pan, S. (2005). Sedimentation rates in the Wanggang salt marshes, Jiangsu. *Journal of Geographical Sciences*, 15(2):199 – 209.

Wang, F. and Wall, G. (2010). Mudflat development in Jiangsu Province, China: Practices and experiences. *Ocean & Coastal Management*, 53:691 – 699.

Wang, R., Zhang, Y., Xia, F., and Zhao, S. (2013). Grain size distibution and transportation trends of bottom sediments in the sand ridge field of the South Yellow Sea, China. *Marine Geology & Quaternary Geology*, 32(6):1–8.

Wang, W., Liu, H., Li, Y., and Su, J. (2014a). Development and management of land reclamation in China. *Ocean & Coastal Management*, 102:415–425.

Wang, X. and Ke, X. (1997). Grain-size characteristics of the extant tidal flat sediments along the Jiangsu coast, China. *Sedimentary Geology*, 112:105–122.

Wang, X. H., Qiao, F., Lu, J., and Gong, F. (2011). The turbidity maxima of the northern Jiangsu shoal-water in the Yellow Sea, China. *Estuarine, Coastal and Shelf Science*, 93(3):202–211.

Wang, Y., Gao, S., and Jia, J. (2006). High-resolution data collection for analysis of sediment dynamic processes associated with combined current-wave action over intertidal flats. *Science Bulletin*, 51(7):866–877.

Wang, Y., Zhang, Y., Zou, X., Zhu, D., and Piper, D. (2012a). The sand ridge field of the South Yellow Sea: Origin by river–sea interaction. *Marine Geology*, 291-294:132–146.

Wang, Y. and Zhu, D. (2006). Characteristics and exploitation of coastal wetland of china. *Resources and Environment in the Yangtze Basin*, 15(5):553 – 559.

Wang, Y., Zhu, D., You, K., Pan, S., Zhu, X., and Zou, X. (1999). Evolution of radiative sand ridge field of the South Yellow Sea and its sedimentary characteristics. *Science in China Series D*, 42(1).

Wang, Y. P., Gao, S., Jia, J., Liu, Y., and Gao, J. (2014b). Remarked morphological change in a large tidal inlet with low sediment-supply. *Continental Shelf Research*, 90:79–95.

Wang, Y. P., Gao, S., Jia, J., Thompson, C. E., Gao, J., and Yang, Y. (2012b). Sediment transport over an accretional intertidal flat with influences of reclamation, Jiangsu coast, China. *Marine Geology*, 291-294:147–161.

Wang, Z., Li, L., Chen, D., Xu, K., Wei, T., Gao, J., Zhao, Y., Chen, Z., and Masabate, W. (2007). Plume front and suspended sediment dispersal off the Yangtze (Changjiang) River mouth, China during non-flood season. *Estuarine, Coastal and Shelf Science*, 71(1-2):60–67.

Wentworth, C. (1922). A Scale of Grade and Class Terms for Clastic Sediments. *Journal of Geology*, 30(5):377–392.

Winterwerp, J. and Van Kesteren, W. (2004). *Introduction to the physics of cohesvie sediment dynamics in the marine environment*, volume 56 of *Developments in Sedimentology*. Elsevier, Amsterdam.

Woodroffe, C. D. and Saito, Y. (2011). River-Dominated Coasts. In *Treatise on Estuarine and Coastal Science*, volume 3.05 of *Estuarine and Coastal Geology and Geomorphology*, pages 117–135. Elsevier, 1 edition.

World Development Indicators database (2017). Gross domestic product 2016. Technical report, World Bank.

Xing, F., Wang, Y. P., and Wang, H. V. (2012). Tidal hydrodynamics and fine-grained sediment transport on the radial sand ridge system in the southern Yellow Sea. *Marine Geology*.

Xinhua News Agency (2018). China names and shames two provinces over slack marine protection effort.

Xu, F., Tao, J., Zhou, Z., Coco, G., and Zhang, C. (2016). Mechanisms underlying the regional morphological differences between the northern and southern radial sand ridges along the Jiangsu Coast, China. *Marine Geology*, 371:1–17.

Xu, Z., Zhang, W., Lu, P., and Chen, K. (2015). The study on the bottom friction and the breaking coefficient for typhoon waves in radial sand ridges—the Lanshayang Channel as an example. *Acta Oceanologica Sinica*, 34(3):99–107.

Xu, Z., Zhang, W., Lu, P.-d., An, X., and Chen, K.-f. (2014). Wave-induced flow and its influence on ridge erosion and channel deposition in Lanshayang channel of radial sand ridges. *Journal of Hydrodynamics, Ser. B*, 26(6):882–893.

Xue, C. (1993). Historical changes in the Yellow River delta, China. *Marine Geology*, 113(3-4):321–330.

Yan, Y., Song, Z., Xue, H., and Mao, L. (1999a). Hydromechanics for the formation and development of radial sandbanks - Vertical characteristics of tidal flow. *Science in China Series D: Earth Sciences*, 42(1):22–29.

Yan, Y., Zhu, Y., and Xue, H. (1999b). Hydromechanics for the formation and development of radial sandbanks - Plane characteristics of tidal flow. *Science in China Series D*, 42(1).

Yang, B., Feng, W.-b., and Zhang, Y. (2014). Wave characteristics at the south part of the radial sand ridges of the Southern Yellow Sea. *China Ocean Engineering*, 28(3):317–330.

Yang, Y., Wang, Y. P., Gao, S., Wang, X. H., Shi, B. W., Zhou, L., Wang, D. D., Dai, C., and Li, G. C. (2016). Sediment resuspension in tidally dominated coastal environments: new insights into the threshold for initial movement. *Ocean Dynamics*, 66(3):401–417.

Yao, H. (2013). Characterizing landuse changes in 1990–2010 in the coastal zone of Nantong, Jiangsu province, China. *Ocean & Coastal Management*, 71:108–115.

Yao, P. (2016). *Tidal and Sediment Dynamics in a Fine-Grained Coastal Region: A Case Study of the Jiangsu Coast*. PhD thesis, Delft University of Technology, Delft.

Yao, P., Su, M., Wang, Z., van Rijn, L. C., Zhang, C., Chen, Y., and Stive, M. J. (2015). Experiment inspired numerical modeling of sediment concentration over sand–silt mixtures. *Coastal Engineering*, 105:75–89.

Yao, P., Wang, Z., Zhang, C., Su, M., Chen, Y., and Stive, M. J. F. (2013). The genesis of the radial tidal current off the Central Jiangsu Coast. In *Proc. of 7th Int. Conf. on Coastal Dynamics*, pages 1947 – 1958, Arcachon. Bordeaux University.

Yin, Y., Gao, J., Zhou, K., and Mu, S. (2017). Dynamic of land use/cover changes under reclamation and Spartina Alterniflora invasion in Jiangsu central coastal wetlands. *Geographical Research*, 36(8):1478 – 1488.

You, K., Zhu, D., Wang, X., Sun, Y., Zhou, L., and Ma, Z. (1998). The stability analysis of Xiyang tidal channel in radial submarine sand ridges along North Jiangsu. *Geographical Research*, 17(1).

Ysebaert, T., Van der Wal, J., Tangelder, M., De Groot, A., and Baptist, M. (2016). Ecotopenkaart voor het Eems-Dollard estuarium. Technical Report Rapport C059/15, IMARES.

Zhang, C., Chen, J., Lin, K., Ding, X., Yuan, R., and Kang, Y. (2011). Spatial layout of reclamation of coastal tidal flats in Jiangsu province. *Journal of Hohai University (Natural Sciences)*, 39(2).

Zhang, C., Yang, Y., Tao, J., Chen, Y., Yao, P., and Su, M. (2013). Suspended sediment fluxes in the radial sand ridge field of South Yellow Sea. *Journal of Coastal Research*, 65(sp1):624–629.

Zhang, C., Zhang, D., Zhang, J., and Wang, Z. (1999). Tidal current-induced formation—storm-induced change—tidal current-induced recovery. *Science in China Series D: Earth Sciences*, 42(1):1–12.

Zhang, C. K. and Chen, J. (2011). Master plan of tidal flat reclamation along Jiangsu coastal zone. In *Proc. of 6th Int. Conf. on Asian and Pacific Coasts*, pages 139–146, Hong Kong, China. Weizmann Institute of Science.

Zhang, C. K. and Ed. (2012). The Comprehensive Survey and Evaluation Report on Coastal Zone of Jiangsu Province. Technical report, Beijing Science Press.

Zhang, R., Pu, L., Li, J., Zhang, J., and Xu, Y. (2016). Landscape ecological security response to land use change in the tidal flat reclamation zone, China. *Environmental Monitoring and Assessment*, 188(1).

Zhang, R. S. (1995). Tidal prism throat area relationships of tidal inlets along Yellow Sea and Bohai Sea coast. *Ocean Engineering*, 13(2).

Zhao, S.-s., Liu, Y.-x., Li, M.-c., Sun, C., Zhou, M.-x., and Zhang, H.-x. (2015). Analysis of Jiangsu tidal flats reclamation from 1974 to 2012 using remote sensing. *China Ocean Engineering*, 29(1):143–154.

Zheng, C. W., Zhou, L., Jia, B. K., Pan, J., and Li, X. (2014). Wave characteristic analysis and wave energy resource evaluation in the China Sea. *Journal of Renewable and Sustainable Energy*, 6(4):043101.

Zhou, L., Liu, J., Saito, Y., Zhang, Z., Chu, H., and Hu, G. (2014). Coastal erosion as a major sediment supplier to continental shelves: example from the abandoned Old Huanghe (Yellow River) delta. *Continental Shelf Research*, 82:43–59.

Zhu, Q., Wang, Y. P., Ni, W., Gao, J., Li, M., Yang, L., Gong, X., and Gao, S. (2016). Effects of intertidal reclamation on tides and potential environmental risks: a numerical study for the southern Yellow Sea. *Environmental Earth Sciences*, 75(23).

Zhu, Q., Yang, S., and Ma, Y. (2014). Intra-tidal sedimentary processes associated with combined wave–current action on an exposed, erosional mudflat, southeastern Yangtze River Delta, China. *Marine Geology*, 347:95–106.

Zhu, Y. and Chang, R. (2000). Preliminary Study of the Dynamic Origin of the Distribution Pattern of Bottom Sediments on the Continental Shelves of the Bohai Sea, Yellow Sea and East China Sea. *Estuarine, Coastal and Shelf Science*, 51(5):663–680.

Zhu, Y. and Chang, R. (2001). On the relationships between the radial tidal current field and the radial sand ridges in the southern Yellow Sea: a numerical simulation. *Geo-Marine Letters*, 21(2):59–65.

Zhu, Y. and Chen, Q. (2005). On the Origin of the Radial Sand Ridges in the Southern Yellow Sea: Results from the Modeling of the Paleoradial Tidal Current Fields off the Paleo-Yangtze River Estuary and Northern Jiangsu Coast. *Journal of Coastal Research*, 216:1245–1256.

Zou, X., Yin, Y., and Ma, J. (2006). The stability of the Lanshayang Channel.pdf. *Quaternary Sciences*, 26(3):334 – 339.

A

Data Analysis

In order to set-up and calibrate the Delft3D model, a data analysis was carried out to obtain information about bathymetry, hydro and morphodynamic quantities and coastline changes. Use has been made of a several data surveys at the Tongzhou coast. In this section, these surveys will be discussed more elaborately.

A.1. tidal level and datum

In absence of clear tidal levels at the Jiangsu coast, conventional tidal levels are based on the waterlevel measurements taken at tidal gauges at Tongzhou bay , including statistical features, such as the mean water level, mean low water (MLW) and mean high water (MHW) (CCCC Third Harbor Consultants Co. Ltd, 2012). Characteristic tidal levels during spring and neap conditions were determined by further analysis of the datasets. The mean high water spring (MHWS) and mean low water spring (MLWS) were defined as the two consecutive maximum and minimum heights respectively, during a period when the tidal range was largest. Consequently, the mean high water neap and mean low water neap were defined as the two consecutive minimum and maximum water levels respectively, during a period when the tidal range was at its smallest. An overview of the tidal levels and the Beijing 54 chart datum are shown in Table A.1

A.2. Measurements

In this study use has been made of two measurement datasets. The first set of measurements was retrieved at 14 mooring stations in the channels and on shoals at the Yaosha-Lengjiasha area from 22 to 23 February 2012 (spring tide) and 29 February to 1 March 2012 (neap tide) (CCCC Third Harbor Consultants Co. Ltd, 2012). These measurements consists of several features; the current velocity, current direction and suspended sediment concentrations, measured at 5 different sampling heights over the watercolumn, the wind speed and wind direction, the depth averaged salinity and the suspended particle grain size, sampled at the bed, middle and surface of the watercolumn. The waterdepth was measured at 6 tidal guages, of which 4 temporary (*e.g.* Xiaomiaohong, Sanshahong, Lengjiasha,Datang) and 2 permanent tidal gauges (*e.g.* Lüsihaiyang, Yangkou). hese gauges measured the waterlevels for 30 days, starting at 21 February till 22 March 2012. The location of all the measuring stations at Tongzhou Bay are shown in Figure A.1.

Table A.1: Tidal datums

Tidal datum	waterlevel w.r.t. MSL [m]
MHWS	2.914
MHW	2.01
MHWN	1.012
1985 National Elevation Benchmark	-0.11
MLWN	-0.633
MLW	-1.868
MLWS	-2.66
Lowest tide observed at Lüsishayang	-3.44

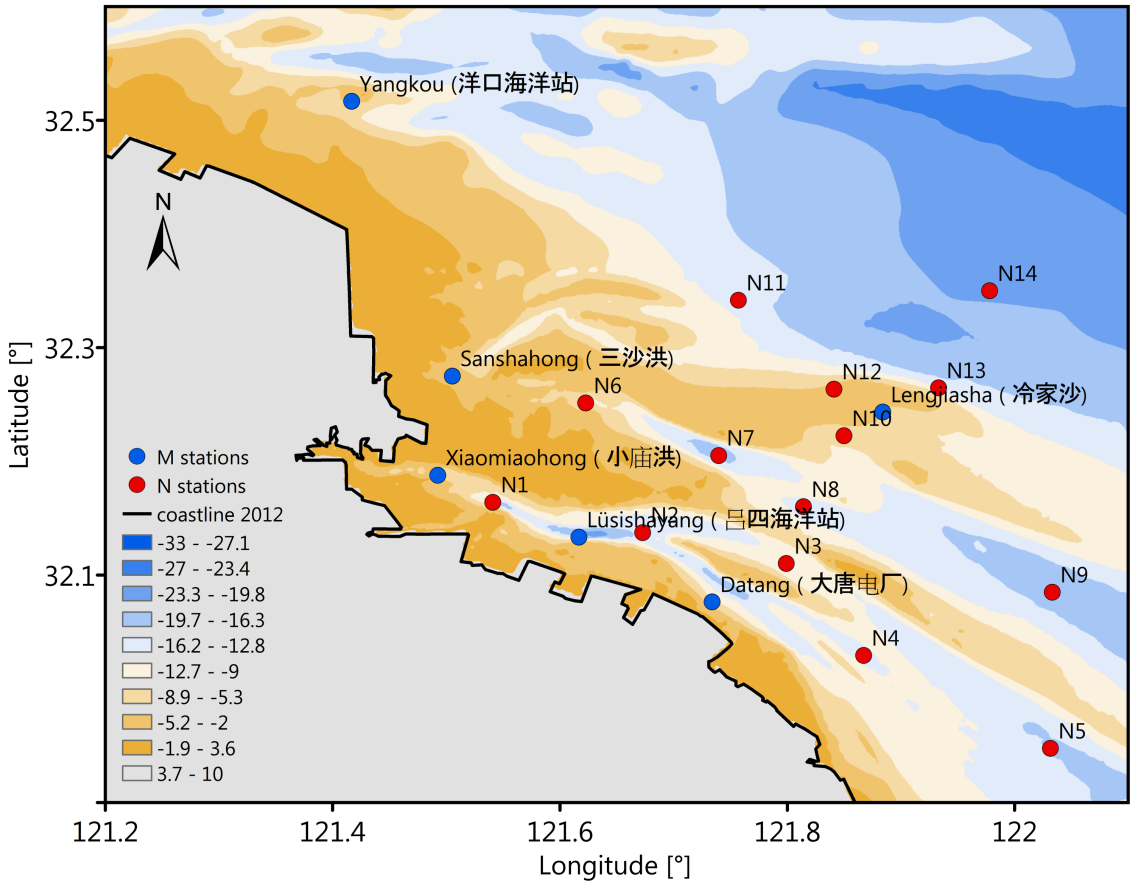

Figure A.1: Measurement locations at Tonghzou bay

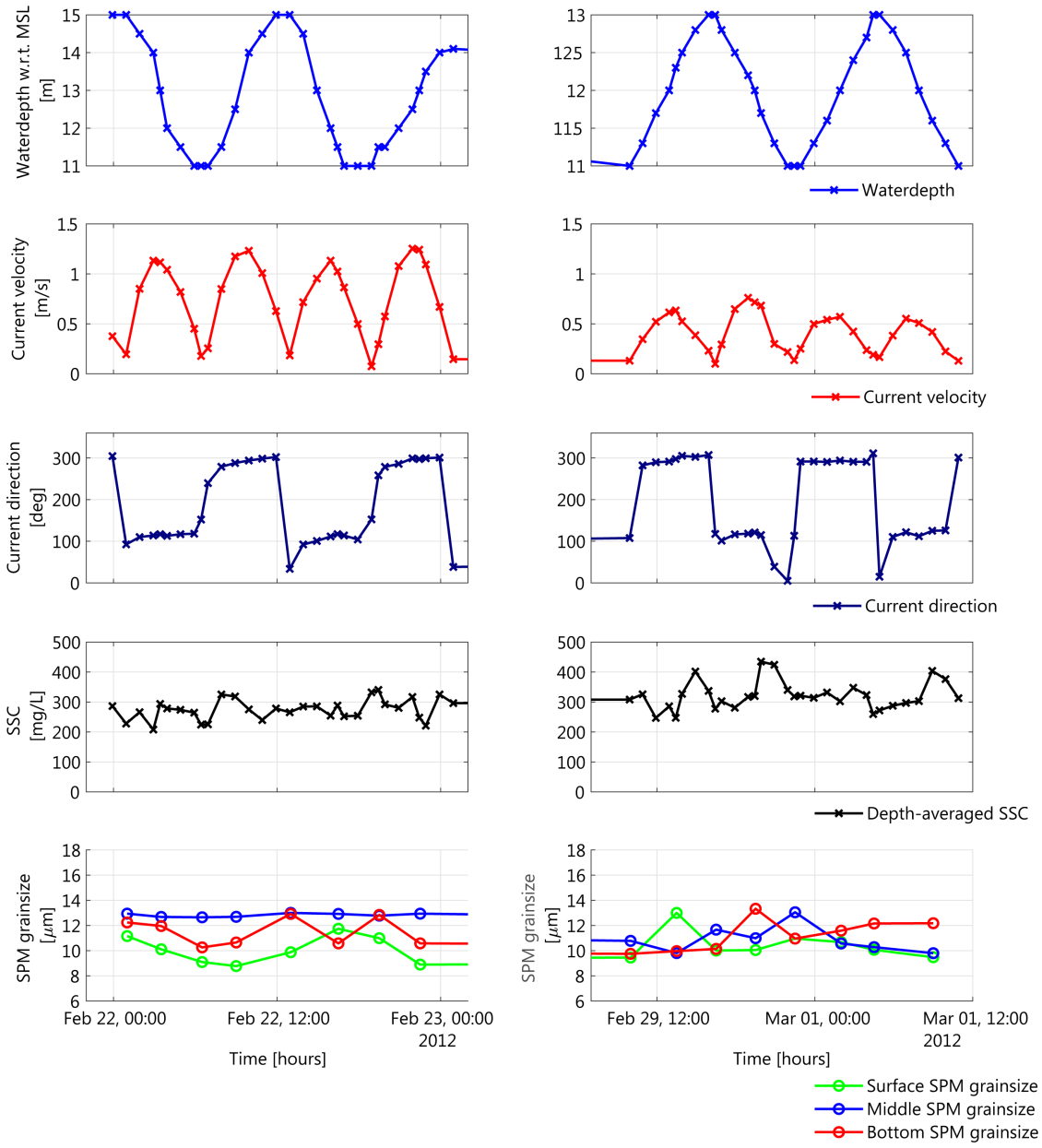

Figure A.2: Measurements taken at the N8 station during 22 to 23 February 2012 (Spring tide, left panel) and 29 February to 1 March 2012 (Neap tide, right panel)

A.2.1. Waterlevels

The waterlevels were measured at the 6 tidal gauges with an interval of 10 minutes. A closer analysis of the time series, show an average tidal range of $4 \sim 6$ m during spring tide. An overall analysis of the retrieved data results in the determining of the tidal datums, as shown in Table A.1.

Comparing the waterlevels from offshore towards nearshore, shows a longer falling tidal period than raising tidal period, suggesting the Xiamioahong and Sanshahong channel to be in the flood dominant regime. This means that the system tends to show a nett transport towards the shore or into the channel.

A.2.2. Velocities

The current velocities and current direction were measured at 14 mooringstations by a Acoustic Doppler Current Profiler at the bed, the water surface and 3 intermediate depths over the watercolumn with an interval of 10 minutes.

By comparing the velocity phase, it can be seen that peak flood velocities are higher than ebb velocities. the average period of flood is shorter than ebb flow. This suggest similar flood dominant patterns in the Xiamioahong and Sanshahong systems. This asymmetry in flow implies several consequences on the sediment transport. With higher velocities during peak, sediment concentration is higher and thus the transport capacity is higher as well. This implies a net transport of sediment towards the coast or into the basin. Additionally, due to the difference in duration of flow reversal (slack water), suspended sediment has less or more time to settle depending on the asymmetry signal. As such, sediment is transported into the basin over a tidal cycle.

Additionally, the wind speed and direction was measured for the same period with an interval of 60 minutes. Velocities during spring tide were relatively low ($< 3 m/s$) . However, during neaptide these velocities increased to more severe wind speeds ($\pm 9 m/s$). These windspeeds did not differ much across the different stations. This suggest of the presence of wind-induced waves during neap conditions. It is unclear how severe these waves were as there are no measurement available during this period. It is unclear if these wind-induced waves had effect on the measured sediment concentrations. Also, it is not known how long these windspeeds were prevailing, prior to the measuring period.

A.2.3. Suspended sediment concentrations

Suspended sediment concentrations were measured at the 14 mooring stations by sampling with several $500 ml$ horizontal water sample collectors at the surface, bed and middle of the water column. Additionally, the samples at these stations were further analyzed and presented in the average, median and peak particle size of the suspended material.

The concentrations measured over different depths and the depth averaged concentration for station N8 are shown in Figure A.2. The concentrations during spring follow the velocity. However, concentration does not follow the flow instantaneous, nor does it goes to zero. An average concentration of $100 \sim 300$ mg/L during spring and neap. During neap tide, similar patterns and concentrations can be measured. However, offshore stations show a more constant, falling trend. This could indicate a certain wash load which is still in suspension during neaptide and is slowly decaying due to the absence of the required flow to entrain new sediment. Another cause could be the local resuspension of sediments in the period around neaptide due to the presence of wind induced waves as suggested by the windspeed measurements.Examination into this similarity despite different hydrodynamic forcing is elaborated in Appendix C.

A.2.4. Suspended particle matter

The suspened particle sizes for station N8 are shown in Figure A.2. The sediment samples were retrieved with an interval of 3 hours and therefore not simultaneous with other measurements. Averaged over all the stations, a depth-averaged mean grainsize of $10 \sim 11$ μm is observed during spring and neap tides.

A.2.5. Salinity

Salinity was measured by taking 500 ml samples 2 depths at the 14 mooring stations. Mean salinity level is at 30.74 ppt with a variation of 0.194 ppt during spring and 31.04 ppt with a standard deviation of 0.08 ppt during neap. Overall, the salinity over the 14 locations does not show a large variety and can be described as brackish to salt. This suggest that the discharge form the agricultural channels is relatively insignificant compared to the salt coastal waters. Also the freshwater discharges from the Yangtze river are not detectable.

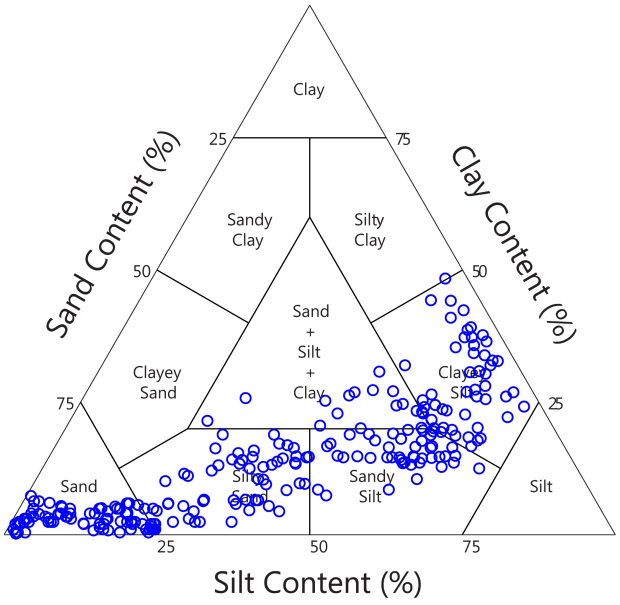

Figure A.3: Tertiary diagram of bed samples taking during measurement campaign in Feb 2012

A.2.6. Bed samples

As part of the measurement campaign, 222 bed sediment samples where retrieved, covering most of the Yaosha-Lengjiasha ridges and channels at Tongzhou. These samples were recorded in grain size classes, which were reclassified into clay, silt and sand classes according to Wentworth (1922); Shepard (1954). The samples are shown in a tertiary diagram in Figure A.3. Further analysis showed that smaller particle classes were mainly located on the shoals and shallower areas. Coarser bed composition was mainly found in the classes or locations were high hydrodynamic conditions were present. Similar observations of this coarsening of the bed sediment towards deeper waters were made at Tongzhou and the Jiangsu coast (Wang and Ke, 1997).

B

Tongzhou Bay site visit: Okt 2017

After the Symposium on Coastal Resources and Environment 2017 (CORE 2017) hosted at Hohai University, Nanjing, a field visit was planned to the Jiangsu coast and several institutions. This trip included visiting the current extend of the reclamations at the Yaosha shoal, Tongzhou Bay. This section show a selection of the photo's taken at the reclamation and several interesting features that have been formed after the completion in 2013. The construction consists of a offshore reclamation in the middle of the Yaosha shoal, connected via a construction road with hinterland. Photos were taken during just before sunset, around 16:00 ~ 17:00, corresponding with low tide.

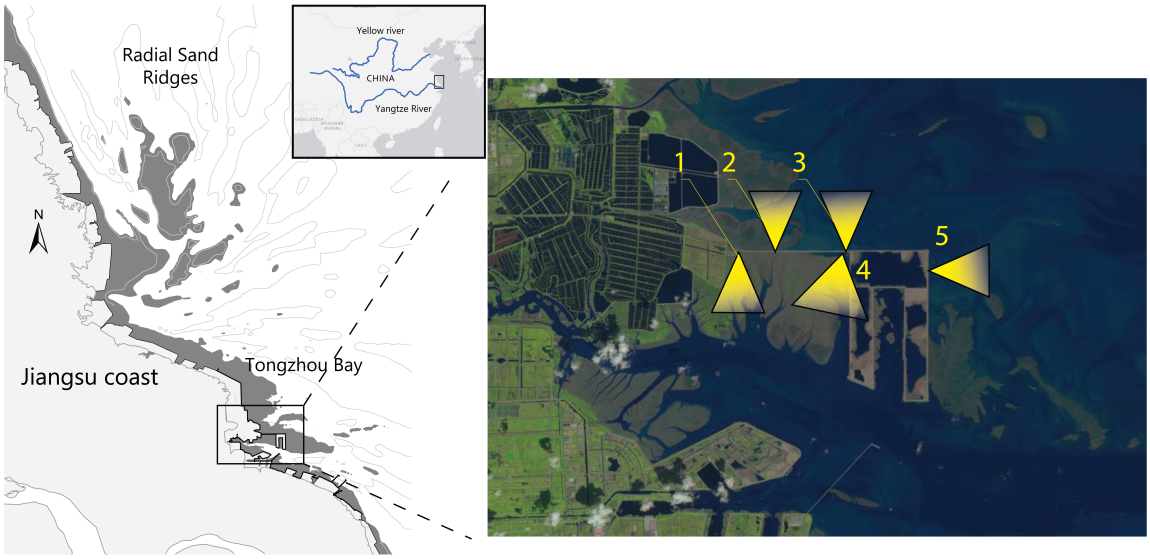

Figure B.1: Overview of the photograph locations during fieldvisit in Oktober 2017 at the current reclamation of the Yaosha shoal at Tongzhou Bay

Figure B.2: . In same order it shows: Photo at the beginning of the construction road showing the relative high nearshore regions with some vegetation (1), photo of the northside of the construction road, showing closer proximity to tidal waters and therefore lower elevations (2), photo of similar location further down the construction road, where tidal waters are even closer to the reclamation (3), photo of the inner section adjacent to the reclamation, where sections of the exposed mudflat can be seen as well as channel formation along the workroad and reclamation (4), photo of the head of the reclamation, looking seaward (5). Photographs courtesy of S.G.J. Aarninkhof

C

Tongzhou Bay Model calibration

The Tonghzou bay region is characterized by complex tidal and sediment dynamics. In order to get satisfactory results for hydrodynamics and sediment transport, several model setups and calibration steps were performed which resulted in the final setup. Starting point was the Jiangsu Regional Model and modified sediment transport formulas as described by Yao (2016). Based on measurements results, several alterations were made to this model into a more confine Tongzhou Bay Model. In this section, these different setups and calibration steps are elaborated.

C.1. Jiangsu Regional Model

C.1.1. Jiangsu Regional Model

Within this study use has been made of the model setup provided by Yao (2016). This hydro, -morphodynamic model encompasses the entire Jiangsu coast. It is able to simulate 2DH sediment transport for sand-silt mixed sediments specifically found at the Jiangsu coast. Yao (2016) confirmed that the present JRM can reproduce good results over a short-term period. The full JRM setup is discussed in section 3.2.1. The model results is compared with measurements,obtained during 22 February to 3 March 2012 at 14 mooring stations and 6 water level gauges (CCCC Third Harbor Consultants Co. Ltd, 2012).

In Figure C.1 the measured an calculated waterlevels for Xiaomiaohong and Lengjiasha stations are shown, situated in the channel and on top of a shoal respectively. Although the JRM was developed for the entire Jiangsu coastal domain, the model already performs relatively well in predicting the water levels with some slight under estimations during neap tide. Same results were obtained for the other 4 locations

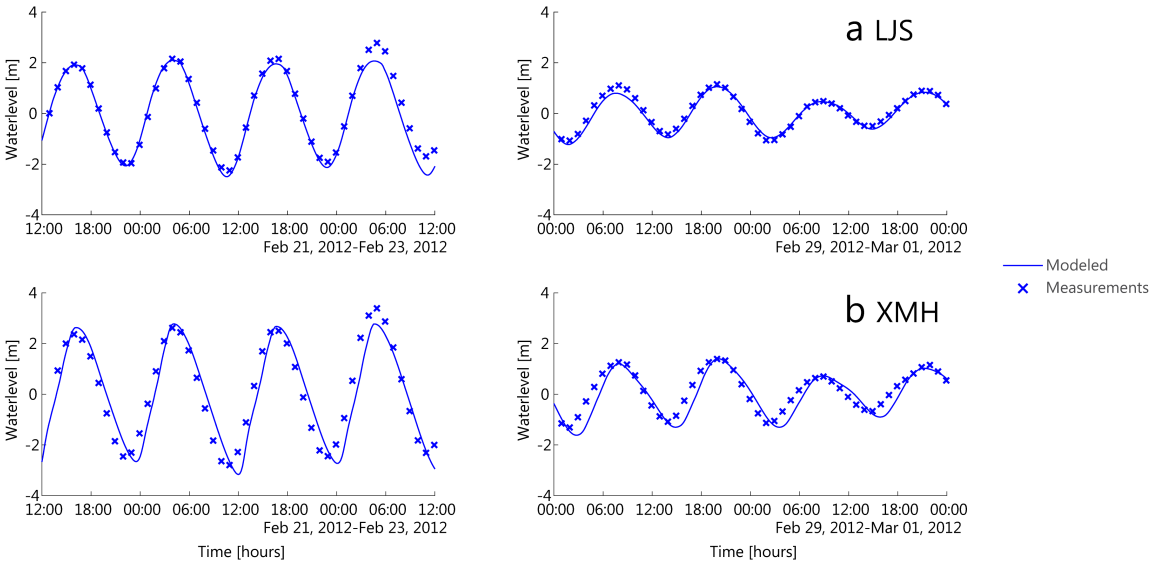

Figure C.1: Calculated and measured waterlevels at two monitoring stations, Lengjiasha and Xiaomiahong

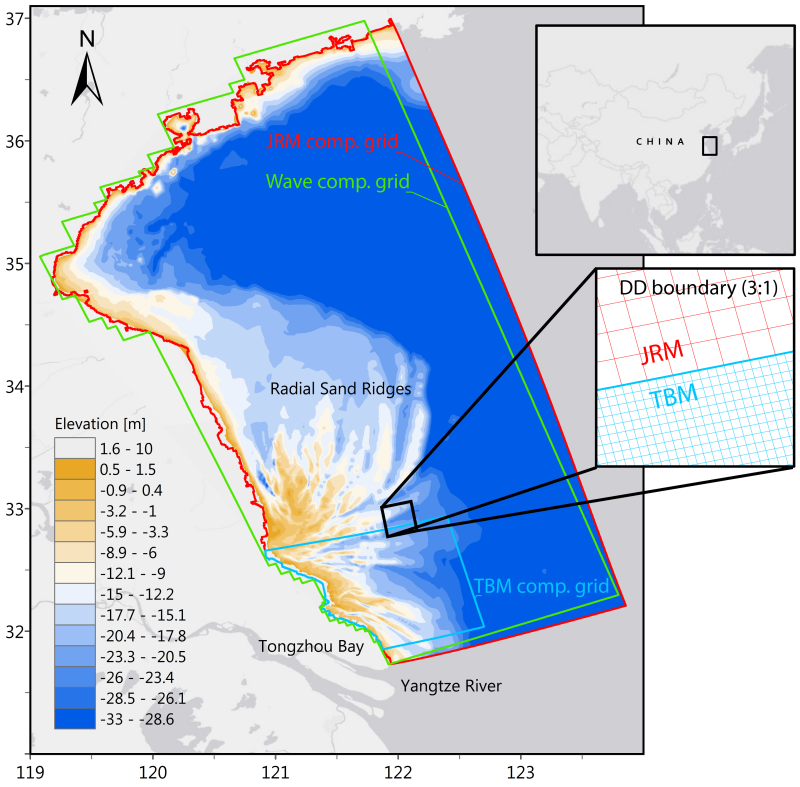

Figure C.2: Used computational grids for the Tongzhou model

The current velocities, directions and suspended concentrations are referenced with the measurements at the 14 mooring stations (see Appendix A). Generally, the model shows a good similarity between the calculated and measured current velocities and directions, as shown in Figure C.3. At more nearshore stations within the tidal channel (*e.g.* N1, N2 , N6 etc.) the model show a large over estimation of the peak velocities. It is presumed that this discrepancy is due to the dissimilarity between the initial bathymetry set in the model

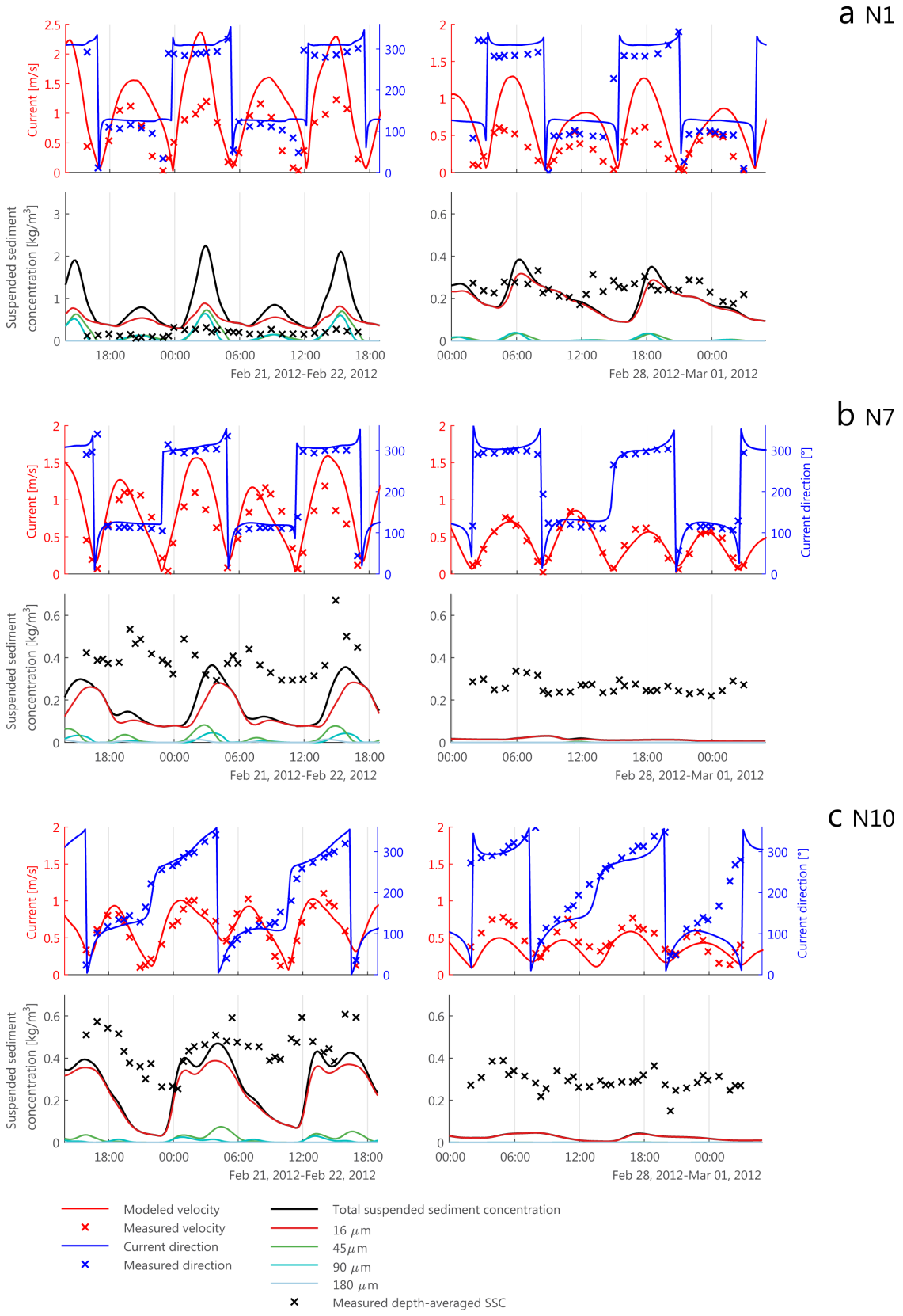

Figure C.3: Calculated and measured current velocities, directions and SSC at station N1, N7 and N10

and in reality. Another short coming was the relative course resolution in the tidal channels. The velocity phase and direction however are still simulated quite well.

Comparison between the calculated and measured sediment concentrations are shown in Figure C.3. Calculated SSC during spring tide conditions show a rough agreement with the measured concentrations. The calculated trend in concentration during the measuring period show a similar behavior to the measured trends. Closer examination of the calculated concentrations show that the model over or under predicts the SSC, due to inconsistent calculated tidal currents or availability of sediment fractions in the spatial varying bed composition.

During neap tide, the sediment concentrations drop at most locations and show very low dynamic. Comparing to spring tide conditions, the overall flow velocities during neap tide are lower and therefore entrainment and transport of the sediment decreases. Apparently, these flow velocities (around <1 m/s) are to low to entrain sediment from the bed. As similar declining trend is suggested by the measured concentrations aswell, however the concentration itself remains higher than calculated.

C.1.2. Tongzhou Bay Model

To increase the model's accuracy in the near shore processes at the shallow waters at Tongzhou Bay, a smaller domain was 'online' nested inside the JRM by use of Domain Decomposition (DD, (Deltares, 2018)) approach. This Tongzhou Bay Model (TBM) consists of 468 by 269 gridcells with a resolution varying from 231 ~ 366 m. This grid size refinement corresponds to 3 : 1 compared to the JRM computational gird. The TBM was initially setup with similar settings as the JRM. Preliminary results of the TBM are shown in Figure C.4 together with the measurements during spring and neaptide periods. Closer examining the results showed no significant improvement in the disagreement of either the predicted waterlevels, current velocities and sediment concentrations. As such, further improvements were made to the TBM.

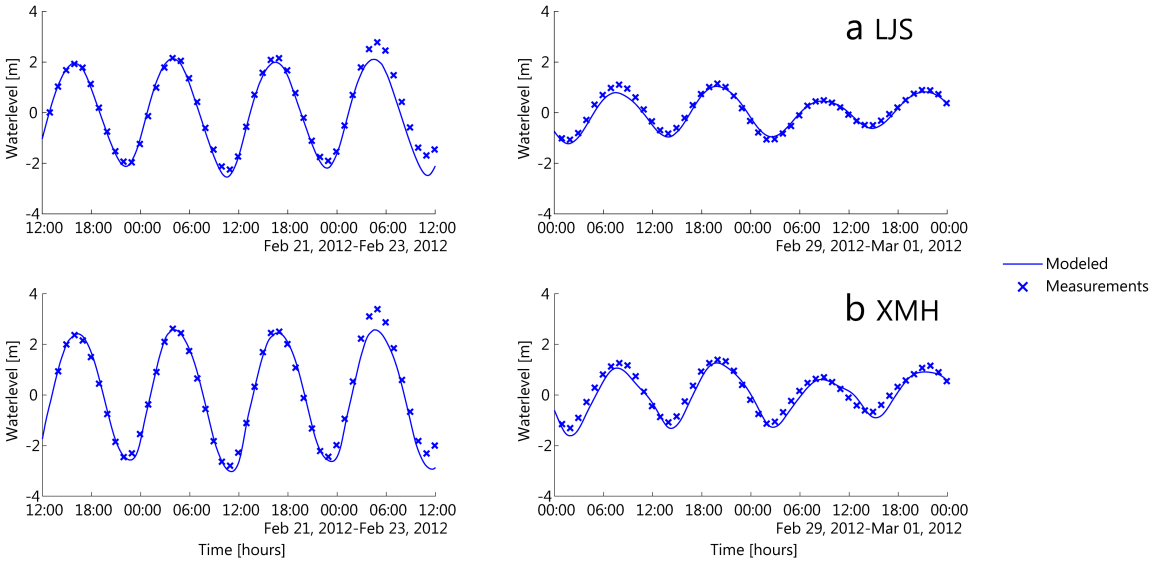

Figure C.4: Calculated water levels with DD setup at Xiaomaiohong channel and Lengjiasha shoal

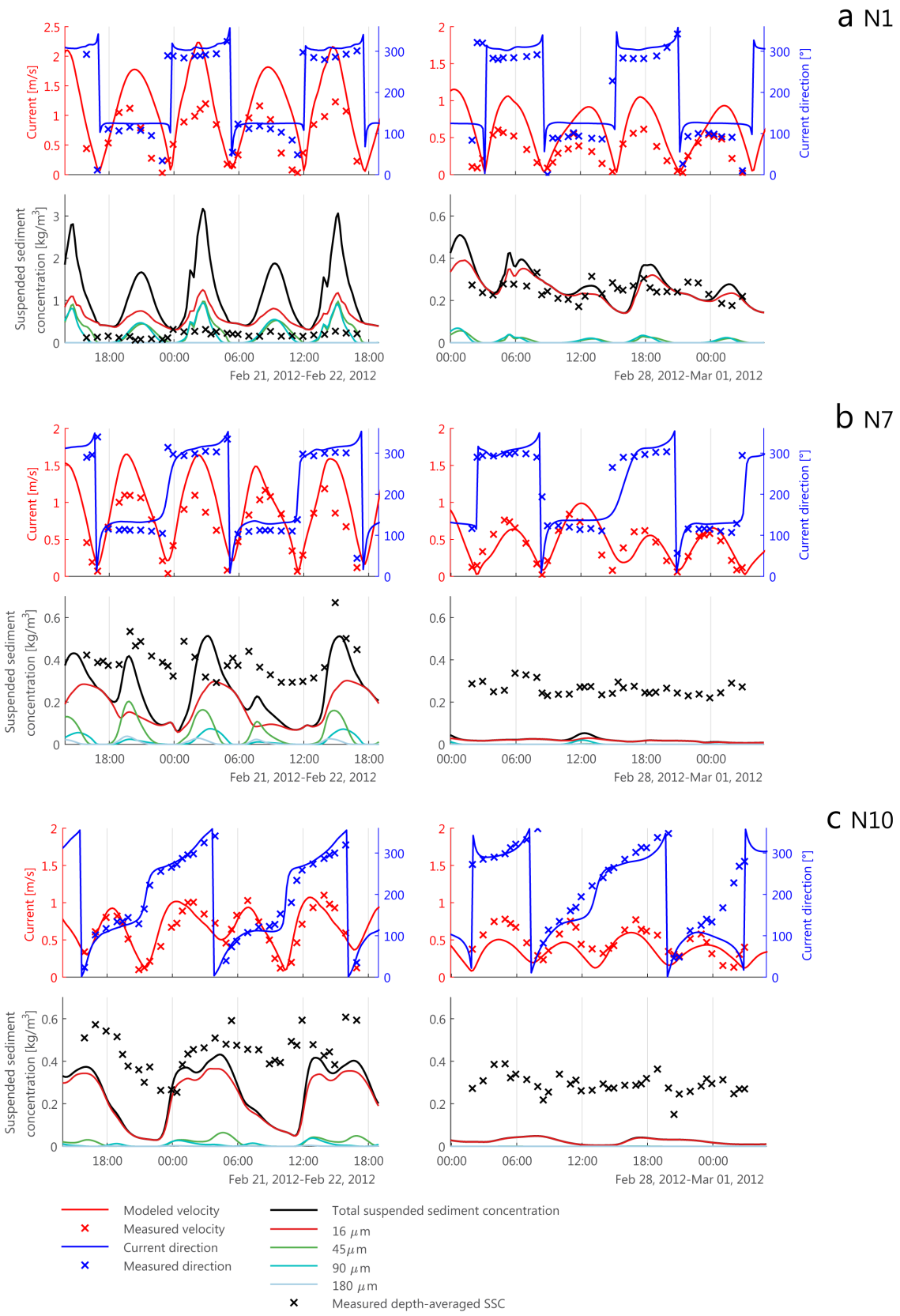

Figure C.5: Calculated flow velocities, direction and SSC with DD setup at stations N1, N7 and N10

C.2. Tongzhou Bay Model improvements

With the preliminary results of the TBM still showing a disagreement with the measured current velocities and sediment concentration, several adjustments were made to the TBM configuration;

- Up-to-date bathymetric data
- Additional mud fraction
- Simplified bed composition
- No further modification of the bed roughness

These alterations were initially tested within a more computational-efficient model of the Tongzhou Bay region. This was done by 'offline' coupling with the JRM, in which it provides the boundary conditions for the smaller domain (not shown here)

C.2.1. Up-to-date bathymetry

Initial bathymetry within the TBM was based on the original data from the JRM, which dates from 2006 (Yao, 2016). More recent surveyed data at the Tongzhou Bay from October 2010 was made available and included in the TBM. The domain with new bathymetry mainly covers the Xiaomiaohong and Sanshahong channel and the Yoasha and Lengjiasha shoal, as shown in Figure C.6.

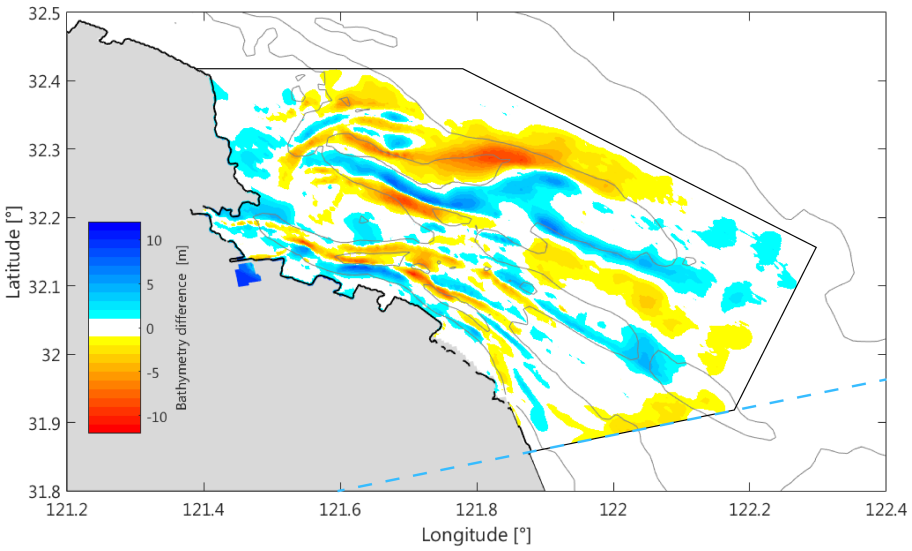

Figure C.6: Difference in initial bathymetry by the JRM and the measured bathymetry in October 2010

C.2.2. Additional cohesive fraction

As described in section 3.2.2, measurement of the average grainsize of the suspended material showed a lower mean grainsize than the lowest fraction (16 μm) present in the model (CCCC Third Harbor Consultants Co. Ltd, 2012). Also the measured concentration showed a lower dependency on the flow conditions than the calculated concentrations by the previous model set-ups . Therefore an additional sediment fraction is added, which is modeled as cohesive sediment as descibed by Partheniades (1965). As it is not clear what sediment properties could represent this observed fraction, a sensitivity study is performed to determine the characteristic parameters of this cohesive sediment, as well the initial and boundary conditions. These parameters include:

- Erosion parameter, M $[kg/m^2/s]$
- Critical bedshearstress for erosion, τ_{ce} $[N/m^2]$
- Settling velocity, w_s $[mm/s]$

- Boundary concentration, c_{SB} $[mg/L]$
- Initial bed layer thickness d_{mud} $[m]$

Erosion parameter The erosion parameter controls the total amount of eroded material, once the erosion threshold is exceeded ($\tau_{ce} > \tau_c$). A total of 3 values were tested (*e.g.* M = 0.01; 0.004 and 0.005). The results are shown for a station N1 (upper the Xiaomiaohong channel) and station N10 (shallow water on top of Lengjiasha shoal) during spring and neap tide. Durations are shown corresponding to spring and neap tide from 22 February to 3 March. It can be seen, that a higher erosive parameter results in an overall higher concentration. Varying the erosion parameter from 0.010 to 0.005 yields a nearly constant difference of 3 mg/L during the simulation.

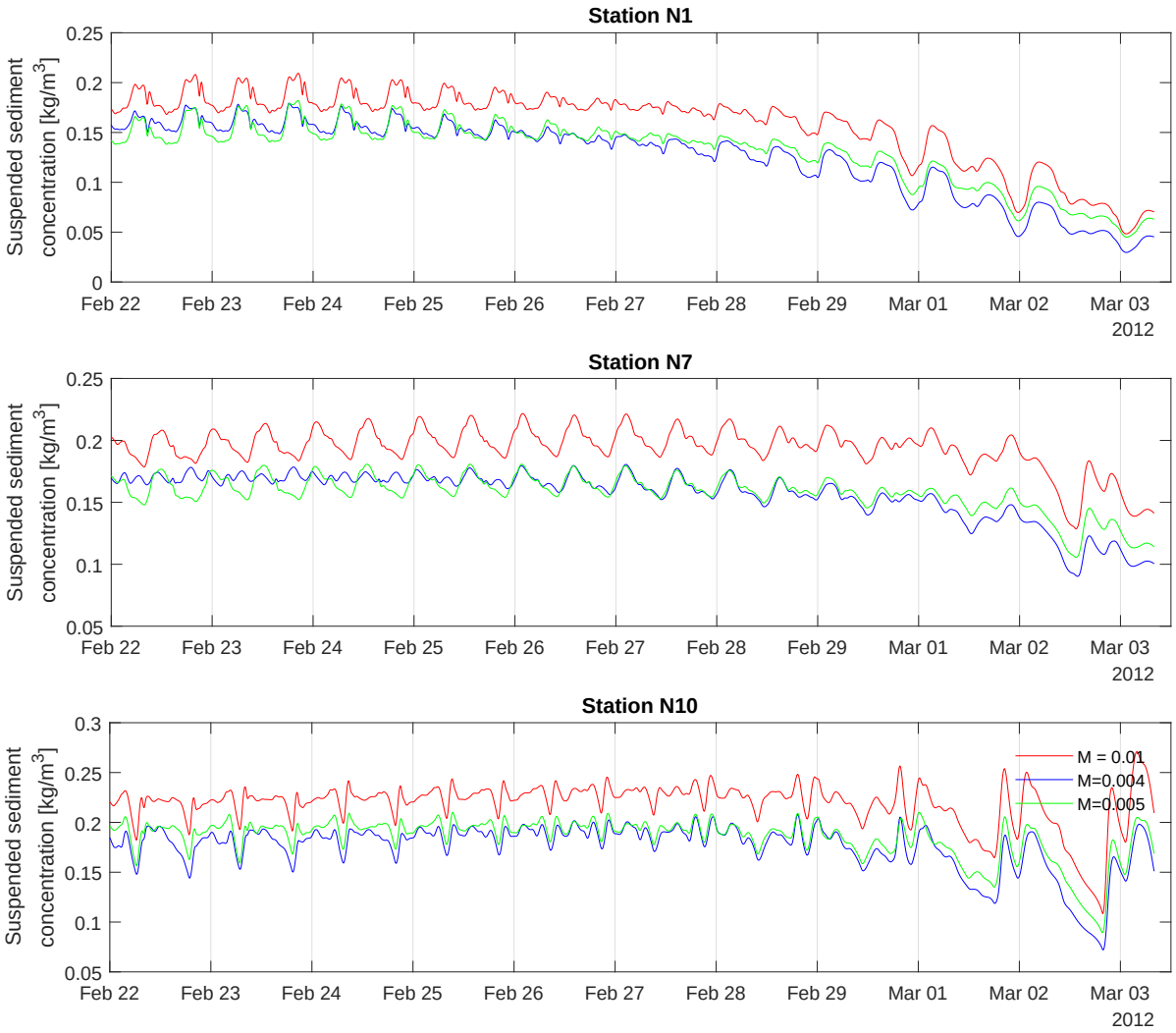

Figure C.7: Difference in calculated suspended sediment concentration due to the erosion parameter M

Critical bedshearstress The critical bedshearstress for erosion describes when the sediment will start to erode as result of the drag inflicted on the bedsurface by the flow. As described in section 2.3, several values for the τ_{ce} are proposed for the cohesive material along the Jiangsu coast, varying form 0.11 to 0.29 N/m^2 (Shi et al., 2016; Yang et al., 2016). For the sensitivity study, τ_{ce} is given a value of τ_{ce} = 0.1, 0.12 & 0.2 N/m^2. Further, it is assumed that deposition of the cohesive sediment fraction always takes place, setting the critical bedshear stress for deposition to τ_{cd} = 1.0 e3 N/m^2 Winterwerp and Van Kesteren (2004).

Again, spring and neap cycle is shown for three stations, namely N1, N7 and N10 located at upper XMH, SSH and on LJS shoal respectively. It can be seen that during high velocities the calculated concentration are roughly the same. This can be explained as the flow velocities are high and the critical bedshear stress for the

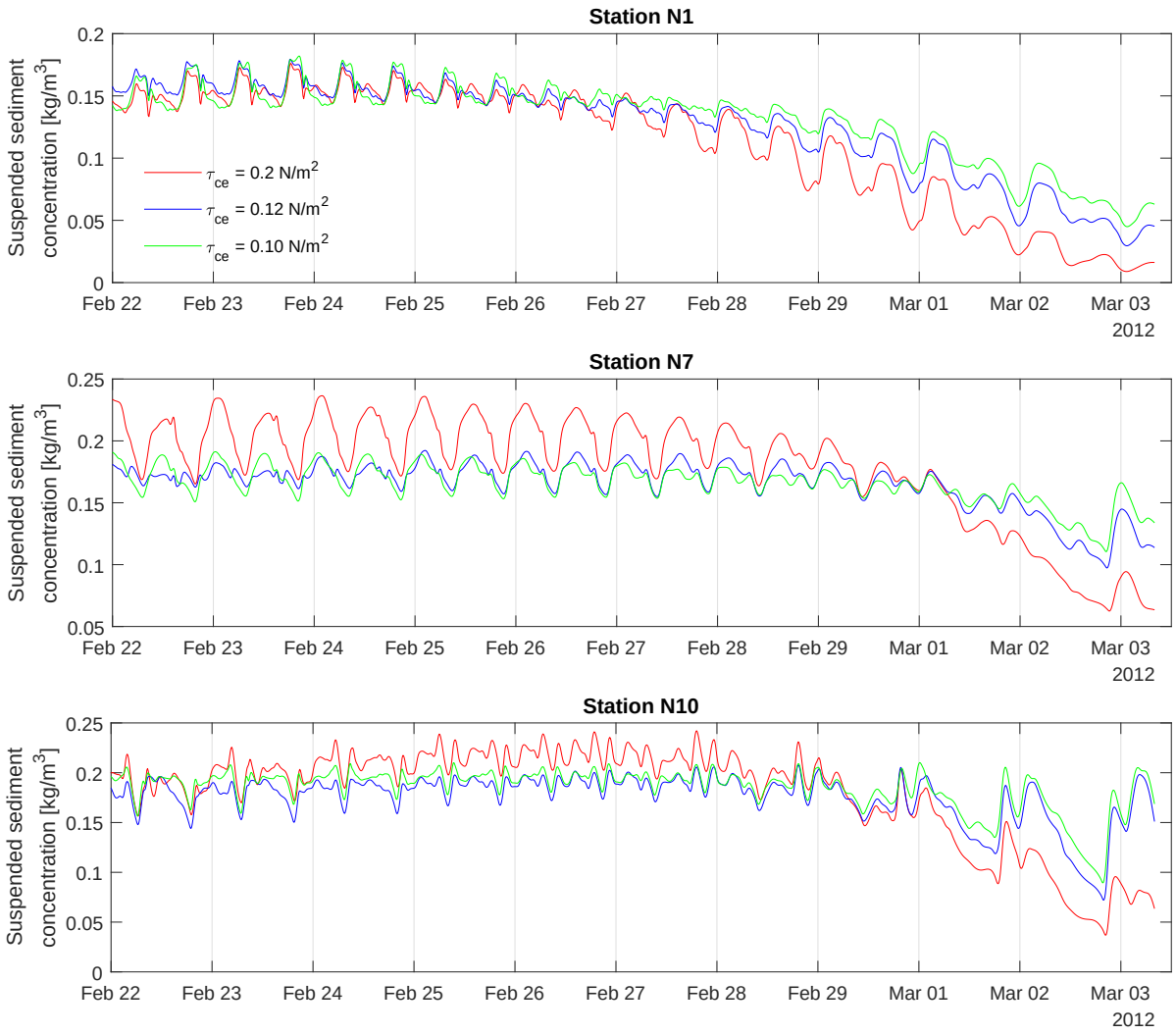

Figure C.8: Difference in calculated suspended sediment concentration due to the critical bed shearstress for erosion

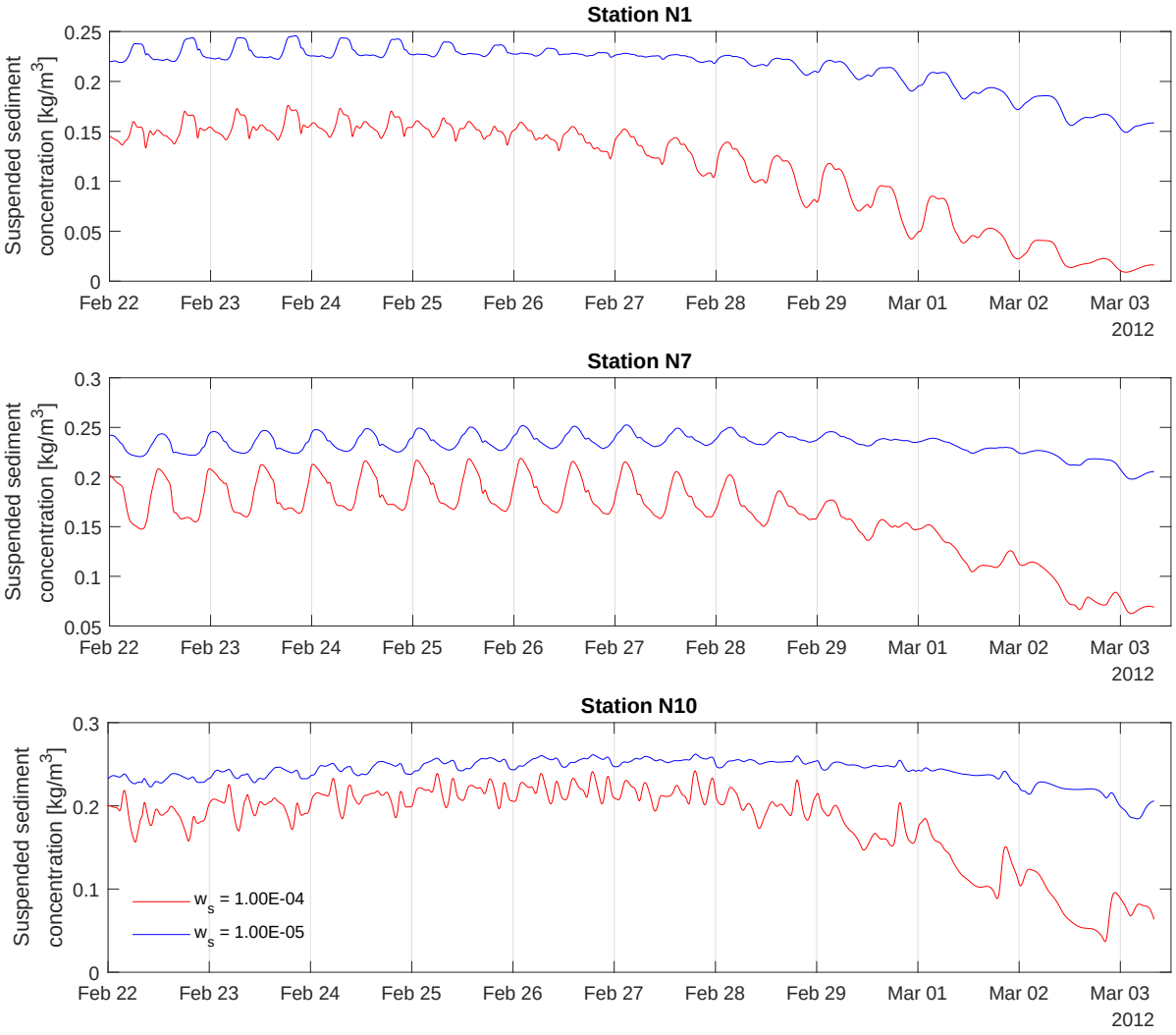

Figure C.9: Difference in calculated suspended sediment concentration due to the settling velocity

sediment to be eroded is surpassed in all cases. During neap tide, the current velocities are low, hence the critical bed shear stress enacted by the flow does not surpass the critical bedshearstress for the sediment to be picked up. Therefore, as the maximum current velocity per tidal cylce steadily reduces, so does the overall sediment concentration. Varying in the critical bedshear stress for the sediment reflect this trend. For lower value of τ_{ce} leads to entrainment even during low current velocities and a higher concentration during neap conditions.

Settling velocity The settling velocity describes the rate at which sediment particles descend towards the bed and determines the time a parcel remains in suspension. In this sensitivity study, the settling velocity is varied between $0.1 \sim 0.01\ mm/s$. Results are shown in Figure C.9.

It can be seen that the sediment property with the high settling velocity is able to maintain the concentration throughout the domain. When velocities are high and the sediment is entrained, this concentration will decay with a smaller gradient that with a higher settling velocity. At station N1, the low settling velocity and high entrainment makes this an almost constant concentration. When the velocities drop, the τ_{ce} is exceeded less often during a tidal cycle. Hence the concentration starts to steadily drop. At shallow zones, this signal is much more episodic as the velocity picks up is short time periods.

C.2.3. No bed roughness modification

The sediment transport within the JRM is calculated by the modified VanRijn transport formulations van Rijn (2007a,b) as described by Yao et al. (2015); Yao (2016). In this approach, the transport is calculated separately

from the flow results. This means that flow-induced transport parameters, the such as the bed shearstress are individually determined for flow and transport. Bed friction was initially described by a spatial varying manning coefficient as $n = 0.015 + 0.1/H$, with H the initial water depth. In order to increase the JRM's flow results accuracy within the complex system of channels and shoals, a spatial varying tuning parameter was introduced by Yao (2016) depending on deep or shallow regions within the domain. This tuning parameter was applied to the bed friction, thereby adjusting the bed roughness and local flow velocities.

However, the introduction of an additional cohesive fraction to the model, as described in previous section, required the use of a different sediment transport formulation as described by Partheniades (1965). Within these formulations, the transport is directly calculated from the flow results. This makes the flow calibration approach as included in the JRM not applicable as it affects both the flow and transport. For example, regions in the JRM where the flow was considered to low were adjusted by multiplying the local manning coefficient with a relatively low calibration factor. As such, the bed shear stress becomes very low and according to the sediment transport formulations for cohesive sediment, siltation occurs. This results in a nearly constant siltation at these areas which has no physical representation anymore. Therefore, the modification of the manning coefficient is not included in the new setup.

The effect of not including the bed roughness calibration factor on the flow velocities was examined by simulation several setups with different bed roughness definitions. Figure C.10 shows the comparison between several bedfriction definitions and additional tuning. The largest effect of the bedfriction can be observed during spring tide when current velocities are highest. The impact of neglecting the tuning parameter in the bed friction is relatively small *e.g.* $\pm$ 0.1 m/s. Some underestimations of the current velocities were calculated, mostly at locations were the tuning parameter was particularly high, such as the main channels. Simplifying the bedfriction by a constant value of $n = 0.015$ leads to large underestimations, especially in the upper reaches of the tidal channel *e.g.* $N1$. Comparison with the measured current velocities suggest that neglecting the tuning parameter on the spatial varying manning coefficient results in acceptable results.

C.2.4. Simplified bed composition

The JRM was setup with a space-varying bed composition that consisted out of 4 fractions (*e.g.* 16, 45, 90 and 180 μm) within a vertical homogeneous active layer with a thickness of 6 m. This bed composition was compiled from different field measurements form other studies reflecting the situation around 2006 Yao (2016). Calculated SSC from this setup show large variations in entrainment of the sediment. This difference could originate from a different bed composition for the situation of 2012 with respect to 2006 due to sorting effects. More recent bed samples, which were retrieved in February 2012 at a section of the Tongzhou Bay, were made available (see section A.2). These samples were reclassified into the 4 sediment fractions and included into the TBM domain. However, this proved to be problematic, as insufficient data was available to make a sound reclassification. Also, integrating this new bedcomposition section into the existing bed composition for the whole TBM created inconsistencies between layers. Calculated sediment concentrations for each fraction did not show an improvement (not shown here). Moreover, the variety in bed composition for both the JRM and TBM setup, made it difficult to analyses the differences in SSC due to the difference in the availability of each fraction. Therefore, a more simplified set up was composed, in which the 16, 45 and 90 μm fractions each made up 25% or 1.5 m of the total depth. The smaller cohesive fraction and 180 μm fraction were included as 0.02 m and 1.48 m respectively.

C.3. TBM altered configuration

C.3.1. TBM altered configuration

The Tongzhou Bay Model was revised with the described alterations (*e.g.* up-to-date bathymetry, neglecting bed roughness tuning, inclusion of the cohesive fraction and the simplified composition). With a better understanding of the sensitivity of several parameters on the overall suspended concentration of the additional cohesive fraction, several combinations are feasible to model comparable sediment concentrations in combination with the existing fractions (*e.g.* 16, 45, 90, 180 μm). Initially, a relative static set of parameters were chosen for the cohesive fraction (very low settling velocity, very low erosion parameter and critical bed shear stress. After calibration, a set of parameters were chosen, which show a more dynamic behavior and can be seen in Table C.1.

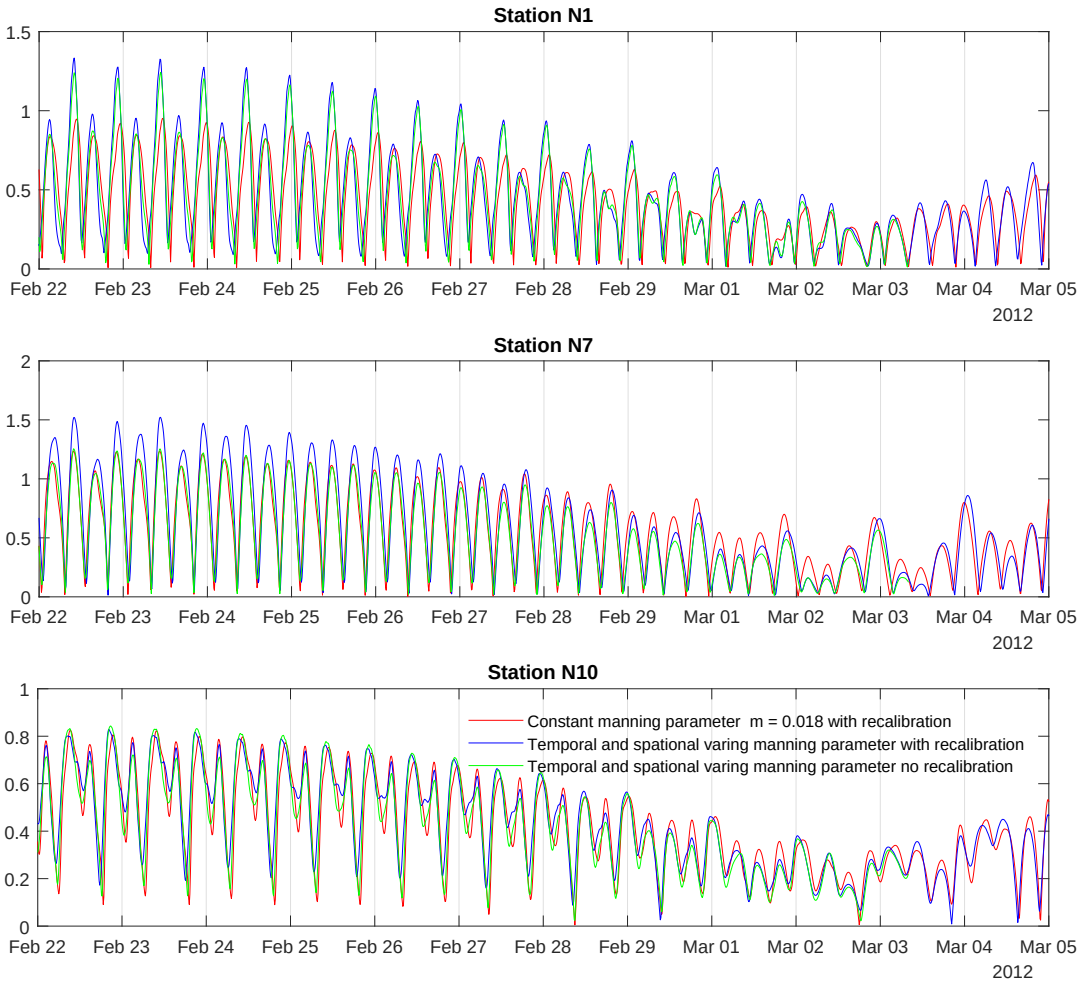

Figure C.10: Difference in flow velocities due to bed roughness definition

Specific density	2.65E+03	kg/m^3
Settling velocity	1.00E-04	m/s
Critical bed shear stress for sedimentation	1.00E+03	N/m^2
Critical bed shear stress for erosion	2.00E-01	N/m^2
Erosion parameter	4.00E-03	$kg/m^2/s$
Dry bed density	3.00E+02	kg/m^3

Table C.1: Finer fraction sediment properties

C.3.2. Boundary conditions

Generally, high concentrations of mud and fines are confined to nearshore coastal zones, due to large-scale processes, such as baroclinic circulations, wave- or tide-driven residual currents or other large scale processes. Similar patterns were found with turbidity satellite images from the Jiangsu Coast Wang et al. (2011). The current model does not incorporate these kind of forcing. Therefore, in order to approximate these nearshore concentrations of the newly added cohesive fraction, different combinations in boundary concentration and initial bed layer thicknesses were tested by means of a sensitivity study.

Boundary concentrations of 0.1, 0.3 and 0.4 g/L were simulated for period of 6 months without other sediment sources present in the model. The results for 3 stations are shown in Figure C.11, which correspond to the upper and entrance of the Xiaomiohong channel and at the more shallow station on the Lengjiasha shoal. It can be seen that for all cases the sediment concentration gradually increases, as more material is being imported up the tidal channels, due tidal asymmetry-induced residual currents. Also, it can be seen that the concentration at different stations approximate the set boundary conditions given enough time elapses for the material to be transported inside the domain.

Yao (2016) included the Yangzte derived SSC, by defining a concentration along the southern boundary for the 16 μm fraction. This set concentration defining a nearshore concentration linearly declined from 0.3 g/L at the nearshore end to 0.015 g/L at the offshore end of the boundary. A similar approach was adopted for the newly added cohesive fraction, describing the boundary concentration of the Yangtze river derived fine material. Comparison with measurements at the 3 stations at the end of the 6 month simulation showed a satisfactory result for a boundary concentration of 0.2 g/l at the offshore boundary and a linear decreasing southern boundary of 0.3 g/L at the near shore to 0.2 g/Lat the offshore end. Finally, by observing the sediment concentration in the domain after 6 months simulation of solely described boundary conditions, an initial concentration of 0.2 g/L for the cohesive fraction was chosen to speed up the simulation duration

So far, the boundary conditions for the smaller domain at Tongzhou have been discussed. However, since the TBM is coupled within the JRM, similar boundary conditions need to be set at the JRM boundaries as well. During simulation, flow and sediment fluxes are exchanged between these coupled boundaries. Since, we are mainly interested in the dynamics inside the TBM, a initial condition of 0.2 g/L for the cohesive fraction was set for JRM domain as well, in order to not disrupt the initial exchange of flow and sediment between the boundaries. The eastern boundary of the JRM was set at a relatively low concentration of 0.015 g/L, as no significant fine sediment fluxes are present at offshore depths. The southern boundary of the JRM is extended with a linear decreasing concentration of 0.3 g/L nearshore and the same 0.015 g/L at the offshore end of the boundary.

C.3.3. Inclusion in the bed

Several simulation were done with varying amount of cohesive material present in the bed. Initial bedlayer thicknesses of 0.01, 0.02 and 0.1 m were set together with 0.25, 0.4 g/L or no concentration at the domain boundary. Preliminary results showed that at all the stations, the material included in the bed is almost completely entrained during strong flow velocities (*e.g.* flood tide) (not shown here). In the case of no additional sediment concentration at the boundaries of the domain, the concentration steadily declines. This can be explained as current patterns and open boundaries transport all the material outside the domain over time. For short time-scale simulations, this decline is not signification. However, for longer timeperiods this approach may not be suitable.

C.3.4. Results

The results of the final setup for the TBM are shown in Figure C.12 and C.13. It can be seen that the current velocities are reproduced quite well. Compared to earlier model setups, this would suggest that a more up-to-date bathymetry has a large impact, especially at the nearshore locations. Closer examination of the current direction shows an overall bias of minus 50 degrees (counter-clockwise). This is due to the simplified test model setup and grid size resolution. Further simplification by not including the roughness calibration did show signification changes.

The introduction of an additional cohesive fraction improved the model's ability of reproducing sediment concentrations during both spring and neap conditions. Furthermore, a higher set cohesive fraction concentration results in lower entrainment of 16 μm. This is probably due to the increase of mud fractions in the bed composition, making it harder to be entrained. It can be seen that the finer mud fraction is partly responsible for the measured concentrations during neap. However, it seems that these concentrations are increased by a missing processes.

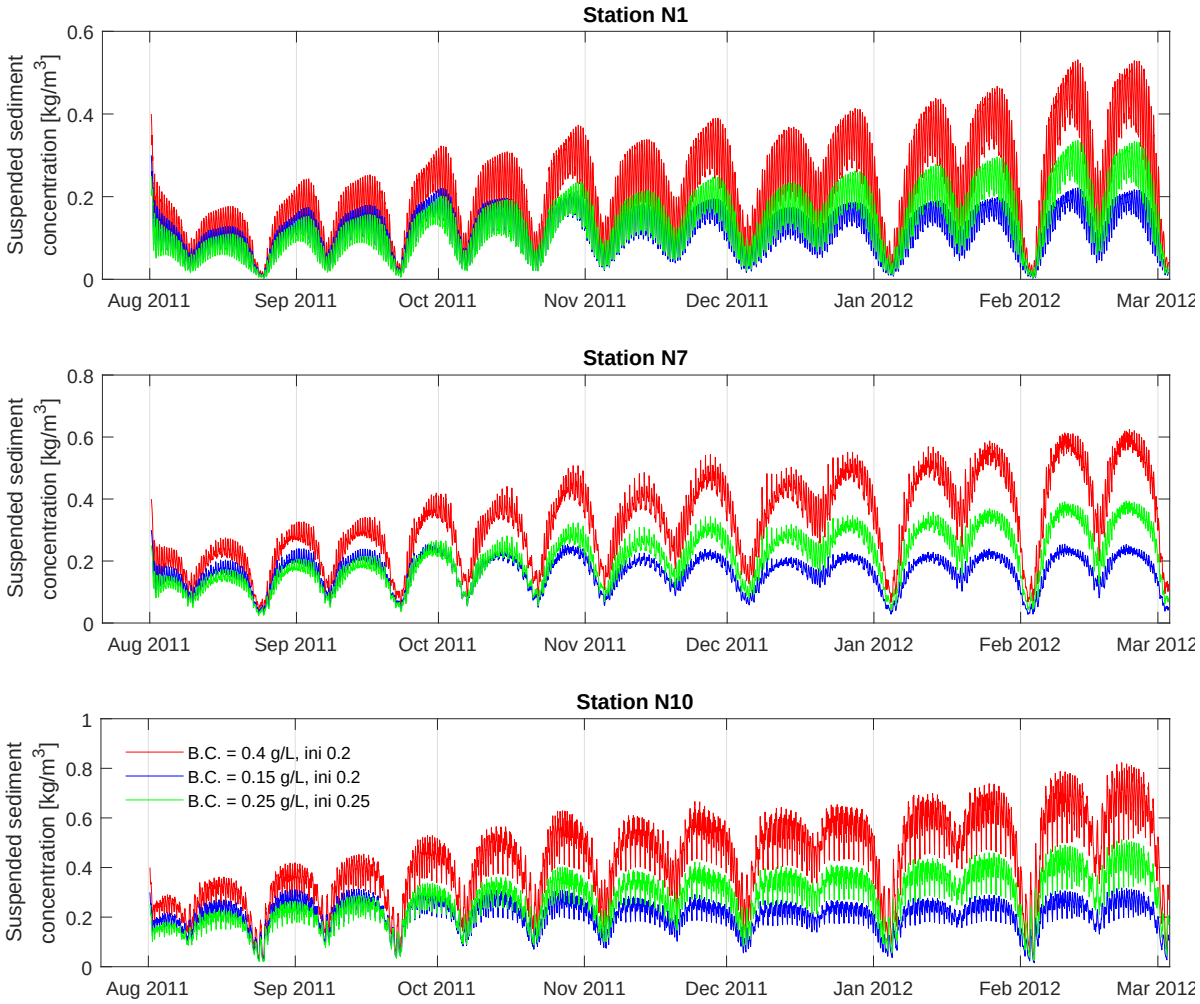

Figure C.11: Difference in calculated suspended sediment concentration due to boundary concentration

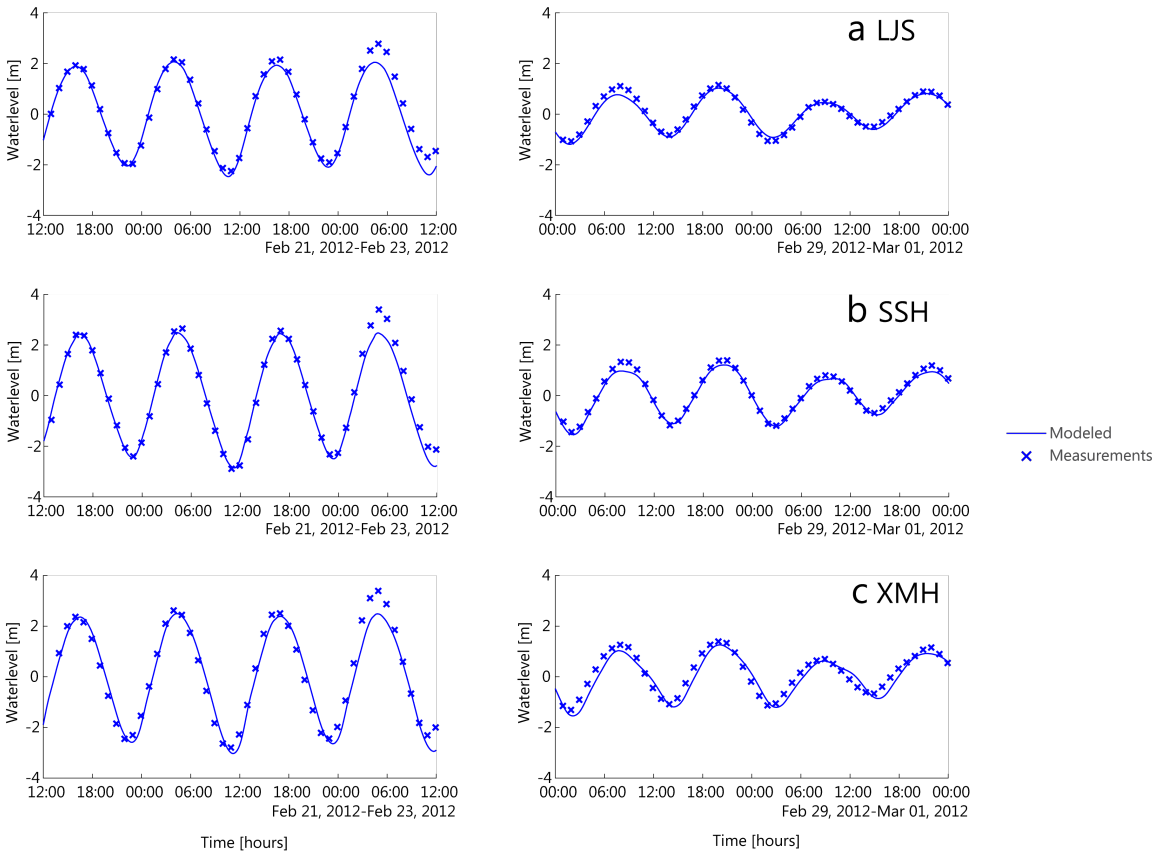

Figure C.12: Final waterlevel results after calibration

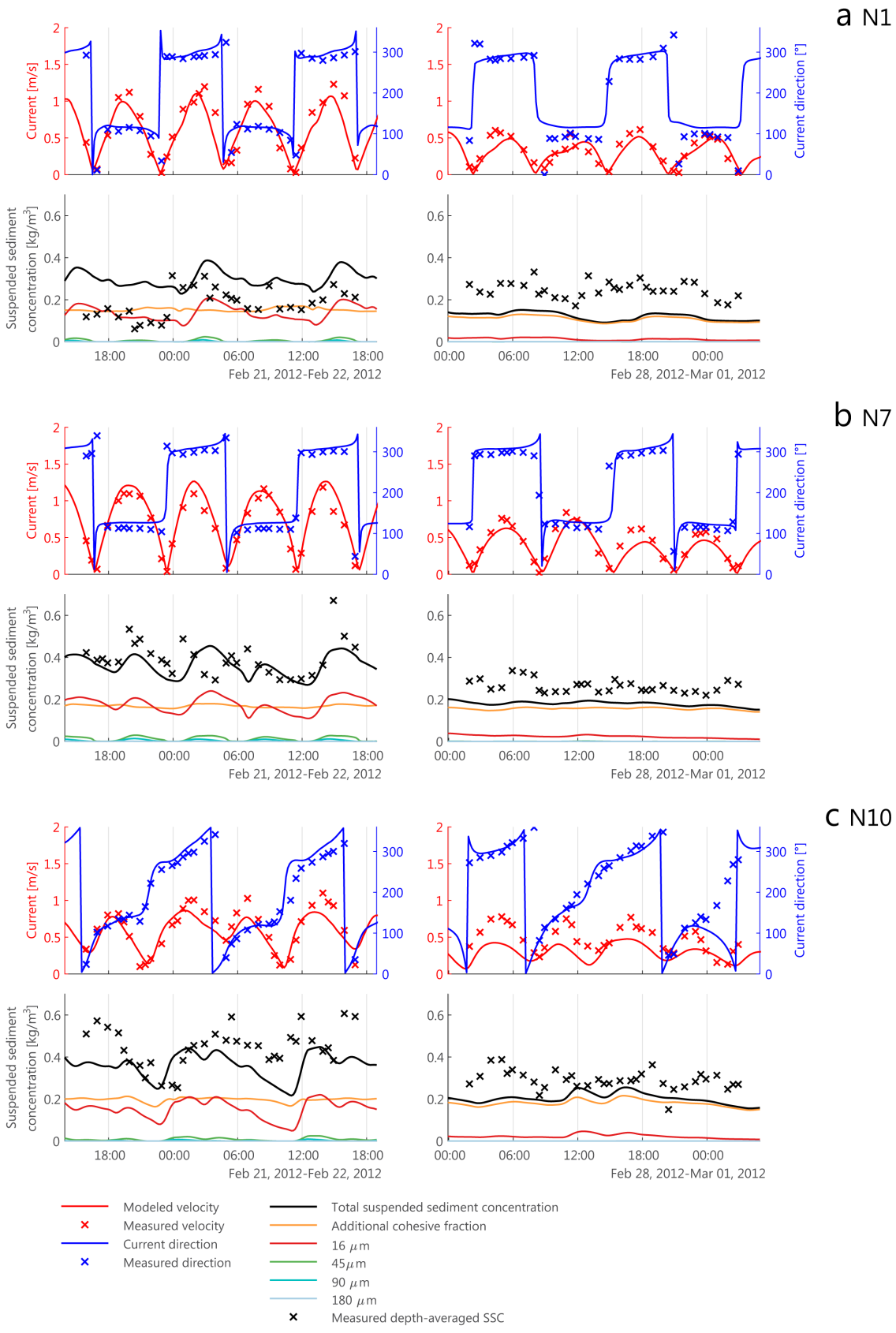

Figure C.13: Adapted TBM results

C.4. Influence of wind-induced waves

As shown in section A, severe wind speeds were measured during the measuring campaign in 2012, especially during neap tide (CCCC Third Harbor Consultants Co. Ltd, 2012). This would suggest the presence of wind-induced waves, which could have a significant role in the resuspension of fine particles during the low flow velocitis in neap tidal conditions. The role of waves in the entrainment of fine sediment at the Jiangsu coast has been investigated in several studies. It was found that during low water conditions, when currents are not as strong, the combined wave- and current-induced bed shear stress, τ_{cw} is larger than the solely current-induced bed shear stress, τ_c (Zhu et al., 2014). Other work showed that the role of currents is far more significant than waves at the Jiangsu coast.

Waves and current interactions are simulated by means 'online' calculation by the numerical model WAVE with the Delft3D-FLOW module (Deltares, 2014). Wave calculation were made on a separate computational grid, as shown in Figure 3.1. It consists of 139 x 238 gridcells with a resolution of 836 $\sim$ 4212 m (see figure C.2). The grid was enclosed by one landboundary at the Jiangsu coast and two open boundaries. The wave and hydrodynamic model exchange information, such as water depth and current velocity with a timestep of 20 min. Wave-current interactions on the bedshear stresses are calculated as described by (Fredsøe, 1984).

Due to the lack of clear wave data at the Jiangsu domain, wave conditions consisted of a combination of incoming wave boundary conditions from offshore and local wind-induced waves. At the eastern offshore boundary, a single wave conditions was defined from mean wave height characteristics found in previous studies. The incoming wave condition was defined with a mean significant waveheight of $H_s = 1.1m$ and a peak wave period of $T_p = 8s$ (Chen et al., 2013; Yang et al., 2014). Further, a directional spreading of 10 ^{o} and normal incident wave direction was assumed. Data analysis showed that the wind velocity and phase did not differ significantly over the 14 measuring locations (see section A.2.2). As such, a constant wind field was assumed over the whole wave computational domain, which consisted the measured wind time series. Missing data between measuring periods were linearly extrapolated with a minimum of 2 m/s

In Figure C.14, the applied windspeed, as well as the calculated significant wave height, current velocity and direction and sediment concentration are shown for spring and neap tide. The current velocity and diction do not show insignificant changes due to the inclusion of waves. The calculated SSC show a general increase during both spring and neap conditions. This can be explained as waves increase the bedshearstress by means of drag. Consequently, the lower tidal flow mixes this enhanced bed concentration over the watercolumn. This increase is particularly apparent during neap conditions when wind velocities and wind-induced waves were highest.

It can be seen that the total sediment concentration during neap conditions is increased due to inclusion of the wave action and matches the measured concentration more accurate. The individual concentration per fraction are shown in the same graph as well. It can be seen that the concentration enhancement by waves is largest with the 16 μm fraction. These results would suggest that the inclusion of a smaller cohesive fraction and the temporal effect of strong waves during neap tide measurements lead to a more accurate calculated sediment concentrations at the Tongzhou domain. Results from stations in the Xiaomiaohong channel, which are more sheltered from waves by the Yaosha-Lengjiasha ridge, show that the waves are not strong enough to entrain significant sediment. However, in reality these waves could come from different directions instead of a single wave direction and will be less damped by the submerged shoals and shallow areas.

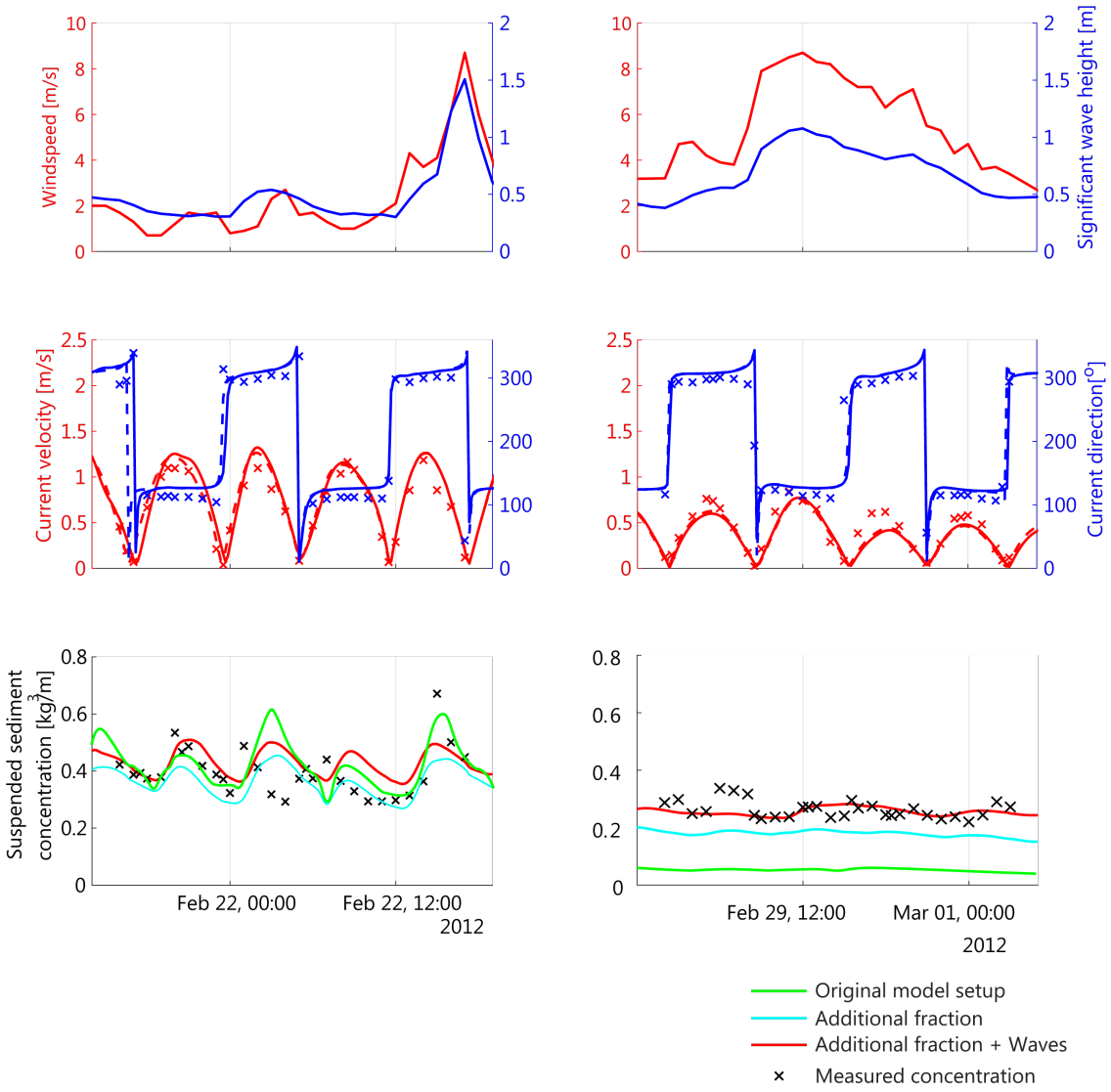

Figure C.14: Effect of wind-induced waves on calculated flow velocities directions, and SSC

D

Alternative port reclamation: Ecotope maps

In this appendix, the comparison between initial and final ecotopemap are shown for all the final alternative port configurations. These correspond to the initial situation in 2012 and after 8 years of morphological development. The ecotope development in case of no additional reclamations is also shown as a reference case. This case represents the hypothetical case of unhinderd natural growth of Tongzhou Bay without any further reclamation of the Yaosha or Lengjiasha shoal.

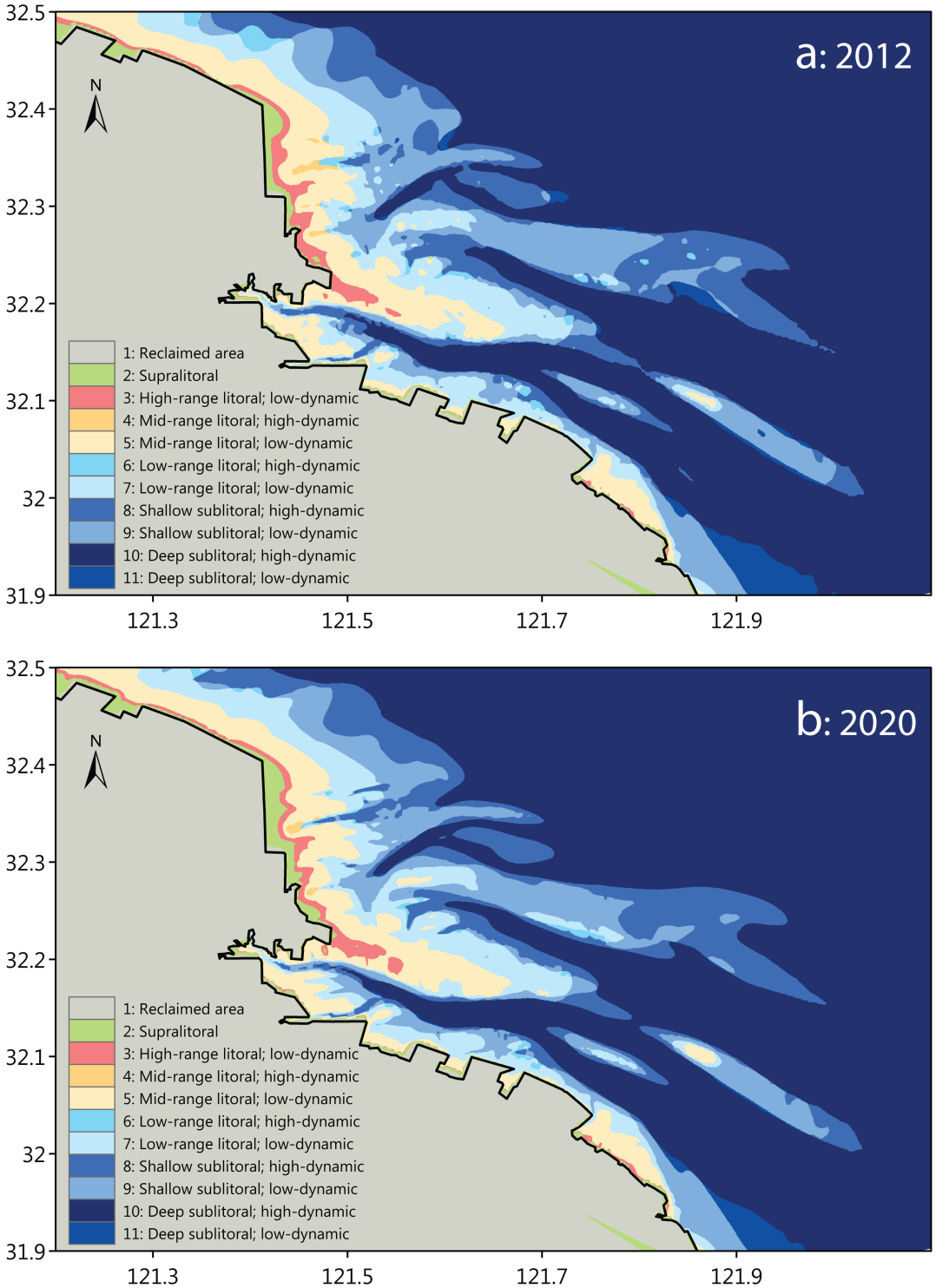

Figure D.1: Ecotopemap for 2012(a) and 2020(b) for the reference case

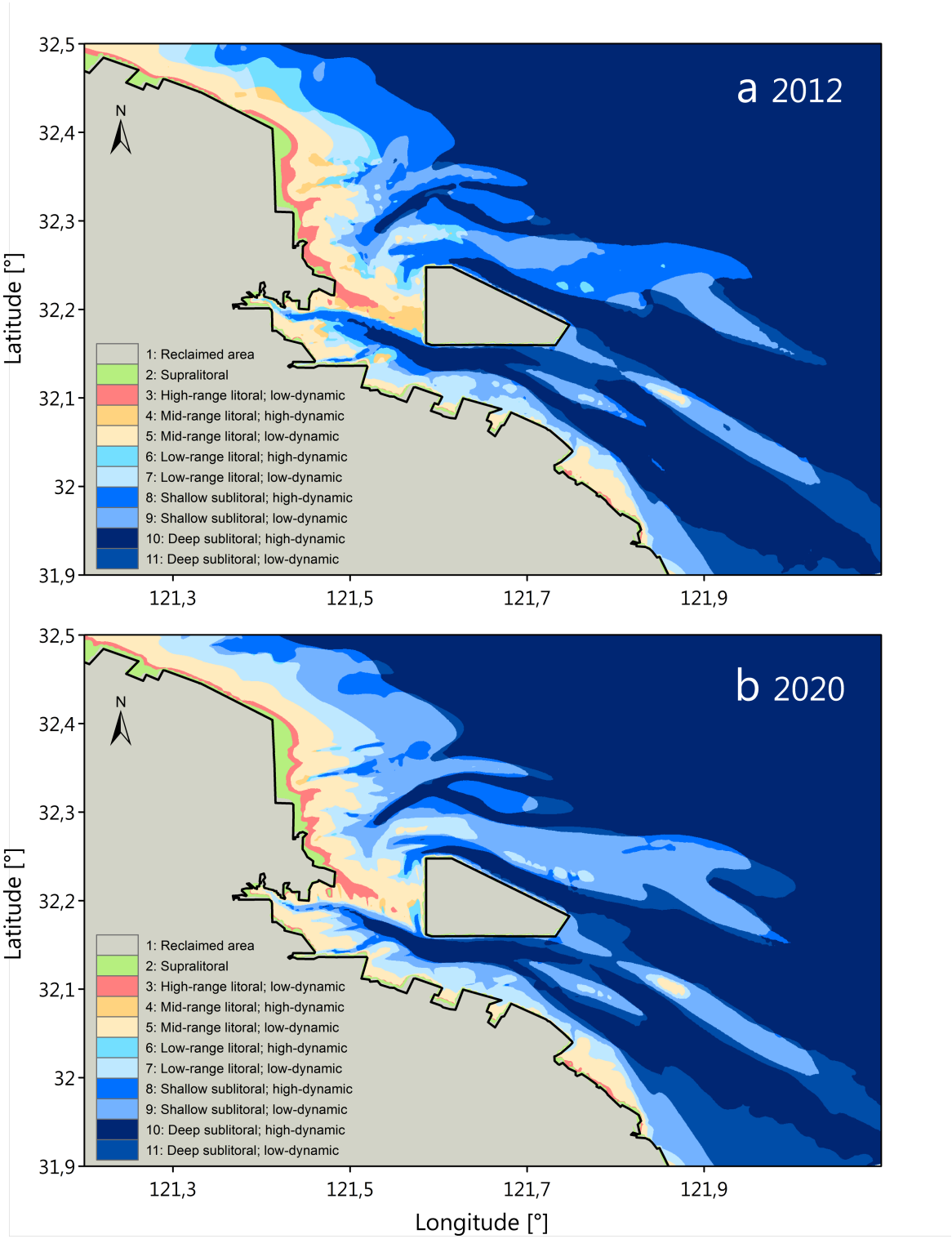

Figure D.2: Ecotopemap for 2012(a) and 2020(b) for scenario $v2$

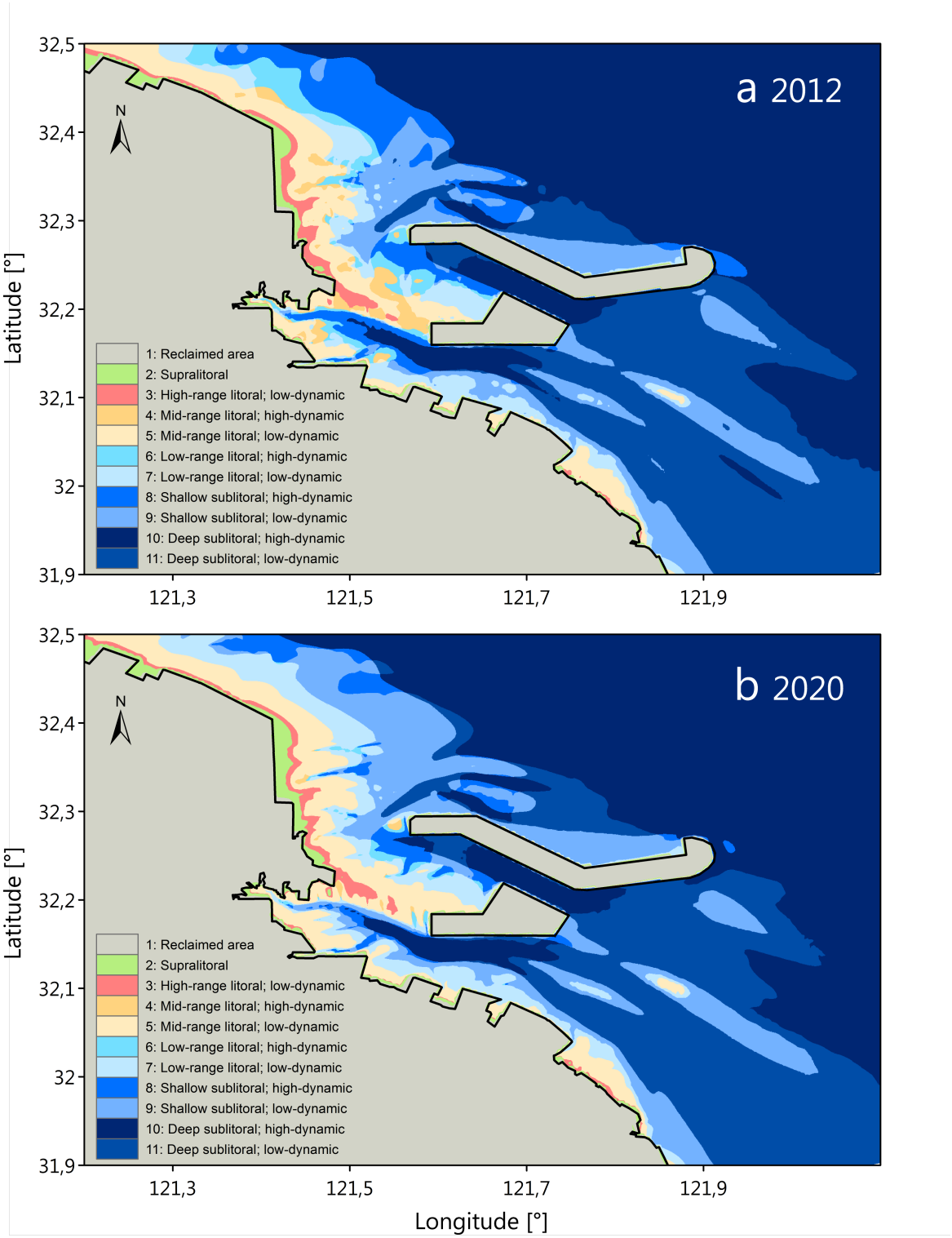

Figure D.3: Ecotopemap for 2012(a) and 2020(b) for scenario $v7$

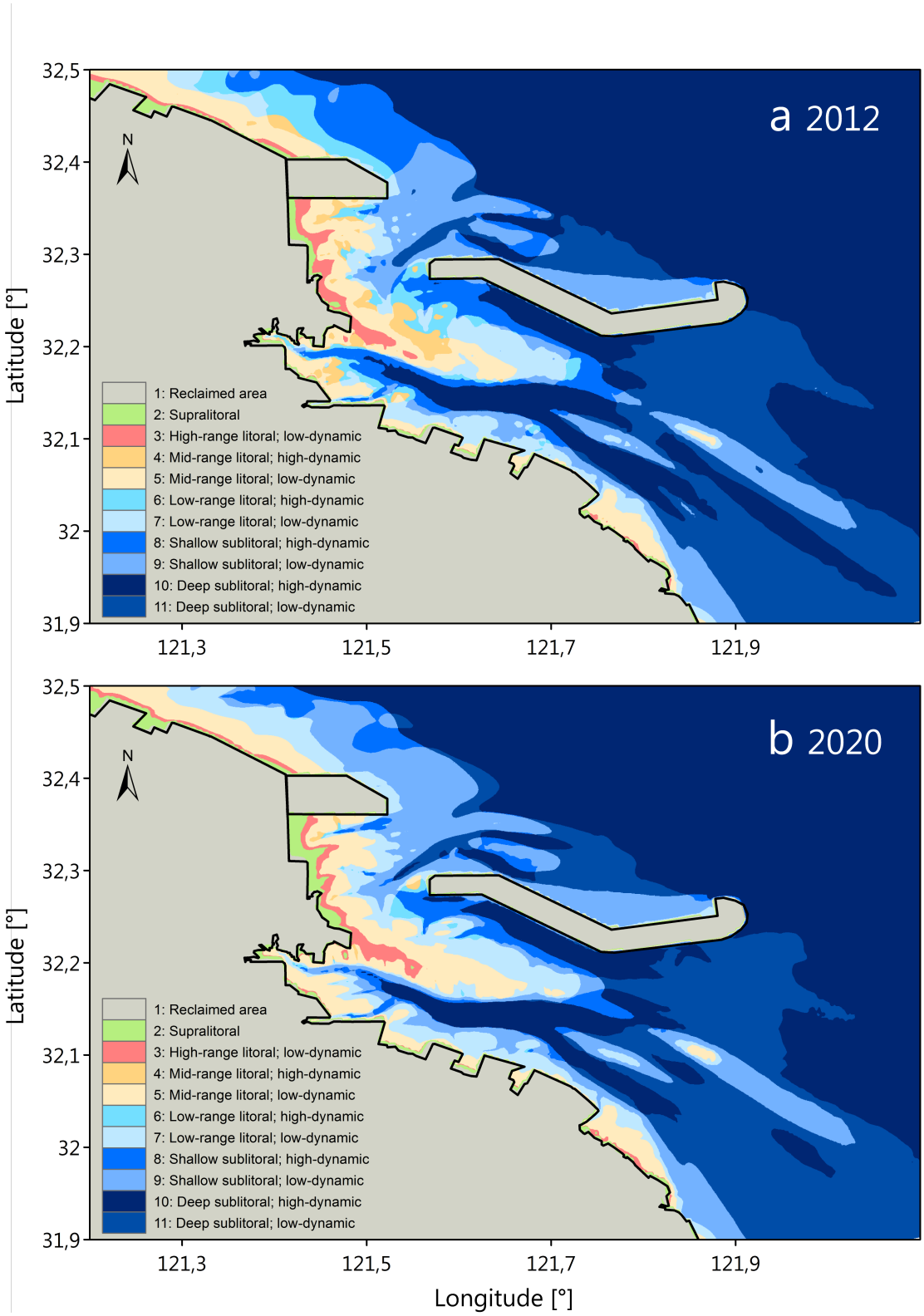

Figure D.4: Ecotopemap for 2012(a) and 2020(b) for scenario *v*8

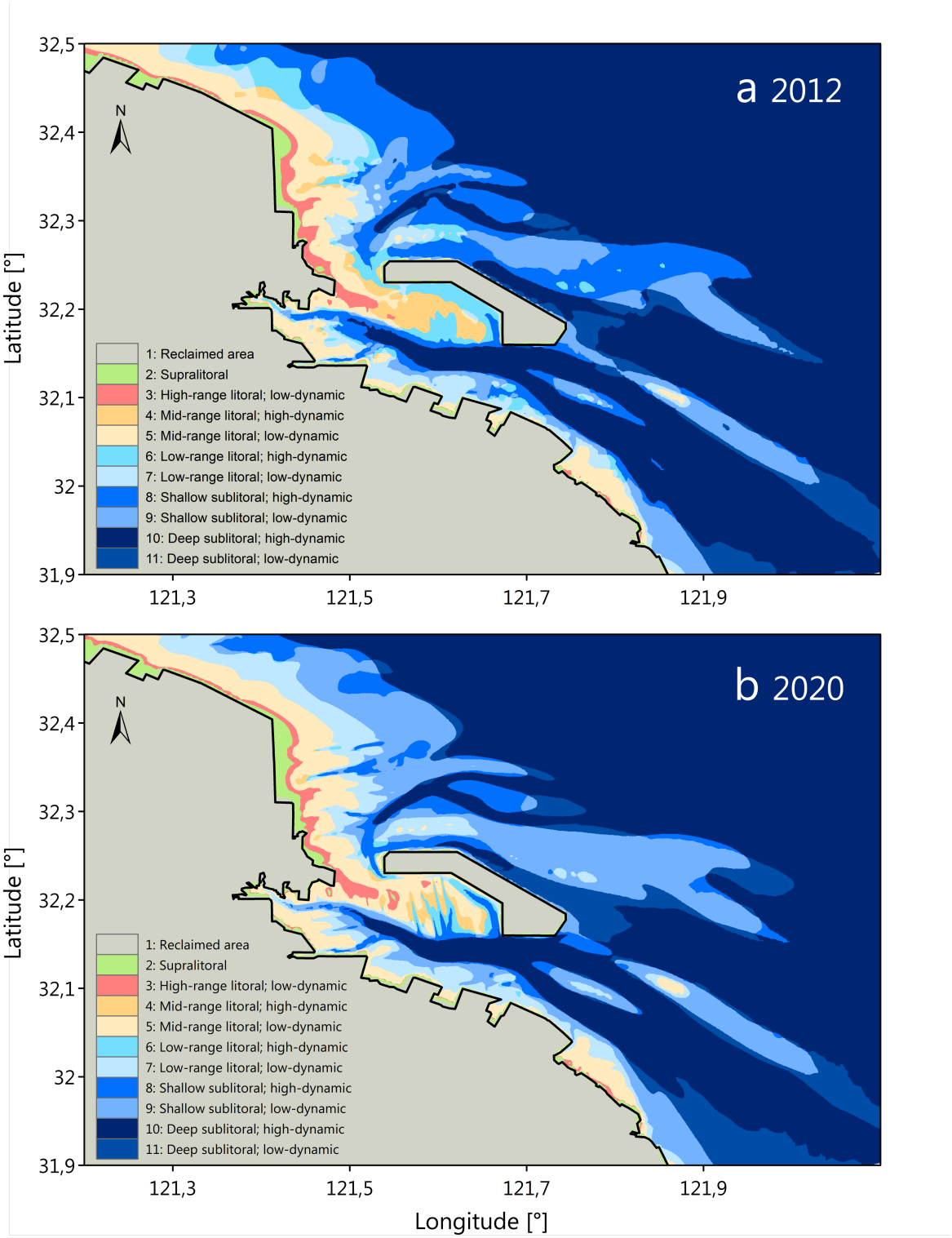

Figure D.5: Ecotopemap for 2012(a) and 2020(b) for scenario $\nu 9$

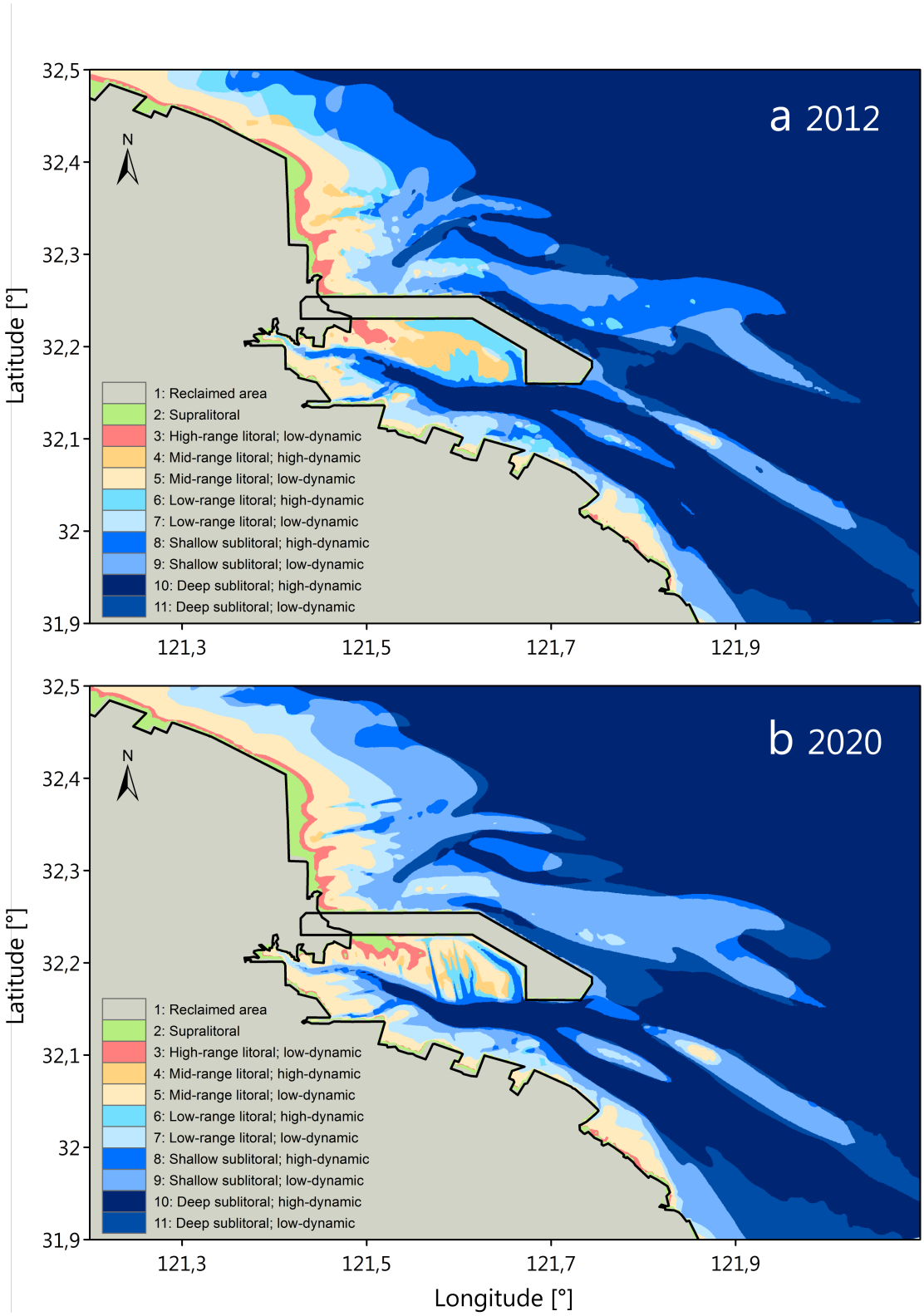

Figure D.6: Ecotopemap for 2012(a) and 2020(b) for scenario $v10$

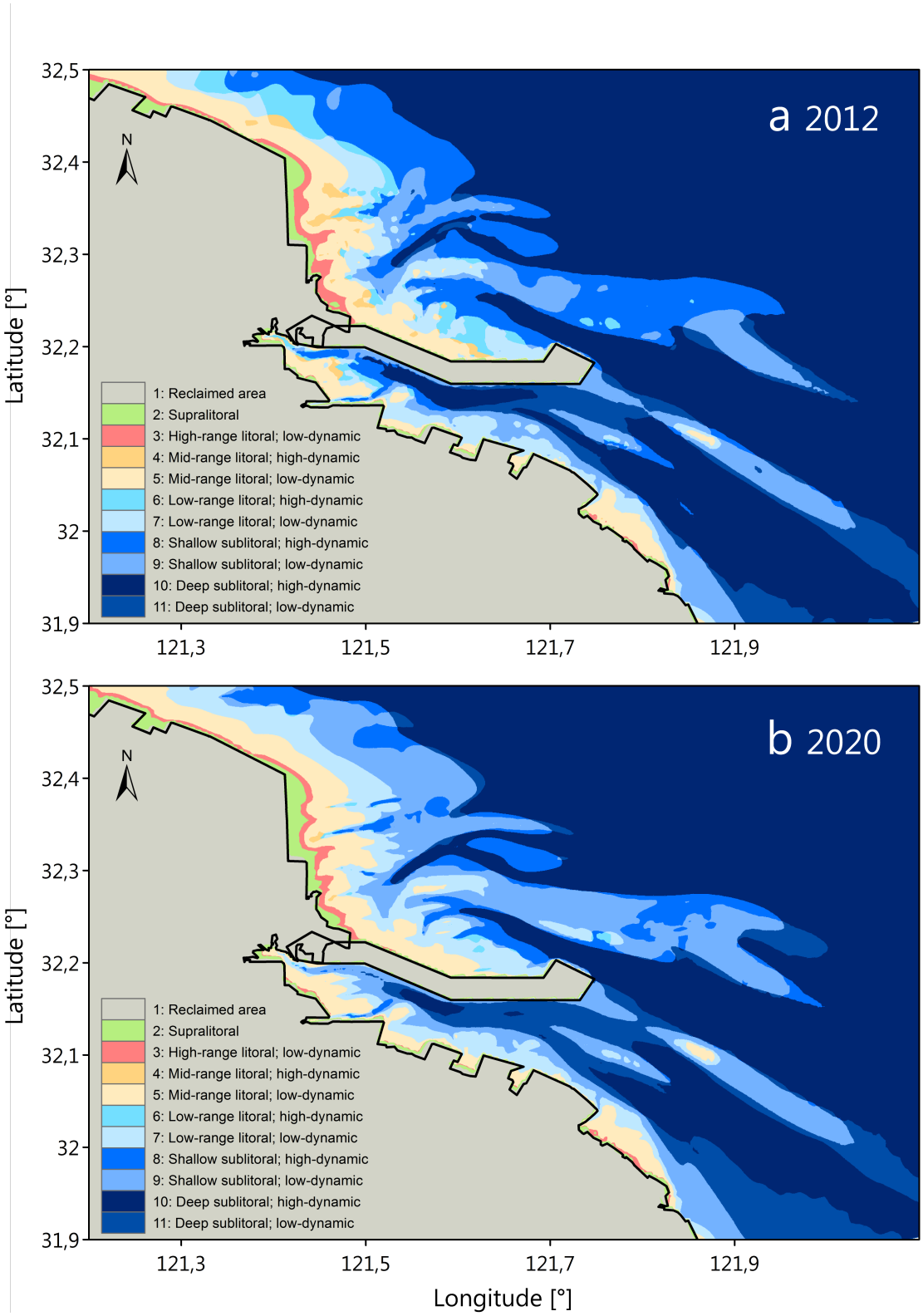

Figure D.7: Ecotopemap for 2012(a) and 2020(b) for scenario $v11$

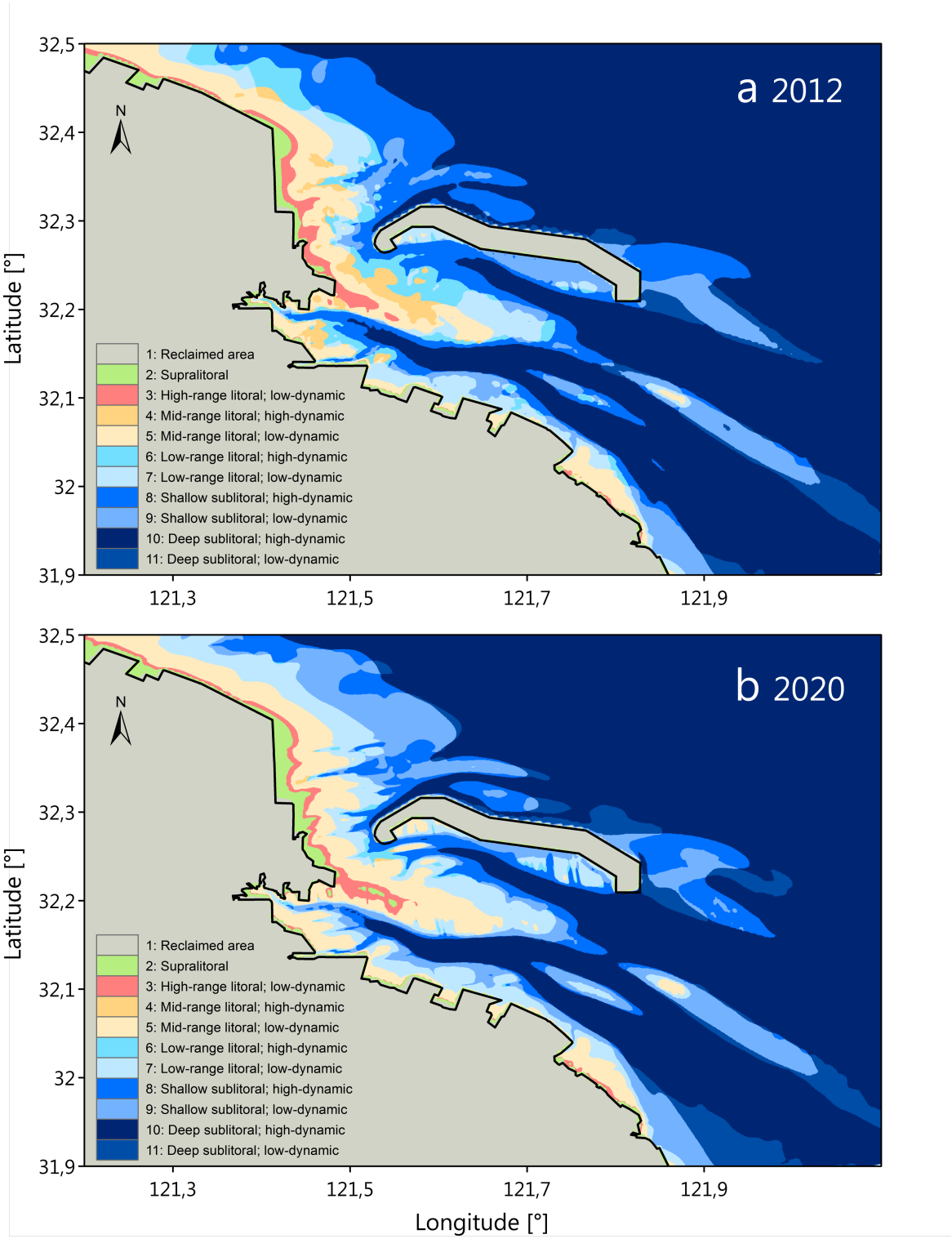

Figure D.8: Ecotopemap for 2012(a) and 2020(b) for scenario $v12$